

PERCOLATE BEHAVIOR OF POLYMER-GEL SYSTEMS

BY

DE-ANNE JOHNSON

A DISSERTATION PRESENTED TO THE GRADUATE SCHOOL
OF THE UNIVERSITY OF FLORIDA IN PARTIAL FULFILLMENT
OF THE REQUIREMENTS FOR THE DEGREE OF
DOCTOR OF PHILOSOPHY

UNIVERSITY OF FLORIDA

1975

NO OF 1 LIBRARIES

To my darling, our little son,

ACKNOWLEDGEMENTS

I would like to thank a number of people for their contributions to this study. First, I would like to express my deep gratitude and appreciation to my research advisors, Dr. R. L. Davis and Dr. J. W. Williams for their guidance, advice, and encouragement in using my graduate work productively and very enjoyable.

I am also grateful to Dr. R. L. Davis and Dr. J. W. Williams of the Department of Materials Science and Engineering and Dr. T. A. Cooper of the Department of Chemistry for their requests, advice and helpful comments.

I would also like to thank my colleagues for their cooperation and friendship. Thanks also go to Cindy Hunsicker for typing this manuscript.

Finally, I would like to thank my parents and my sister for their ever-present support and encouragement.

TABLE OF CONTENTS

	<u>Page</u>
ACKNOWLEDGMENTS	iii
LIST OF TABLES	v
LIST OF FIGURES	viii
ABSTRACT	xvi
CONTENTS	
I INTRODUCTION	1
II BACKGROUND	2
Styrene Characterization.....	3
Mechanism of Polymer Synthesis.....	4
III EXPERIMENTAL PROCEDURES	10
Thermal Analysis.....	10
Infrared Analysis.....	10
Viscous Analysis.....	11
IV SYNTHESIS BEHAVIOR OF POLY(S-VP, BUTYRAL) HOMOPOLYMERS	12
Literature Review.....	13
Monomers and Methods.....	14
Results and Discussion.....	15
Summary and Conclusions.....	17
V SYNTHESIS BEHAVIOR OF POLY(METHYL METHACRYLATE) HOMOPOLYMERS	18
Literature Review.....	18
Monomers and Methods.....	19
Results and Discussion.....	20
Summary and Conclusions.....	21
VI SYNTHESIS BEHAVIOR OF POLY(METHACRYLIC ACID) HOMOPOLYMERS	22
Literature Review.....	22
Monomers and Methods.....	23

Summary and Introduction	100
Summary and Conclusions	100
1. SUMMARY AND CONCLUSIONS	107
Pyrolytic Behavior of PMA and Al_2O_3 -PMA Mixtures	107
Pyrolytic Behavior of PMA and Chlorinated PMA Mixtures	108
Pyrolytic Behavior of PMA and Boron-Substituted Mixtures	110
APPENDICES	
A. LOGGED CHROMATOGRAMS OF PMA MIXTURES	116
B. ^{13}C NMR SPECTRA OF PMA MIXTURES	118
C. FTIR SPECTRA AND STRUCTURAL FORMULA OF THE VOLATILE PRODUCTS	120
D. ADSORPTION THERMALS OF PMA MIXTURES ONTO Al_2O_3 SURFACE THROUGH PULSED SOLVENTS	122
REFERENCES	125
BIOGRAPHICAL SKETCH	126

LIST OF TABLES

Table	Page
1-1 Functions of General Screening Tests.....	2
2-1 Basic Formulations for Tape Casting.....	3
3-2 Mechanisms of Thermal Degradation of Polyethylene Glycol.....	16
4-1 FTIR Peak Assignments for PEG Series.....	41
5-1 Molecular Weight, Molecular Weight Distributions, and Compositions of PEGG Series.....	49
5-2 Conditions of Collecting PEGG Samples.....	162
5-3 GC Operational Variables for PEGG Volatiles Degradation Products.....	181
5-4 FTIR Peak Assignments for PEGG Series.....	177
5-5 Decomposition Products from the Pyrolysis of PEGG to Air.....	124
5-6 Decomposition Products from the Pyrolysis of PEGG in Nitrogen.....	125
5-7 Decomposition Products from the Pyrolysis of $Al_2O_3/PEGG$ in Nitrogen to Air.....	126
5-8 Decomposition Products from the Pyrolysis of $Al_2O_3/PEGG$ in Nitrogen to Nitrogen.....	127
5-9 Decomposition Products from the Pyrolysis of $PEGG/Al_2O_3$ in Nitrogen to Air.....	128
5-10 Carbon Residue Densities of $Al_2O_3/PEGG$ Mixtures Fired Under Selected Conditions.....	171
6-1 Conditions of Collection of PEGG Volatiles.....	162
6-2 GC Operational Variables for PEGG and $Al_2O_3/PEGG$ Volatile Degradation Products.....	177

4-3	FTIR Peak Assignments for PMAA Residues.....	270
4-4	Decomposition Products from the Pyrolysis of PMAA in Air, 30-250°C.....	308
4-5	Decomposition Products from the Pyrolysis of PMAA in Nitrogen, 30-250°C.....	311
4-6	Decomposition Products from the Pyrolysis of PMAA in Air, 250-1000°C.....	340
4-7	Decomposition Products from the Pyrolysis of PMAA in Nitrogen, 300-1000°C.....	353
4-8	Decomposition Products from the Pyrolysis of Al_2O_3 /PMAA Mixtures in Air, 30-250°C.....	358
4-9	Decomposition Products from the Pyrolysis of Al_2O_3 /PMAA Mixtures in N_2 , 30-250°C.....	359
4-10	Decomposition Products from the Pyrolysis of Al_2O_3 /PMAA Mixtures in H ₂ , 250-1000°C.....	359
4-11	Decomposition Products from the Pyrolysis of Al_2O_3 /PMAA Mixtures in N_2 , 300-1000°C.....	359
4-12	Carbon Residue Compositions of Al_2O_3 /PMAA Mixtures Formed in the Presence of Low Condensability Gases.....	359

LIST OF FIGURES

Figure	Page
1.1	Classification of polymers.....14
1.2	Approximate effect of partial thermal history, and some consideration of distance from center to back for successive stages of natural history, for known temperature regime.....14
2.3	Flow diagram of the tape casting process for various substrates.....15
2.4	Thermal degradation reactions of polymers.....16
2.5	Diagram of polymerization mechanism yield in a repeating polymer.....17
2.6	Graphs showing curves for collecting polymers: 140 pure polymer; 140 polymer with added hydroperoxide; 140 polymer with added catalyst.....17
2.7	Schematic diagram of reaction reactions with polymer development and decay with uncontrolled color and odors.....18
3.1	Block diagram of the TSP/MS system.....18
3.2	Schematic diagram of the PIR system.....18
3.3	Structure of the PIR system.....18
3.4	Diagram of the off-line reflective stage in process.....18
3.5	Cross-sectional view of the high temperature reaction chamber.....18
3.6	Block diagram of the carbon analyzer.....18
3.7	Block diagram of the pyrolysis apparatus.....18
3.8	Diagram of the MS/MS system.....18
3.9	Separation reactions of polymer of vinyl alcohol and vinyl alcohol.....18

4.5	FTIR spectra of the polymer residue at the indicated temperatures during synthesis of PVB in nitrogen.....	65
4.6	The FTIR spectrum of the primary volatile product is compared to the reference spectrum for isopropylalcohol.....	67
4.6	The FTIR spectrum of another primary volatile product is compared to the reference spectrum for water.....	67
4.6	FTIR spectra of the polymer residue at the indicated temperatures during synthesis of PVB in air.....	68
4.6	TGA results for PVB in air and nitrogen.....	69
4.7	Plots of the indicated percentage of the PVB residue vs. time (reaction time at 150°C) in air and nitrogen.....	69
4.8	PVB and PVA results for PVB in air.....	71
4.8	FTIR spectra of Al_2O_3 (anhydrous) and Al_2O_3 containing adsorbed PVB (100%). The difference spectrum (adsorbed) is obtained by subtracting the anhydrous spectrum from the film spectrum.....	75
5.10	FTIR spectra of the polymer residue at the indicated temperatures during synthesis of Al_2O_3 /PVB mixtures in nitrogen.....	75
5.11	FTIR spectra of the polymer residue at the indicated temperatures during synthesis of Al_2O_3 /PVB mixtures in air.....	76
5.1	TGA results showing (a) the effect of initial molecular weight on the thermal stability of polyfunctional methacrylate(s) samples prepared by the free radical technique at 60°C, and (b) comparison of TGA thermograms for high and low molecular weight polyfunctional methacrylate(s) samples prepared by an anionic technique with the thermograms for a low molecular weight free radical sample.....	81
5.2	Effects of amount of methylalumoxane on DSC curves for samples degrading in nitrogen, sample A (1-8.8), B (1-8.88), and C (18-21).....	81
5.3	Thermal analysis results showing (a) effects of initial molecular weight on DSC curves for samples degrading in nitrogen, sample C ($M_n = 44,800$, $D_n = 176,000$), and E ($M_n = 320,000$), and (b) effects of polymerization method on DSC curves for samples degrading in nitrogen: sample C free-radically polymerized and E anionically polymerized.....	82

1.1.4	Mass spectrometry results showing 141 thermal degradability with fragments during synthesis of alkanes $M_n = 105,100$, $M_w/M_n = 1.031$, approximately 100% cyclic, $M_n = 11,200$, $M_w/M_n = 1.031$, and isomeric (C ₁₄ H ₂₈) _n , $M_n = 2,155,100$, $M_w/M_n = 1.031$ poly(methyl methacrylates), and (C ₁₄) mass spectra of the volatile products of pyrolysis heated in the temperature range 200°-500° of alkanes 141, approximately 140 and isomeric 140 poly(methyl methacrylates).....104
1.1.5	FTIR spectra for 141 minimally polymerized PMA isomers B1, and C1 from radically polymerized PMA (sample C) degrading at 410°C and 400°.....105
1.1.6	GC results for PMA in air and nitrogen.....106
1.1.7	MS and MS results for PMA in air.....106
1.1.8	MS and MS results for PMA in nitrogen.....107
1.1.9	MS and MS results for PMA/Hexanol polymer mixtures in nitrogen.....108
1.1.10	GC results for Hexanol ($M_n = 11,270$, $M_w/M_n = 10,603$) in air and nitrogen.....110
1.1.11	MS and MS results for PMA-B in 141 air and (C) nitrogen.....111
1.1.12	GC results for PMA-B ($M_n = 258,120$, $M_w/M_n = 105,071$) in air and nitrogen.....112
1.1.13	MS and MS results for PMA-B in 141 air and (C) nitrogen.....113
1.1.14	GC results for PMA results with different molecular weights in 141 air nitrogen and (C) nitrogen.....114
1.1.15	FTIR spectra of the polymer residues at the indicated temperatures during synthesis of PMA in air.....115
1.1.16	Relative peak information shows the FTIR spectra as a function of temperature during synthesis of PMA in air.....116
1.1.17	FTIR spectra of the polymer residues at the indicated temperatures during synthesis of PMA in nitrogen.....116
1.1.18	Relative peak information shows the FTIR spectra as a function of temperature during synthesis of PMA in nitrogen.....118

5-19	The structures of PBA swollen samples in air from 30°C to 100°C.....	110
5-20	The FTIR spectra of the primary volatile product, as compared to the reference spectrum for acryl. methyl plate.....	115
5-21	The structures of PBA swollen collected in nitrogen from 30°C to 100°C.....	116
5-22	FTIR spectra of the polymer residue at the indicated temperatures during pyrolysis of Al_2O_3/PBA mixtures in air.....	117
5-23	Relative peak intensities (from the FTIR spectra) as a function of temperature during pyrolysis of Al_2O_3/PBA mixtures in air.....	119
5-24	The structures of Al_2O_3/PBA swollen collected in air from 30°C to 100°C.....	121
5-25	The results for PBA and Al_2O_3/PBA mixtures in air.....	122
5-26	FTIR spectra of the polymer residue at the indicated temperatures during pyrolysis of Al_2O_3/PBA mixtures in nitrogen.....	124
5-27	Relative peak intensities (from the FTIR spectra) as a function of temperature during pyrolysis of Al_2O_3/PBA mixtures in nitrogen.....	126
5-28	The structures of Al_2O_3/PBA swollen collected in nitrogen from 30°C to 100°C.....	128
5-29	The results for Al_2O_3/PBA mixtures in air and nitrogen.....	130
5-30	FTIR spectra of the polymer residue at the indicated temperatures during pyrolysis of oxidized Al_2O_3/PBA mixtures in air.....	140
5-31	Relative peak intensities (from the FTIR spectra) as a function of temperature during pyrolysis of oxidized Al_2O_3/PBA mixtures in air.....	141
5-32	FTIR spectra of the polymer residue at the indicated temperatures during pyrolysis of oxidized Al_2O_3/PBA mixtures in air.....	142

5-27	Relative peak intensities (from FTIR spectra) as a function of temperature during synthesis of PMDA/ODA mixtures in air	154
5-28	FTIR spectra of the polymer residues at the indicated temperatures during synthesis of PMDA/ODA mixtures in air	155
5-29	Relative peak intensities (from FTIR spectra) as a function of temperature during synthesis of PMDA/ODA mixtures in air	156
5-30	FTIR spectra of the polymer residues at the indicated temperatures during synthesis of PMDA/ODA mixtures in nitrogen	157
5-31	Relative peak intensities (from FTIR spectra) as a function of temperature during synthesis of PMDA/ODA mixtures in nitrogen	158
5-32	The thermograms of PMDA/ODA mixtures collected in air from 20°C to 220°C	159
5-33	The FTIR spectrum of the volatile product (Peak 400) as compared to the reference spectrum for adipic bromide	159
5-34	FTIR spectra of the polymer residues at the indicated temperatures during synthesis of PMDA/ODA mixtures in air and on PMDA/Calixol AgO substrates	159
5-35	FTIR spectra of the polymer residues at the indicated temperatures during synthesis of ODA/ODA mixtures in air	160
5-36	Relative peak intensities (from FTIR spectra) as a function of temperature during synthesis of ODA/ODA mixtures in air	160
5-37	FTIR spectra of the polymer residues at the indicated temperatures during synthesis of PMDA/ODA mixtures in air	160
5-38	FTIR spectra of the polymer residues at the indicated temperatures during synthesis of PMDA/ODA mixtures in air	161
5-39	The results for detection and quantitative TGA in nitrogen	162

5-46	FTO and FTR results for isotactic PMA in nitrogen.....	160
5-47	FTO and FTR results for syndiotactic PMA in nitrogen.....	162
5-48	FTR spectra of the polymer reaction at the indicated temperatures during synthesis of isotactic PMA/CO mixtures in nitrogen.....	163
5-49	FTR spectra of the polymer reaction at the indicated temperatures during synthesis of syndiotactic PMA/CO mixtures in nitrogen.....	164
5-50	FTR results for (4) Al_2O_3 /PMA mixtures and (8) Al_2O_3 /PMA mixtures in air and nitrogen.....	167
5-51	FTR results for (4) Al_2O_3 /PMA mixtures and (8) Al_2O_3 /PMA mixtures in diffuse air and flowing air.....	168
5-52	FTR results for Al_2O_3 /PMA mixtures with different sample size in (4) air and (8) nitrogen synthesis.....	170
5-53	FTR results for Al_2O_3 /PMA mixtures with different sample size in (4) air and (8) nitrogen synthesis.....	172
5-54	FTR results for (4) Al_2O_3 /PMA mixtures and (8) Al_2O_3 /PMA mixtures in air at the indicated reaction rate.....	174
5-55	FTR results for is-zeolined PMA and PMA films cast from chloroform and acetone in air.....	175
5-56	FTR results for PMA films cast from different solvents.....	176
5-57	FTR results showing the effects of expansion, contraction and oxidation procedures on PMA weight loss in nitrogen.....	177
5-58	FTO and FTR results for PMA/CO.3 and PMA/CO_2 mixtures in nitrogen.....	178
5-59	FTO and FTR results for PMA/CO.3 and PMA/CO_2 mixtures in nitrogen.....	180
5-60	FTR results of the polymer reaction at the indicated temperatures during the synthesis of PMA/ $\text{Pn(COOCH}_3)_2$ mixtures in nitrogen.....	182
5-1	Definitive spectra of (4) poly(methacrylate) and (8) PMA, and (4) film reaction after heating at 200°C.....	188

6.2	Weight loss curves of (a) standards and (b) poly(methyl methacrylate) (PMMA) between 100°C and 200°C.....	188
6.3	FTIR spectra and spectra of various poly(methacrylate) solid samples: (a) Sublimated PMMA samples; (b) PMMA heated at 200°C for 1 h; (c) PMMA heated at 200°C for 2 h; (d) PMMA heated at 400°C for 30 min; (e) PMMA heated at 200°C for 1 h. (F), (G), (H), (I), and (J) are the corresponding spectra obtained with the compressed carbon collection system.....	190
6.4	The residue for PMMA in air and nitrogen.....	193
6.5	FTIR spectra of the polymer residue at the indicated temperatures during synthesis of PMMA in air.....	194
6.6	Relative peak intensities (from the FTIR spectra) as a function of temperature during the synthesis of PMMA in air.....	195
6.7	FTIR spectra of the polymer residue at the indicated temperatures during synthesis of PMMA in nitrogen.....	196
6.8	Relative peak intensities (from the FTIR spectra) as a function of temperature during the synthesis of PMMA in nitrogen.....	197
6.9	The thermograms of PMMA residues collected in air from 10°C to 200°C.....	198
6.10	The FTIR spectra of the primary volatile product as compared to the reference spectrum for water.....	201
6.11	The thermograms of PMMA residues collected in nitrogen from 10°C to 200°C.....	203
6.12	The FTIR spectrum of the primary volatile product as compared to the reference spectrum for water.....	204
6.13	FTIR and TGA results for PMMA in air.....	205
6.14	FTIR and TGA results for PMMA in nitrogen.....	207
6.15	The FTIR spectrum of peak A in the gas chromatogram as compared to the reference spectrum for methacrylic acid anhydride.....	208
6.16	Plot of the detectable percentage of the PMMA residue vs. heat treatment time at 200°C and 250°C in air.....	211

5.77	Flask of the insoluble percentage of the PMA residue vs. heat treatment time at 400°C and 450°C in nitrogen.....	217
5.78	Flask of the insoluble percentage of the PMA residue vs. heat treatment time at 300°C in air and nitrogen.....	218
5.79	Gas chromatogram of PMA volatiles collected in air from 300°C to 400°C.....	219
5.80	Gas chromatogram of PMA volatiles collected in nitrogen from 300°C to 400°C.....	221
5.81	IR results for $\text{Al}_2\text{O}_3/\text{PMA}$ mixture in air and nitrogen.....	222
5.82	Gas chromatogram of $\text{Al}_2\text{O}_3/\text{PMA}$ volatiles collected in air from 300°C to 450°C.....	223
5.83	Gas chromatogram of $\text{Al}_2\text{O}_3/\text{PMA}$ volatiles collected in nitrogen from 300°C to 400°C.....	225
5.84	Gas chromatogram of $\text{Al}_2\text{O}_3/\text{PMA}$ volatiles collected in air from 400°C to 450°C.....	226
5.85	Gas chromatogram of $\text{Al}_2\text{O}_3/\text{PMA}$ volatiles collected in nitrogen from 400°C to 450°C.....	227
5.86	FTIR spectra of the polymer residue at the indicated temperatures during synthesis of $\text{Al}_2\text{O}_3/\text{PMA}$ mixture in air.....	228
5.87	FTIR spectra of the polymer residue at the indicated temperatures during synthesis of $\text{Al}_2\text{O}_3/\text{PMA}$ mixture in nitrogen.....	229
5.88	Relative peak intensities (from the FTIR spectra) as a function of temperature during synthesis of $\text{Al}_2\text{O}_3/\text{PMA}$ mixture in air. Intensity of Al_2O_3 and heat at 140, while Al_2O_3 at 1000° for 24 h was used as 100.....	230
5.89	FTIR spectra of the polymer residue at the indicated temperatures during synthesis of reduced $\text{Al}_2\text{O}_3/\text{PMA}$ mixture in air.....	232
5.90	FTIR results showing 140 spectra of the polymer residue at the indicated temperatures, and (b) relative peak intensities as a function of temperature during synthesis of PMA/PMA mixture in air.....	233

3-34	FTIR results showing (a) spectra of the polymer residues at the indicated temperatures, and (b) relative peak intensities as a function of temperature during pyrolysis of PMAA/PMR mixtures in nitrogen.....	261
3-35	FTIR spectra of the polymer at the indicated temperatures during pyrolysis of isolated Si_3H_7 /PMAA mixture in air.....	262
3-37	Relative peak intensities (from the FTIR spectra) as a function of temperature during pyrolysis of isolated Si_3H_7 /PMAA mixture in air.....	264
3-39	IR results for PMAA and Si_3H_7 /PMAA mixtures in air.....	265
3-40	FTIR results showing the effects of silver acetate and potassium permanganate on PMAA weight loss in air.....	266
3-41	FTIR results showing the effects of potassium permanganate on PMAA pyrolysis behavior in air.....	267
3-42	FTIR results showing the effects of silver acetate on PMAA pyrolysis behavior in air.....	268
3-43	IR results showing the effects of nickel acetate on PMAA weight loss in air.....	269
3-45	FTIR results showing the effects of 0.1% addition of nickel acetate on PMAA pyrolysis behavior in air.....	270
3-46	FTIR results showing the effects of 0.1% addition of nickel acetate on PMAA pyrolysis behavior in air.....	271
4-1	Liquid chromatograms of PMAA-8.....	283
4-2	Liquid chromatograms of PMAA-10.....	283
4-3	Liquid chromatograms of PMAA-41.....	283
5-1	^{13}C NMR spectrum of PMAA-8.....	285
5-2	^{13}C NMR spectrum of PMAA-10.....	287
5-3	^{13}C NMR spectrum of PMAA-41.....	288
5-4	Absorption techniques for PMAA/light absorption prepared with 40-50% 104-PMAA.....	289

Abstract of Dissertation Presented to the Graduate School
of the University of Florida in Partial Fulfillment of the
Requirements for the Degree of Doctor of Philosophy

PHYSICAL CHEMISTRY OF POLYMER DEGRADATION

BY

DAVID LEE

January, 1968

Chairman: Dr. Richard W. Stone

Co-Chairman: Dr. Jerry W. Williams

Major Department: Molecular Science and Engineering

The pyrolytic behavior of a vinyl polymer (i.e., polyvinyl
toluene) and two acrylic polymers (i.e., polymethyl methacrylate and
polydimethylsiloxane) was investigated. Degradation studies were
carried out for polymers alone and for copolymer/polymer mixtures by
heating both residues and volatiles. Information concerning the
degradation mechanism was obtained using a variety of techniques,
including mass spectrometry (MS), differential thermal
analysis (DTA), Fourier transform infrared spectroscopy (FTIR), and
gas chromatography (GC). Detailed pyrolysis was carried out using a
unique technique, i.e., by combining the FID system with a hot
stage to provide information into the chemical changes of polymer as a
function of temperature. The final carbon residue concentrations
found were analyzed.

Results show that early stage pyrolysis of polyvinyl toluene,
PMT, involves ring group elimination, with chain scission,

crosslinking, and oxidation. Degradation is mainly dependent on the pyrolytic atmosphere. Pyrolysis is initially accelerated in air due to oxidative reactions. However, a larger weight loss was observed in nitrogen at intermediate temperatures due to slower development of degraded groups and less rapid development of crosslinked structures. Intermediate degradation in the absence of oxygen is extremely difficult due to uncertainties.

Depolymerization reactions of polyacryloyl methacrylates, PMA, was monitored by TGA, MS, FTIR and GC results. The reaction was accelerated by the presence of oxygen. Results also showed that higher molecular weight PMA resins were more stable than the lower ones due to the presence of a greater number of weak chain linkages.

Degradation of polyacrylamide acid, PMAA, occurred in three stages. The first stage was dominated by a depolymerization reaction between the neighboring carboxyl groups which formed a polyacrylate structure. This structure breaks down during the second stage, but crosslinking and oxidation especially occur during the process. These degradation reactions occur and crosslinked structures can be broken down relatively at higher temperatures in air conditions. In contrast, there is a large amount of residue at high temperatures in nitrogen pyrolysis.

Comparisons of the degradation behavior between "pure" polymer and monomer/polymer mixtures indicated that a surface reaction, i.e. formation of carboxylic anhydride, between acrylic polymer chain groups and Al_2O_3 takes place at higher temperatures. No chemical reaction was

observed between PVE and $M_n \bar{M}_w$. This reaction complicates the degradation behavior of the acrylic polymers, and such higher temperatures are required to achieve complete conversion. This surface interaction appears stronger with dehydrochlorinated metal oxides and highly acidic oxides. No reaction was observed when the oxides had a more neutral character. A reaction mechanism was proposed to describe this high-temperature interaction.

Finally, the effects of important processing variables on wall as strategies for controlling the degradation reactions are discussed.

CHAPTER I INTRODUCTION

Oxygen polymers are important additives in many polymer processing operations, such as dry pressing, tape casting, film casting, extrusion, injection molding, etc. They are generally used as stabilizers, free-radical, and chelating modifiers. In some instances, they may serve some other functions as summarized in Table I-1. Although oxygen polymers are also used to fulfill the various functions listed, however, the role of polymer additives in thermal protection is temporary; polymers must be removed completely prior to charring of the ceramic. Incomplete "burnout" of the polymer can adversely affect the subsequent oxidation behavior, e.g., retard the oxidation rate and lower the final density achieved. In some extreme cases, blocking and cracking of the ceramic may occur. In addition, impurities can cause any form undesirable effects on the physical properties of the ceramic. In order to optimize the charring removal process, it is important to develop a thorough understanding of the polymer thermal degradation mechanism. A variety of degradation phenomena can occur during polymer pyrolysis, including decomposition, side chain scission, side group elimination, cyclization, cross linking, etc.

The overall objectives of this study are to gain an improved understanding of the polymer degradation mechanism and factors affecting major product species in selected ceramic/polymer systems;

Table 1.1 Functions of Certain Processing Additives

additive	function
Binder	Providing green strength
Plasticizer	Reducing britt, improving fluidity and flexibility of ceramic/binder mixture
Lubricant	Mold release, interparticle sliding
Suspensant	Particle surface charge control, pH control, anti-coagulation agent
Flocculating agent	Rheological property control of particle/liquid and particle/particle systems
Wetting agent	Altering surface tension of liquid
Water retention agent	Preventing spontaneous of water during pressure application
Chelating or sequestering agent	Sequestering undesirable ions

This study focuses on materials of interest in forming oscillatory ceramic substrates used in micro-electronics packaging. The polymers under investigation include vinyl and acrylic polymers, i.e., poly(vinyl butyral) (PVB), poly(methyl methacrylate) (PMMA), and poly(methyl methacrylate) (PMMA). The ceramic used in this study was mainly Al_2O_3 .

Poly(vinyl butyral) resins are commonly used in large coating operations for forming ceramic substrates. Although there have been numerous studies concerning thermal degradation of vinyl polymers, relatively few studies have been reported for PVB. Investigations which directly compare the degradation behavior of PVB in oxidizing and nonoxidizing atmospheres are particularly limited. Furthermore, studies concerning the pyrolytic behavior of PVB in the presence of ceramic particles are lacking.

Acrylic polymers are used in a variety of ceramic forming operations. Some acrylics, such as PMMA, are known to thermally degrade by depolymerization (i.e., "backbiting"). This mechanism may be advantageous in producing ceramics since pyrolysis of the pure polymer (i.e., with no ceramic present) tends to be completed at relatively low temperatures in both oxidizing and nonoxidizing atmospheres. Although pyrolysis of the pure polymers has been well studied, there is not much information on their degradation behavior in the presence of ceramic.

The research approach used in this study consists of the following two main components:

- (1) development of a mechanistic understanding of the degradation behavior of the "pure" polymer and
- (2) development of a mechanistic understanding of the degradation behavior of polymer/ceramic mixtures.

A variety of techniques, including thermal gravimetric analysis (TGA), differential thermal analysis (DTA), Fourier transform infrared spectroscopy (FTIR), and gas chromatography (GC), were used to provide insight into the thermal degradation reactions of polymer/ceramic mixtures, as well as the pure polymer.

The review of kinetic characterization and mechanistic aspects of polymer pyrolysis is given in Chapter II. The experimental techniques used for kinetic and volatile analysis are described in Chapter III. The pyrolysis behaviors of PBO, PBA, and PBAI systems are described in Chapters IV, V, and VI, respectively. Each chapter contains three parts, i.e., literature review, materials and methods, and results and discussion. It should be noted, however, that the major research focus is on Chapters V and VI. Finally, summary and conclusions are given in Chapter VII.

CHAPTER 11 BINDERES

Binder Classification

Binders are essential for the processing of many commercial ceramics. Their major function is to bind ceramic powders together before sintering and to provide the green strength needed to form the ceramic into shapes. In the modern ceramic industry, many binders have been introduced to fulfill the demand of automated mass production at high speed. These binders are often designed to enhance compaction and application.

Generally speaking, binders can be divided into two categories, i.e., clay binders and nonclay binders, as shown in Figure 3.1 [1].

Clay binders Since ancient times, clay has been used for making pottery, but bricks and earthenware, etc., due to its dimensional behavior in combination with water, clay powder takes any desired shape, which after a lapse of time acquires some rigidity and strength. According to Williamson [2], strength of dried clay is due to bonding between platelets of clay which have high surface area. Its binding property is dependent upon its mineralogy (e.g., whether it is montmorillonite or kaolinitic/etc.). The nonclay-based clay binder, however, is found to be inadequate for many applications, particularly when material other than clay is used for ceramic fabrication.

This has resulted in development of various new blends out of natural and synthetic materials.

Blending Blends- These blends can be classified as following according to their application.

a. Decorative Blends- These blends belong to the inorganic group of materials which develop tools due to a change in their optical structure. These blends retain their good bonding characteristics even after subsequent processing and firing. They are now finding increasing use in the refractory industry where usually ceramics such as silicon, alumina, silicon carbide, etc., are used.

b. Temporary Blends- These are all organic compounds, either natural or synthetic. The binding property of these organic materials can be attributed to their high molecular weights and/or the interactions between their polar groups and active sites on the ceramic surface. For example, polyacrylic, polypropylene, styrene-butadiene copolymer, methylmethacrylate monomer copolymer, etc., have been used as binders for injection-molded silicon-based ceramics [2-6]. Harris and Associates (7) have successfully injection-molded silicon using polyimide binders. They found that this binder system provides for easy and defect-free burning. De Gennaro Research workers [8] used color-stable anthracene-based pigments as binders for extraction of silicon. They reported that the thermal oxidation characteristics of the anthracene-based polymers imparted high green strength to ceramic films [9] and also eliminated binder degradation during drying [10,11]. It should be noted, however, they also reported that the color-stable pigments used may suffer loss of strength in high

Notably, acrylonitrile [17] and styrene copolymers of some styrene monomers at high temperatures [18]. Thermosetting plastics such as epoxy resins or phenolic resins have often been used as major binders [19,21] for silicon nitride powders. The major advantages for these materials include reduced thermal deformation of the mixed mass during polymer removal [14] and the production of strong bodies in the sintered condition [22]. Rogers [23] reported the use of poly(vinyl acetate), poly(methyl methacrylate), and poly(vinyl alcohol) binders for processing multilayer ceramic capacitors (e.g., BaTiO_3 and TiO_2) by tape casting and doctor blade process. Poly(vinyl acetate) (PVA), due to its high strength and molding ability, is another popular binder for manufacturing ceramic articles for use in electronic devices by tape casting operation. A formulation for this process is listed in Recipe 2-3.

Binder Properties

The role of organic binders in ceramic processing is quite multifaceted. Generally speaking, a good binder has the following properties:

1. Is free of carbonaceous residues after firing;
2. provides adequate strength;
3. contributes to dimensional;
4. is stable during storage;
5. is soluble in suitable solvents;
6. is inexpensive; and
7. is available.

Nevertheless, the most important binder selection factors among them are good molding, drying, and degreasing properties.

Table 2.1 Batch Formulation For Tape Casting

Amount (g/g)	Material	Function	Parts by Weight
5(1) for 20 sheets (10mm stage)	Aluminum powder	Substrate material	100.0
	Nigrosin black	Grain growth inhibitor	0.05
	Isobutyl zinc salt ¹	Surface-treated	1.7
	Diethylenetriamine	Solvent	20.0
	DMF + alcohol	Solvent	70.0
Add to above and fill for 20 sheets (5mm stage)	Poly(vinyl acetate) ²	Binder	1.0
	Poly(methylmethacrylate)	Flattener	0.1
	Other plasticizer	Flattener	3.4

Adapted from [14].

1. Synite Type D-3 Zinc isobutyl, Johns E. Young Company, New York, New York.

2. Type D-66 Molecular weight approximately 10,000, Monsanto Company, St. Louis, Missouri.

Sliders tend to stick together before starting and provide the green strength needed to form the various thin shapes. The green strength depends on the amount and the distribution of sliders in the green body. Davis (12) presented a theoretical study of some characteristics of organometallic intermediates that strengthen bodies. He indicated that there exist three classes of slider distribution in green compacts: (1) a random slider, (2) a whisker (pendular) slider, and (3) a coated slider. The random slider, intermediate between whiskering and total coating stages, produces the highest green strength. He concluded that the important properties in creating high green strength include the amount of sliders, the strength of the slider, and the packing density of the particles.

In a patent, Bailey (13) stated that the binder concentration in injection molding process should be at least 2 vol in terms of the mold volume. Barry and Johnson (14) studied spray-dried agglomerates pressed at various pressures to form compacts. They found that there exists an upper limit on binder concentration for maximum green strength at a given forming pressure. Matsuda (15) applied a technique used extensively in the plating industry to provide a quantitative assessment of the critical powder volume concentration in the plating form of nitrocellulose.

However, in most cases of ceramic processing, except injection molding and compression molding, it is common in practice to find that the amount of binder used corresponds to the ratio of binder volume to particle volume of between 0.08 to 0.15. This quantity is

approximately the minimum amount that could be added without filling up the pore spaces in the body which would be detrimental to burning (26).

The firing properties are very much dependent on the rheological characteristics of the binder solution which includes viscosity, rheopneumatism and gelation. Owen (11) mentioned that the viscosity imparted by binders is one of the primary considerations in the selection of a binder for a specific process. On the other hand, the pumpability of a binder can prevent rapid penetration from setting out of solution and yet still supply enough fluidity for the firing process. Finally, the advantage of a gelated structure is to prevent the binder from migrating to the drying surface.

Removal of water from the green body is one of the most critical steps in the firing process. Capillary action, evaporation, and external suction have been used to remove the organic binders. However, they are relatively time-consuming and only applied for low molecular weight binders, such as oils and paraffin waxes. The most widely used method to remove binders is by thermal degradation (i.e., burning). Binder removal is reviewed in the next section.

Binder Burning

Binder removal is a time-consuming and expensive process in ceramic processing. A significant fraction of the microstructural defects (i.e., shrinkage) are caused by the (excessive) binder removal during the initial period of the firing schedule. Presently, detailed information on the thermal removal of organic binders is not readily

available in the open literature. Usually the heating schedule (i.e., heating rate, temperature, and time) during the burning period is dependent on trial and error for each system. In some cases, this process may even comprise up to 40 percent of the entire firing schedule (17). Thus, a thorough understanding of the binder decomposition mechanism and a detailed study of the effect of processing variables are very important in optimizing the burning schedule.

Burnout is affected by the microscopic geometry of the polymerizable materials. For example, the microscopic distribution of polymer and powder determine the homogeneity, porosity, permeability, and packing density of the green body. Upon heating, these variations affect the transformation of polymers to low molecular-weight solids, liquids, or gases, and thus influence the formation of paths for liquid or gas transport. However, because these variations change during heating, the total process is even more complicated.

Gas transport plays an important role in the burning process. During burnout, there exists a counter-diffusion of gases. There is an inward diffusion of oxygen (if burnout is carried out in O_2 or air) and an outward diffusion of product gas. An increase of the outward gas diffusion can increase the burning rate and prevent surface oxidation.

Wells and Goetsch (18) studied the oxidation of carbonaceous deposits within porous catalytic particles. They found that at low

described the oxidation process presented throughout the particles homogeneously (Figure 8-1), which meant that the chemical reaction was the rate limiting factor. (Reaction stages of burnout are represented by a series of arrows indicating increasing time.) At a sufficiently high temperature, the process was found to proceed from the outside of the particle to the inside with a sharp interface between the burnout and unburnout zones. In this case, the rate of combustion is controlled primarily by oxygen diffusion through the reacted portion of the sphere. At an intermediate temperature, a transition state existed where the chemical reaction competes with diffusion. They also indicated that the characteristic time for total burnout is fully determined by initial carbon content, thickness of the body, gas diffusivity, and oxygen partial pressure.

Seifert [9] studied the burnout of carbonaceous reaction from a porous body. Equations for the burnout time were derived based on the following mass transport steps:

- (1) transport of oxygen from the bulk gas to the spherical surface of the body and reverse transport of product gases,
 - (2) diffusion of oxygen into the porous body and reverse diffusion of reaction products, and
 - (3) chemical reaction between the carbonaceous residue and oxygen.
- The results are qualitatively in agreement with the findings of Wise and Goshalski.

The stoichiometry is also an important factor affecting burner burnout. If denitrogenation occurs before burnout is complete, the pure

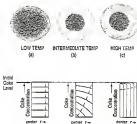


Figure 8.2 Apparatus after partial burnout (below), and coke concentration vs. distance from center (in beds) for successive stages of burnout (above). For three temperature regions. (Adapted from [28].)

structures, which similarly also are disrupted, begin to close and limit the oxygen supply, the reaction may only partially decompose. In some cases, high pressures may build up from swelling trapped within pores and pathways, which can lead to cracking or blistering [30].

Carbonaceous residues are especially undesirable for electronic ceramics. For example, in determining multilayer substrates (Figure 8.3), residual carbon may be fired either at low temperatures or in a reducing atmosphere to avoid oxidation of the metal (e.g., copper, silver, and nickel). Under these various conditions, incomplete removal of carbonaceous materials from the binder component tends to occur. Iremonger and Flinnell [16] reported that black ceramic bodies were obtained after the sintering and deoxidation heating cycle was completed. The carbon remaining in the ceramic formed numerous pores, which resulted in poor electrical and dielectric properties. However, by adding pyrolytic materials (such as silicon and polycarbonyl resin), into the binder system, they could produce ceramic bodies substantially free from carbonaceous residues. Tseng [13] and Tseng [18] studied the effect of low-temperature-oxidation-energy materials on the thermal stability of polymers. It was found that addition of substances with low activation energies for decomposition can significantly lower the decomposition temperature and reduce the amount of residue of the polymer, and the decomposition rate of polymer was highly dependent upon the concentration of the oxidant. Tseng further pointed out that the more effective



Figure 8-3 Flow diagram of the test matching process for sludge substrates.

additives but inhibitors in the melting region of polymers. However, whether these energetic additives still work in the presence of ceramic oxide further investigation.

Another important factor affecting fiber formed behavior is the nature of the polymer/ceramic interface. Organic materials may undergo oxidative reactions at the ceramic surface. The type and rate of these reactions would depend on the polymer functional group attached to the ceramic surface, and on the characteristics of the metal oxide surface [16,19,21].

These catalytic reactions include isomerization (movement of the carbon double bond along the chain) [34], dehydrogenation (removal of hydrogen from the polymer chain); formation of carbon-carbon bonds (directly or indirectly using boronides) [37]; catalytic cracking (hydrocracking); formation of small hydrocarbons from the polymer chain); polymerization [38]; hydrogenation (formation of acetone and carbon monoxide) [39]; hydrogenation (adding hydrogen to unsaturated hydrocarbons); thermal cracking (cracking without); hydroformylation (partial oxidation) [40]; free radical reactions [41]; and oxidation [42].

The types and rates of the catalytic reactions occurring at the organic/ceramic interfaces affect carbon formation. Gas flows on the metal surface due to carbon adsorption/desorption, carbon ring formation, and polymerization reactions. To avoid carbon formation, the dehydrogenation, polymerization, and aromatization reactions should be "poisoned," and the oxidation and hydrogenation reactions be

enhance. Brownell [17] reported that oxides with acidic behavior oxygen are enhance polymer oxidation reaction, while oxides with highly bonded oxygen (e.g., Al_2O_3 , Ag_2O , and SnO_2) enhance dehydrogenation reaction.

Thermal Degradation of Polymer Polyimide

Thermal Degradation of Polymer

Organic polymers consisting essentially of carbon, hydrogen, oxygen, and nitrogen are composed of macromolecules which are joined by chemical bonds to each other. In general, organic polymers degrade at considerably lower temperatures than most ceramics and metallic materials. At elevated temperatures, the chemical bonds in the polymer backbone and the side groups may be ruptured and form lower molecular weight polymer fragments. Under certain conditions, these fragments may not be stabilized without further extensive chain rupture. In addition to the changes of molecular weight and molecular weight distribution, thermal degradation reactions generally involve complex chemical processes which completely changes the structure of the polymer.

Generally speaking, thermal degradation reactions can be divided into several subcategories [18-20], namely:

- (1) random main chain scission,
- (2) side group elimination,
- (3) depolymerization,
- (4) carbonization (dehydrogenation, cyclization), and
- (5) crosslinking.

A schematic depiction of the degradation reactions is shown in Figure 2.4 [47]. Although these two types of degradation processes seldom take place separately, some understanding may be gained by studying the degree of polymerization vs. monomer feed ratios shown in Figure 2.3 [48].

3. Random main chain scission

Random main chain scission is the breaking of the main chain to produce smaller molecules of old chain. The molecular weight of the residual polymer falls rapidly from the start. Little soluble material is produced until late in the reaction. This reaction can be represented by pathway B in Figure 2.2.

4. Side group elimination

Elimination reaction of the type



has been observed in some polymers derived from vinyl monomers, e.g., the elimination of hydrogen chloride from poly(vinyl chloride) or acetic acid from poly(vinyl acetate). The elimination reaction can be rationalized as the unsaturated species formed attacks the adjacent group:



Figure 3-4 Thermal degradation reactions of polymers. (Adapted from COTS.)



Figure 3.3 Degree of polymerization vs. monomer yield in a degrading polymer. $P_n(1)$ is the number average degree of polymerization of the residual polymer. (Adapted from [16].)

3. Depolymerization

Depolymerization ("unzipping") reaction is a process in which monomer units are released from the polymer chain ends. Such a process can be viewed as the reverse of the propagation step in addition polymerization. In the final case, monomer is the only product. Polymers derived from 1,1-disubstituted alkenes sometimes are often susceptible to this type of degradation (48); a typical example is poly(methyl methacrylate). Figure 8 in Figure 8.5 is characteristic for depolymerization with $\alpha \approx 1$. As soon unzipping is initiated, the whole macromolecule depolymerizes at the average chain length \bar{L}_0 (i.e., the average number of monomer molecules formed between initiation and termination) is greater than the degree of polymerization (\bar{L}_0). Figure 9 is typical for depolymerization with $\alpha < 1$.

4. Cyclization

This reaction is known to define a key kinetic competition, polymer formation, and decomposition by depolymerization. There is usually some random scission occurring concurrently.

5. Crystallization

Crystallizing reaction can be represented by primary R_1 , which results in the formation of three-dimensional "gel-like" cross molecules.

A diagram of the most probable reactions involved in the thermal degradation of polymer is given below:



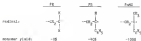
It is important to realize that the chemical structure of the polymer affects the degradation reaction greatly [26]. For example, a comparison of the monomer units in the degradation of PEEK and Polyimides revealed Oved notes that aceto ketone groups in the aromatic group in PEEK stabilizes the free radical. Thus, PEEK undergoes more facile depolymerization [26].



The free radicals are also stabilized by resonance stabilization as in polystyrene (PS) [30]:

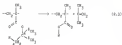


These two stabilizing effects can work together as shown in the degradation of monomer units of polystyrene (PS), PE, and poly(methyl styrene) (PmSt) [34]:



Another example to illustrate the importance of chemical structure in the degradation reaction is given by poly(methyl methacrylate). Although, as described earlier, poly(methyl methacrylate) degrades thermally in a radical process to give quantitative yields of monomer, in higher polystyrenes decomposition of the ester group may occur. This ester decomposition

reaction may result in formation of anisomeric acid anion by the polymer and the evolution of the corresponding oxoan (VI). For example, in the case of poly(hydroxyethyl methacrylate),



(where α and β represent the location of carbon atoms of the ester group), the reaction proceeds by a molecular mechanism involving interactions between the carbonyl group and hydrogen atoms on the α carbon atom of the ester group (12). The importance of β hydrogen atoms in facilitating ester decomposition at the expense of depolymerization is illustrated in Table 4-2. Ester decomposition only becomes important when the monomer will incorporate at least five hydrogen atoms on the α carbon, and depolymerization is quantitative when there are at least six or ten β hydrogen atoms.

From the kinetic point of view, random chain scission and depolymerization, under a combination of mass, can be expected by the free radical chain reaction mechanism, i. e., a chain reacting with

Table 2.2. Reduction of thermal degradation of poly(alkyl methacrylates). Numbers indicate the number of hydrogen atoms on the pendant group.

Isopropyl acrylates		Methyl methacrylates		Other methacrylates	
isobutyl	0	ethyl	2	iso-propyl	4
sec-pentyl	0	isopropyl	2	sec-butyl	6
tert-butyl	0	tert-butyl	2	tert-butyl	6
2-ethylhexyl	2	tert-butyl	2		
		tert-butyl	2		
		tert-butyl	2		

reduced from (18).

Free radical intermediates. The four essential reactions are:

1. Initiation

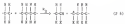


2. Propagation



3. Chain transfer, followed by re-initiation

a. Inter-molecular



b. Termination by disproportionation



c. Termination by disproportionation



where k_1 , k_{t1} , k_2 and k_d are rate constants.

The free radical species are formed by the initiation process. The radicals bring about further extension of the polymer chain by a chain reaction represented by the propagation and chain transfer steps, and the chain is ended as the radicals are removed by the termination reaction.

The initiation process can occur either at random points along the main chain or at some lines resulting from monomer structure [23-26] such as

- (a) chain ends free initiator radicals or unsaturated end groups,
- (b) branches or side groups,
- (c) moieties substituted with suitable side groups.

(4) separated structures, and

(4) head-to-head diads.

These "separated" structures are separated interspersed during polymerization process, such as residual monomer and peroxide catalyst, may not be suitable for the initiation of degradation process.

The activation energy for the degradation reaction can be estimated as the sum of the heat of polymerization and the activation energy for propagation in polymerization with the assumption that in radical polymerization the termination reaction occurs with near zero activation energy [31]. The lower the heat of polymerization (and) i.e. the smaller $|\Delta H_p|$, the lower the activation energy of degradation, thus the higher the probability of depolymerization.

For chain transfer step, the activation energy varies with the type of hydrogen which is abstracted and in the level for tertiary, allylic, and benzylic hydrogens [32,33-35].



respectively. It has been shown [36,37] that the free radical can abstract the hydrogen at consecutive distances (e.g. five carbon atoms from the free radical) from the carbon chain before the intermediate

ultrapure β -cellulose to give the final viscose product. This is often called a "wash-mung" reaction. It is also reported to realize that intramolecular transfer allows a way of producing molecules in the lower and lower size range much earlier and in much greater proportions than would be expected from random scission alone.

Termination can be achieved by a bimolecular disproportionation reaction. This is additionally accounted and is the most probable mechanism at the high temperature limit. However, it should be noted that the rate of all these reactions are affected to an ascertainable degree by the hindrance or action due to surrounding molecules. Thus a molecule dissolves, the surrounding molecules can keep the fragments in one another's proximity for up to a hundred collisions, with opportunity to recombine, before they escape. This "cage effect" [42,43] could be even more important in a highly viscous primer melt than in less viscous liquids. Thus the termination rate constant, k_{tp} , may be much smaller for large polymeric radicals than for small ones.

Solution Degradation of Polymers

Although polymers degrade at high temperatures in the absence of oxygen, degradation is always always faster in an oxidizing atmosphere and is strictly auto-catalyzing [44] (Figure 3.6). The exposure of a polymer to oxygen is characterized by an induction period during which the polymer does not show any obvious changes and there is little oxygen absorption as shown in Figure 3.7 [45]. This period is

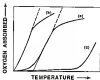


Figure 2.2 Oxygen absorption curves for various polymers: (a) pure polymer, (b) polymer with added hydroperoxide; (c) polymer with added antioxidant. (Adapted from [20].)

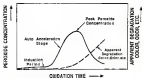


Figure 3-7 Schematic diagram of oxidation reactions with peroxide development and decay with noticeable color and odor (adapted from [44].)

overlappings important in the process of initiation, "benzene rings" amounts of hydroperoxides are formed which can initiate the subsequent rapid auto-oxidation reaction. In some cases, when the polymer contains trace amounts of peroxide impurities or catalyst, the initiation period is not observed at all and the oxidation process begins immediately (Figure 2.8). During the reaction, various low molecular weight products are evolved and groups containing oxygen atoms (e.g. hydroxyl, carbonyl, and aldehyde) are formed along the polymer chain or at its ends. Formation of a cross-linked structure may also be observed.

The primary reaction steps of the free radical oxidation reaction are initiation, propagation, and termination reactions. In reaction the parent compound, the R being the most labile hydrogen atom, R[•] is the radical formed by removal of the hydrogen atom, ROO[•] is the peroxy radical formed by the addition of oxygen to R[•] and ROOH is the corresponding hydroperoxide.

1. THE INITIATION REACTION



The formation of the mono-radical depends on the chemical structure of the polymer, or more precisely on the dissociation energies of particular bonds between the atoms forming the polymer. The initiation reaction may be induced by temperature, high energy radiation, catalysts, direct attack of oxygen or ozone, and ultraviolet light.

4. Dehydrohalogenation reactions



The propagation reaction involves formation of peroxo radicals and hydroperoxides. Since reaction (8.11) is a radical pairing process, it has a low activation energy and occurs with high frequency. The second step (8.12) on the other hand involves the breaking of a carbon-hydrogen bond and has a higher activation energy. In some circumstances the propagation rate constant, k_p , is a composite of the rate constants for several possible reactions of peroxo radicals. The hydroperoxide formation reaction is fairly sensitive to the substitution of the attacking radical and to polar and steric effects, and is also dependent on temperature (49-51). Free-radicals are relatively selective electrophilic species abstracting tertiary hydrogen in preference to secondary and primary ones. (Tertiary hydrogen have the lowest activation energy for chain transfer, i.e., they are the least stable hydrogen. In other words, tertiary free radicals are the most stable species compared to secondary and primary ones.)

Hydroperoxide can then decompose by reaction of the oxygen-oxygen bond:

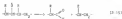


It is also clear that various transition metal ions, such as Cu^{2+} , Fe^{3+} , and manganese promote the decomposition of hydrogen peroxide by a redox mechanism (11).



and the catalytic activity of the metal ions increases with the increase of the oxidizing-reducing potential of the metal ion. These free radicals formed are very unstable and are subject to reaction for the initiation of further oxidation reaction. The alkoxy radicals may also undergo the following reaction to give aldehydes, ketones, and associated structures which are typically found in oxidized polymers (10-11):

(a) Formation of aldehydic groups through fragmentation process, e.g.



(b) Formation of ketonic groups, e.g.



1c) Formation of hydroxyl groups



1d) Formation of cross-links



3- The termination reaction

The termination of the chain is due to reactions of free radicals with each other; in which reactive products are formed:



Since usually reaction (2.19) is rate determining, peroxyl radicals are the dominant radical species present in autooxidation and termination occurs primarily through reaction (2.20). If, however, oxygen access is limited by diffusion, reactions (2.19) and (2.21) may play a more important role [74].

The kinetic consequence of the relative efficiencies of reactions (2.21) and (2.12) is that at ambient pressures, the rate of oxidation

is given by equation 3.10 (74),

$$-\frac{d[X_2]}{dt} = k_2 k_3 \frac{1}{k_1} \frac{[X_2]^{1/2} [X_1]^{1/2}}{[X_1]} \quad (3.11)$$

where k_1 is the rate of initiation. The rate of initiation is independent of oxygen pressure. However, at low oxygen pressure, equation 3.11 holds,

$$-\frac{d[X_2]}{dt} = k_2 k_3 \frac{1}{k_1} [X_1]^{1/2} [X_2]^{1/2} \quad (3.12)$$

and the initiation rate is dependent on the concentration of oxygen.

CHAPTER III EXPERIMENTAL TECHNIQUES

The experimental techniques used in this study to characterize the degradation reactions are described in this chapter. Selected sample preparation procedures and operation variations for each polymer are given in the following chapters.

Thermal Analysis

Thermal Gravimetric Analysis (TGA) and Differential Thermal Analysis (DTG)

Weight changes and heat effects (i.e., endothermic and exothermic reactions) were monitored during analysis by simultaneous thermal gravimetric analysis (TGA-differential thermal analysis (DTG)).¹ A block diagram of the TGA/DTG system is shown in Figure 3-1.

The TGA curves were obtained by simultaneously recording the weight of the sample and temperature. Two sizes of crucibles, 0.3 g. and 1 g., were used for polymers and ceramic/polymer mixtures, respectively. A blank buoyancy run was conducted under the exact same conditions as the sample runs in order to compensate for the buoyancy effect at different temperatures.

¹ Model 900, DuPont Co., Eden, Pa.

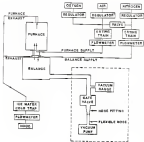


FIGURE 3.1 Block diagram of the SOLVOS system

The DTA curves were obtained by comparing the temperatures recorded by the two thermocouples (Pt/Pt-10Rh), each of which was inserted into the bottom end of the alumina crucibles holding the sample and reference materials. The size of the crucibles used was 0.2 in. and heavily sintered alumina was used as the reference material.

The heating rate was 5°C/min and the gas flow rate (air or nitrogen) was approximately 50 cc/min. All the samples were dried at 100°C under vacuum for 24 hours before testing.

Residue Analysis

Pyrolytic Residue Analysis (FTIR Spectroscopy)

The residual polymer was analyzed in several stages during pyrolysis. The polymer residues were analyzed in-situ using a FTIR spectrometer¹ equipped with a hot stage.

The schematic diagram of the FTIR system and the layout of the optical bench are shown in Figures 3.2 and 3.3. The spectrometer consists of a Glaser 24 source, the beam splitter, and liquid-nitrogen-cooled KBrTe (MTE-4) detector. A high temperature reaction chamber, coupled with a diffusion reflectance stage,² was used to obtain spectra under controlled atmosphere (air or nitrogen) and temperature conditions.

¹ Model 600, Nicolet, Madison, WI.

² Model 884-50A, Harrick Scientific, Ossining, NY.

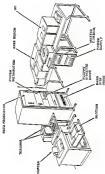


Figure 3-1 Assembly diagram of the P228 pistol.

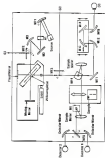


Figure 3-1 Schematic of the PTM applied bench

The diffuse reflectance stage, as shown schematically in Figure 1-4, has two 8.5 cm² elliptical mirrors. One of them focuses the incident beam on the sample, while the other one collects the diffusely reflected radiation off the sample. The radiation was collected at an elevated angle of 180° to minimize the intensity of specularly reflected light and thus to achieve high energy throughput.

The high temperature reaction chamber, as shown in Figure 1-5, supports the sample in a way located at the top of a temperature controlled pot. A water cooling jacket is provided to control the temperature of the outer chamber and station during very high temperature conditions. The temperature was controlled externally at a rate of 20°C/min from 30° to 1000°C. Spectra were collected every 10°C over the range 4000-700 cm⁻¹ for one minute (100 scans), with a 4 cm⁻¹ resolution.

The samples used include polycyclic aromatic (PAs) and diamond powder. The graphitic PA was finely ground and heated to remove adsorbed moisture before use. Diamond powder¹ was used as received.

Hot-stage FTIR spectra were also obtained for ceramic/polymer mixtures. In order to exclude the changes that occur in the polymer pyrolysis behavior due to the presence of the ceramic, the hot-stage spectra were collected for the ceramic by itself (using identical heating conditions) and these spectra were subtracted from the corresponding spectrum for the ceramic/polymer mixture.

¹ 30 PA grade, manufactured diamond powder, Eagle Co., Norton Green, UK.

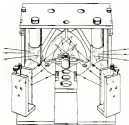


Figure 3-4. Diagram of the diffuser vane stage.

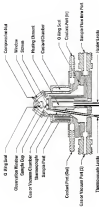


Figure 3-2. Cross-sectional view of the high temperature reaction chamber.

In most cases, relative peak intensities plots were constructed for major absorption peaks as a function of temperature. Relative peak intensity was calculated based on the ratio of the peak height of that particular peak to that of the carbonyl peak at 1700 μ .

Carbon Analyzer

In some cases, condensable gases after heat treatment under various conditions were collected for carbon fraction concentration measurements. The carbon fraction concentrations were obtained using a carbon analyzer by LECO Co.¹ A block diagram of the carbon analyzer is shown in Figure 1-4. The prepackaged samples were introduced in a fixed flow rate, purified oxygen stream at 4000-10000 cc. hourly, carried into various stages. The carbon fraction was monitored by an IR detector. Finally, a peak integrator was used to calculate the CO₂ peak area and then convert this value to the carbon concentration.

Thermal Analysis

Gas Chromatography (GC)

Small amounts formed during condensation were analyzed by gas chromatography (GC).² A vial/vial rack containing the sample was inserted into a sample tube which was heated in a LECO furnace. A

¹ Model D-204, LECO Co., St. Joseph, MO.

² Type Mass Spectral Library, Hewlett, Packard, Co.

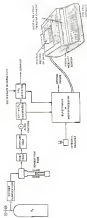


Figure 3.6 Block diagram of the screen analyzer.

flow diagram of the pyrolysis operation is shown in Figure 3.1. The volatile products formed during pyrolysis were collected in a liquid nitrogen cold trap. After the cold trap was removed, samples were injected into the GC in order to separate the volatile components. The GC has an on-column injection port and a 50 gauge methyl silicemicrotreated 30 x 0.25 mm capillary column. Helium (He) was used as the carrier gas.

The GC was interfaced with the infrared spectrometer (IR-DT10), as shown in Figure 3.2, in order to identify the volatiles. The species of the volatiles were taken in a registering mode when they passed through the GC-IR light pipe. The species were then compared with the NPL (U.S. Environmental Protection Agency) vapor phase library¹ by computer for identification. The GC was also equipped with a flame ionization detector (FID) and peak integrator² in order to determine volatile concentration.

¹ Vapor Phase Spectral Library, NIOSH, Madison, WI

² Model 3392A, Model 67000, Palo Alto, CA.

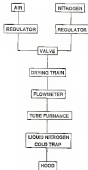


Figure S.7 Block diagram of the synthesis apparatus.

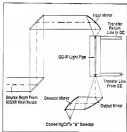


Figure 3-8 Diagram of the CO-PTC solution

CHAPTER IV
THERMAL DEGRADATION OF POLY(VINYL PYRROLIDONE)

Literature Review

Polystyrene, butyral resin are commonly used in tape casting operations for forming ceramic substrates. Although there have been numerous studies concerning thermal degradation of vinyl polymers, relatively few studies [71-75] have been reported for vinyl acetal polymers, such as poly(vinyl butyral) resins.

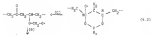
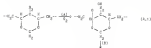
Goodell and co-workers [76] investigated the catalytic degradation of poly(vinyl formal (PVF). Studies of weight loss,



PVF

coloration, and infrared spectral changes were carried out using a series of poly(vinyl formal) having varying amounts of acetoxy and alcohol groups. It was found that, as the content of the acetoxy groups increased, the overall weight loss increased. However, with alcohol groups present, the weight losses tended to follow the same trend as those found for polymers containing the acetoxy group, but the total increases was less than that found for the acetoxy-containing

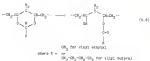
polymers. In general, it was observed that the higher the β -oxygen content, the lower the weight loss. On heating in air, the polyvinyl formate changes from colorless to yellow and finally to deep brown. It was noted that polymers with the greater amount of acetate groups colored more readily than those polymers containing the greater number of hydroxyl groups after 10 hr of heating. Infrared spectral examination indicated an increase in the hydroxyl and the carbonyl absorptions after prolonged heat treatment. At the same time, the carbon-hydrogen stretching bands and absorptions characteristic of the acetal group disappeared. A new absorption assigned to a carbon-carbon double bond appeared in the spectrum. Randall and co-workers interpreted the data in the following manner:





The process is free radical and primarily involves reaction at the formal group rather than at either the hydroxyl or carboxyl groups which are randomly distributed along the polymer chain. This mechanism appears to be quite reasonable and accounts for the ratio of groups and formal ring in the initial degradation. The product produced in step B is responsible for the change of the formal ring. Step C accounts for the increased carbonyl absorption observed in the infrared spectrum and for the presence of formaldehyde among the volatile degradation products.

In 1955, Kurekian and Jeynes [70] studied the infrared spectral changes accompanying the heat treatment of polyvinyl acetate and polyvinyl formal. Absorption in the spectrum attributed to carbon-oxygen, carbon-hydrogen, and hydroxyl functionalities decreased, whereas the carbonyl absorption increased significantly. These data were interpreted as the formation of esters of acetic and valeric acid.



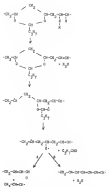


Figure 4-1 Degradation mechanism of copolymer of styrene (St) and methyl methacrylate. (Adapted from [81].)

Recently, investigations which directly compare the degradation behavior of PVB in acidifying and neutralizing atmospheres cannot be found in the literature. Furthermore, studies concerning the pyrolytic behavior of PVB in the presence of various solvents are lacking. Thus, the research objectives of this study are focused on these two aspects.

Materials and Methods

Materials

Polymer.— The polymer used in this study was a poly(vinyl butyral) resin,¹ PVB. This resin is a copolymer with butyral, residual hydroxyl and acetate groups attached to the carbon backbone at these sites,



According to the manufacturer, the residual butyral content, expressed as weight percentage of poly(vinyl butyral), is 40% and the residual hydroxyl content, expressed as weight percentage of poly(vinyl butyral), is 17.5-50%. The resin also contains a residual acetate content, expressed as weight percentage of poly(vinyl butyral), of 0-2.5%.

¹ Polysar-B, Monsanto Co., St. Louis, MO

Carbon. Carbon/polymer mixtures were prepared with a high purity (99.999%) Al_2O_3 having a defined Stokes diameter (determined by x-ray scattering¹) of 6-8 μ and a specific surface area (determined by nitrogen gas adsorption²) of 1.1 m^2/g .

Sample Preparation. Carbon/polymer mixtures were initially prepared as suspensions, using methanol as the solvent for the PVB resin. The suspensions, consisting of 1 vol% polymer, 35 vol% ceramic, and 64 vol% solvent, were made up by adding the ceramic powder to the polymer solution at one time. Cooled resins (c. 50 ml) suspensions were then forced pinch-rolled for 30 min to break down the coarse agglomerates followed by 15 min of ultrasonic treatment. Suspensions were cast onto water-cooled glass plates and the residual was allowed to evaporate at room temperature. The cast samples were ground to a powder in a mortar and subsequently dried at 100°C under vacuum for 24 h in order to remove any residual methanol. The final Al_2O_3 /PVB mixtures contain 1.1 vol% PVB.

Results

Thermal Analysis (TGA and DSC). The sample size was approximately 50 mg for pure polymer, and 175 mg and/or 5000 mg for

¹ BOD-980, Boynton Metal Co., Little Rock, AR

² Jet-Dry Particle Size Analyzer, Micromeritics Instrument Corp., Norcross, GA. The nitrogen Stokes diameter value was provided by R.K. Lee, Department of Materials Science and Engineering, University of Florida, Gainesville, FL.

³ Model 99-T, Thermogravimetric Corp., Swanton, VT. The specific surface area value was provided by R.K. Lee, Department of Materials Science and Engineering, University of Florida, Gainesville, FL.

$\text{Al}_2\text{O}_3/\text{FTB}$ mixtures. The heating rate was $5^\circ\text{C}/\text{min}$ and the gas flow rate (air or nitrogen) was approximately 40 cc/min.

Further treatment infrared (FTIR) spectroscopy The residual polymer was analyzed at various stages during pyrolysis using a Frontier Infrared Instrument (FTIR) spectrometer equipped with a hot stage. Potassium bromide (KBr) was used as diluent in this study.

For pure FTB samples, 50 μl of polymer solution (10 mg/ml solvent) was dried with 500 mg of diluent in a vial. After the solvent evaporated completely, the polymer-diluent mixture was transferred to the sample cup and was subsequently analyzed.

For $\text{Al}_2\text{O}_3/\text{FTB}$ mixtures, 10 μl of the mixture was dried with 500 μg of diluent in a vial before transfer to the sample cup.

The heating rate was $5^\circ\text{C}/\text{min}$ from 30-400°C. Spectra were collected every 30s under a controlled atmosphere (air or nitrogen) over the range 4000-500 cm^{-1} , with 4 cm^{-1} resolution.

Gas chromatography (GC) Volatile products formed during pyrolysis were collected in a liquid nitrogen cold trap. Samples were then injected into the gas chromatograph (GC) in order to separate the volatile compounds. The GC was interfaced with the infrared spectrometer (GC-FTIR) in order to identify the volatiles.

Results and Discussion

In this study, degradation behavior of FTB in oxidizing and nonoxidizing atmospheres were compared. The principal evaluation of FTB is the production of various products was also investigated.

Pyrolytic Behavior of PVE

Figure 4.1 shows the FTIR spectra for polymer residues at different temperatures during the pyrolysis of PVE in nitrogen. A list of the FTIR peak assignments for the initial PVE is given in the Table 4.1 [31]. The results in Figure 4.1 indicate that substantial side group elimination reaction occurs between 300 and 400°C. Degradation of poly(vinyl halogen) segments is indicated by decreases in intensity for the C-H stretching peaks at 2900 and 2870 cm^{-1} , C-Cl bending peaks at 1460, 1420, and 1330 cm^{-1} , C-Br-C stretching peak at 710 cm^{-1} , and the ring vibration peak at 1600 cm^{-1} . The increases in the intensity of the C=C stretching peak at 1670 cm^{-1} and the C-C stretching peak at 1100 cm^{-1} are associated with the elimination of hydrogen groups from the poly(vinyl chloride), PVE, segments. Removal of chlorine groups from poly(vinyl acetate), PVAc, segments is indicated by the decrease in the C-Cl stretching peak at 1260 cm^{-1} .

Side group elimination was also indicated by GC-FTIR analysis of the volatile products formed during pyrolysis. The primary volatile component identified (see Figure 4.10) was tetrahydroxy 1,2,3,4-dioxo which can be formed by separation of the ring structure in the poly(vinyl halogen) segments from the carbon backbone. Another major volatile product was water (Figure 4.8) which forms by a side group elimination reaction involving the hydrogen group in the poly(vinyl chloride) segments.

Although most of the absorption peaks in Figure 4.1 decrease as a result of side group elimination, there is a small increase in

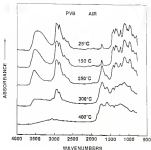


Figure S.2 FTIR spectra of the polymer residues at the indicated temperatures during pyrolysis of PM in nitrogen

Table A.1: FTIR Peak Assignments for PEG Series

Peak (cm^{-1})	Assignment
3710	$\nu(\text{O-H})$, residual PEG
2900	$\nu_{\text{as}}(\text{CH}_2)$
2850	$\nu_{\text{s}}(\text{CH}_2) + \nu_{\text{as}}(\text{CH}_2)$
1730	$\nu(\text{C=O})$, residual PEG ₆₀
1450	$\delta_{\text{as}}(\text{CH}_2) + \nu(\text{C-O})$
1421	$\nu(\text{CH}_2) + \nu(\text{C-O})$
1400	$\nu(\text{C-O})$
1270	$\nu_{\text{s}}(\text{CH}_2) + \nu(\text{CH}_2)$
1240	$\nu(\text{C-O}) + \nu(\text{C-O}), \nu(\text{C=C})$
1200	$\nu(\text{C}_2\text{H}_5) + \nu(\text{CH}_2) + \nu(\text{C-O}), \text{PEG}_{60}$
1100	$\nu_{\text{as}}(\text{C-O-C})$
1060	$\nu(\text{C-O}), \text{PEG}$
1000	ring vibration
911	$\nu(\text{CH}_2)$
800	$\nu(\text{CH}_2)$, ring vibration

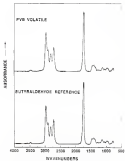


Figure 6.3 The IR spectrum of the primary volatile product is compared to the reference spectrum for butraldehyde.

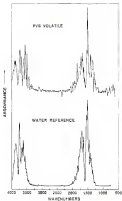


Figure 3.4 The FTIR spectrum of another primary volatile product is compared to the reference spectrum for water.

intensity of the carbonyl (C=O) peak at 1720 cm^{-1} between 300 and 400°C. In addition, a weak peak (at 1500 cm^{-1}) associated with carbon-carbon double bonds (C=C) develops in this temperature range. The formation of (al and β -) bonds is indication of both side group elimination and evolution of the carbon backbone (Fig. 3).¹ These observations are also indicated by GC-FTIR analysis which shows that small amounts of low molecular weight alcohols, ketones, and carboxylic acid compounds² are formed during pyrolysis (18).

Figure 5.1 shows the FTIR spectra for polymer residues at different temperatures during pyrolysis in air. The spectra have similar features to those in Figure 4.2 for nitrogen pyrolysis, but several important differences should be noted. First, the side group elimination reactions begin at lower temperatures in air pyrolysis. The peaks associated with C-H stretching and bending, C-H stretching, C-C stretching, C-F stretching, and the methyl ring vibration all decrease significantly between 150 and 200°C. In short, the C-H stretching peak has disappeared in air pyrolysis, while significant peaks remain in the spectrum for the corresponding nitrogen sample. Another important difference between the air and nitrogen FTIR spectra in Figures 5.1 and 4.2 is the development of a strong carbonyl peak between 150 and 200°C in air pyrolysis indicative of oxidative mechanisms. This result indicates that side group elimination and main chain evolution is assisted by an oxidative mechanism. This is also indicated by TGA and TTA results discussed below.

¹ Identification of alcohols, ketones, and carboxylic acid compounds was provided by R.E. Smith, University of Florida, Gainesville, FL.

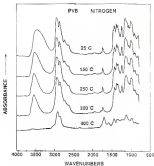


Figure 3.5 FTIR spectra of the polymer residue at the indicated temperatures during pyrolysis of PVB in air.

The GC-FTIR analysis of volatile products formed during air pyrolysis showed similar results as in nitrogen. (Although, more volatile products were detected during air pyrolysis.) The major volatile product was again isopropenol. Significant concentrations of water and hydroxy acid were also detected, as well as smaller amounts of alcohols, ketones, and carboxylic acid compounds.

Figure 4.3 shows the TGA results for air and nitrogen pyrolysis of PBI. Both TGA curves show two weight loss stages. The first stage in each case is associated with side group elimination, as well as main chain scissions. The TGA curves are consistent with the FTIR results in that the weight loss rate in the first stage is enhanced in air. This first stage also ends with less overall weight loss (i.e. more residual) for air pyrolysis. This is attributed to the extensive development of carbonyl groups in the polymer residue (Figure 4.4).

The existence of a second (higher temperature) weight loss stage in the TGA curves suggests that degradation-resistant cyclic and crosslinked structures form at lower temperatures during the side group elimination and chain scission reactions. The development of cyclic structures in the polymer residue during the early stages of degradation was indicated by GC-FTIR analysis of volatiles collected after being heated to 500°C. In both air and nitrogen pyrolysis, a variety of aromatic compounds¹ were detected, including benzonitriles, phenol, naphthalene, etc.

¹ Identification of aromatic compounds was provided by R.D. Smith, University of Florida, Gainesville, FL.

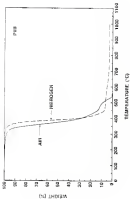


Figure 3. TGA results for PPS in air and nitrogen.

Available evidence indicates that cyclic and crosslinked structures develop at lower temperatures in air pyrolysis. This is suggested by the first crossover of the air and nitrogen TG curves (Figure 4.8). The second stage in air pyrolysis begins after some overall weight loss (i.e., with more volatile products). The FTIR results in Figure 4.9 also indicate that cyclic structures develop at lower temperatures in air. Between 700 and 1000 cm^{-1} , the δ -ring breathing peak shows a significant increase in intensity and the C-H stretching peak broadens considerably. Both observations are consistent with the development of cyclic structures [75,84]. In addition, the absorption around at 1400 cm^{-1} is associated with structures containing acetylenic carbon-carbon bonds [87]. Evidence that crosslinking occurs at lower temperatures in air was obtained by monitoring changes in weight loss of the polymer residue in ethanol after heat treatment.³ Samples were heated at a relatively low temperature (110°C) so that the overall weight loss resulted low (4%), even after long treatment times. Initially, the PBI is completely soluble in ethanol. As crosslinking occurs during heat treatment, the percentage of the polymer that becomes insoluble in ethanol increases. Figure 4.7 [8] shows that about 100% of the residue formed after 4 hours at 100°C in air is insoluble, while only ~10% of the residue is insoluble for the same heat treatment in nitrogen.

³ Solubility measurements were provided by R.E. Smith, University of Florida, Gainesville, FL.

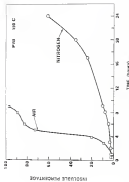


Figure 1-7 Plots of the percentage of the PVB residue vs. time treated at 100°C in air and nitrogen. Adapted from [11].

While there is less development of vesicles and crystallized structures at low temperatures in nitrogen, the first stage in the TGA curve (Figure 4.4) runs with a greater overall weight loss than does residual trapped in air pyrolysis. Further, since oxidative degradation mechanisms are not likely in nitrogen pyrolysis, the crystallized and cyclic structures that do form during the first stage are extremely difficult to break down at the higher temperatures. Thus, a second crossover in the air and nitrogen TGA curves is observed. More importantly, large amounts of residual C-HO remain at high temperature up to 1000°C in nitrogen pyrolysis, indicating that a carbon char forms.

The importance of oxidative degradation mechanisms in air pyrolysis was also illustrated by FTIR results.¹ Figure 4.5 shows plots of the IR curve and the derivative of the TGA curve (DTG) for air pyrolysis. Although the weight loss in the second stage, the second FTIR peak, is much smaller than the first stage, the carbonyl peak is considerably larger in the second stage. This is indicative of the oxidative breakdown of the crystallized and cyclic structures that developed during the earlier stages of pyrolysis. The features observed during the first weight loss stage is consistent with the strong carbonyl peak development that was observed at low temperatures in the FTIR spectra (Figure 4.11). The reactions associated with the first stage have great oxidative and acid char removal are generally irreversible when

¹ IR and FTIR results in Figure 4.5 were provided by D.G. Schultze, University of Florida, Gainesville, FL.

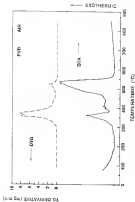


Figure 3. DSC thermograms of PPS and PPS-DBO.

signal is not present. (Indeed, small endothermic peaks were observed at $+150$ and $+180^\circ\text{C}$ during nitrogen pyrolysis of PVB.) In air pyrolysis, the heat released due to oxidation is more than sufficient to produce a net peak that is endothermic.

Pyrolysis behavior of $\text{Al}_2\text{O}_3/\text{PVB}$ mixtures

Pyrolysis studies were also carried out with $\text{Al}_2\text{O}_3/\text{PVB}$ mixtures. In order to demonstrate the bonding interaction between Al_2O_3 and PVB at room temperature, PVB spectroscopy was used to illustrate the importance of Al_2O_3 surface hydroxyl groups in PVB adsorption. The IR spectrum in Figure 4.3 shows the unadsorbed Al_2O_3 . The very broad peak over the range $3700\text{--}3000\text{ cm}^{-1}$ is associated with O-H stretching vibrations in physically adsorbed hydrogen-bonded molecular water and in surface hydroxyl groups (i.e., Al-OH hydrogen-bonded to molecular water [30]). The small absorber at $\sim 1700\text{ cm}^{-1}$ is associated with isolated surface hydroxyl groups (i.e., Al-OH). The small broad peaks at ~ 1650 and $\sim 1500\text{ cm}^{-1}$ are attributed to O-H stretching vibrations. (These peaks arise from transients formed at the moment in which the Al_2O_3 powder was dried.) The IR spectrum in Figure 4.4 shows the IR spectrum of Al_2O_3 powder with adsorbed PVB. A large increase in the peaks associated with O-H stretching vibrations is obtained due to the adsorbed PVB. A more subtle, but important, effect is the disappearance of the absorption absorber at $\sim 1700\text{ cm}^{-1}$. The difference spectrum in Figure 4.5, obtained by subtracting the IR spectrum from the dry spectrum, more clearly

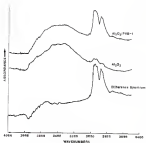


FIGURE 4.5 FTIR spectra of Al_2O_3 (middle) and Al_2O_3 containing species for 10p1 (top). The difference spectrum (bottom) is obtained by subtracting the whole spectrum from the top spectrum.

shows the decrease in isolated hydroxyl groups as $\sim 1710\text{ cm}^{-1}$ as a result of PVB adsorption. This also indicates that the polymer is binding strongly to the isolated surface hydroxyl groups. Thus, polymer/particle attachment involves hydrogen bonding between isolated hydroxyl groups on the Al_2O_3 surface and PVB hydroxyl side groups.

The PVB degradation mechanism in Al_2O_3 /PVB mixtures was found to be very similar to that of the polymer alone. This is illustrated by hot-stage FTIR results for Al_2O_3 /PVB mixtures that were pyrolyzed in air and nitrogen. In order to monitor the PVB degradation behavior when the ceramic is present, hot-stage spectra were collected for the ceramic by itself under the same heating conditions used for the mixtures and these spectra were subtracted from the corresponding spectra for the ceramic/polymer mixtures. The "difference" spectra are shown in Figures 4.10 and 4.11 for nitrogen and air pyrolysis, respectively. The changes that occur during heating are very similar to results shown in Figures 4.2 and 4.3 for "pure" polymer. This indicates that although PVB attaches to the Al_2O_3 particles via hydrogen bonding between hydroxyl side groups in the polymer and hydroxyl groups on the particle surfaces, no direct chemical reaction takes place at higher temperatures between PVB and Al_2O_3 .

Summary and Conclusions

The initial pyrolysis of PVB is dominated by the elimination of side groups (aliphatic, hydroxyl). Subsequent reactions indicate that main chain cleavage, crosslinking, and cyclization also occur during the

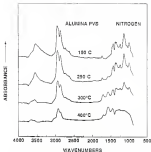


Figure 9.10 FTIR spectra of the polymer residues at the indicated temperatures during pyrolysis of AlkylPVS samples in nitrogen.

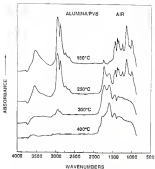


Figure 4.11 FTIR spectra of the polymer residue at the indicated temperatures during pyrolysis of $\text{Al}_2\text{O}_3/\text{PVBS}$ mixture in air.

early stages of pyrolysis. Higher temperatures are required to break down the degradation-resistant spiro and crosslinked structures.

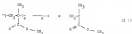
Degradation behavior of PFB is highly dependent on the pyrolysis atmosphere. Pyrolysis is initially accelerated in air (compared to nitrogen) due to oxidative mechanisms. Selective degradation is initiated by the extensive development of carbonyl groups during air pyrolysis. At intermediate temperatures, a larger weight loss was observed in nitrogen (compared to air). This apparently reflects the slower development of carbonyl groups and the less rapid development of crosslinked structures during nitrogen pyrolysis. During the later stages of pyrolysis, degradation in the absence of oxygen is extremely difficult due to crosslinking.

PFB adsorbed onto the Al_2O_3 particle surface via hydrogen bonding between hydroxyl side groups in the polymer and hydroxyl groups on the particle surfaces. During pyrolysis, the PFB degradation behavior was found very similar to that of the polymer alone. An overall chemical reaction takes place at higher temperatures between PFB and Al_2O_3 .

CHAPTER V THERMAL BEHAVIOR OF POLY(ETHYL METHACRYLATE) KIDNEY

Literature Review

It has long been established [10-11] that poly(ethyl methacrylate), PEMA, upon thermal degradation gives almost quantitative yields of monomer. This degradation process has been regarded as the reverse of polymerization, since the same diorganotinide ("catalytic") is given in this type of degradation reaction. [12]



The degradation was first investigated by Gulderson and others. Gulderson and Melville [10,11] reported that the thermal degradation of PEMA occurs in two distinct stages. Approximately 50% of the PEMA sample degrades between 300-350°C in vacuum while the remainder requires temperatures well in excess of 500°C. In the other work, Brinkman and Jansma [13] working at 100°C obtained quantitative yields of monomer. These workers, however, were able to separate the reaction into two stages, the first part a very fast reaction producing about 50% monomer, followed by a second, slower reaction

which continues until all the polymer has degraded. In both of these investigations, the change in molecular weight of the polymer complex was measured as a function of conversion to monomer. Based on these results, they further indicated that there are two types of chain initiation reactions for PPS degradation. One is chain-end initiation [9] which takes place at lower temperatures due to the reaction of pre-formed chain ends formed as a result of dispropagation termination during polymerization. The other, taking place at higher temperatures, is initiated at random positions along the polymer chain. They also stressed that the relative importance of these two reactions depends on the temperature of depolymerization. Their results were later confirmed by other workers [10-12], and it is noted that the correct kinetic interpretation of PPS degradation requires both rates of initiation to be taken into account [10-12].

The kinetic rate equations for the depolymerization reaction can be expressed by the following elementary steps:

Initiation



Propagation



Unimolecular chain transfer, which can be considered as a special case of equation 18-3, gives fragments larger than monomer, i.e.,



Termination



where k_1 , k_2 , k_3 , k_3' and k_4 are the rate constants for random scission, and initiation, propagation, intramolecular chain transfer, and termination reactions. The rate of change in concentration of macromolecules, P_{p} , can be given by the difference between the rate of formation by equations 5.1-5.3 and the rate of disappearance by equations 5.2, 5.3 and 5.4:

$$\begin{aligned} \frac{dP_{\text{p}}}{dt} = & k_1(2n-1)P_{\text{in}} + k_2P_{\text{p}} + k_3\left(\frac{P_{\text{p}}}{V}\right)(2n-1)P_{\text{in}} + k_3'\left(\frac{P_{\text{p}}}{V}\right) \sum_{j=1}^n \frac{1}{j} P_j \\ & + k_4 \sum_{j=1}^n \sum_{k=1}^n \frac{1}{j+k} dP_{jk} + k_4'P_{\text{p}}^2 \end{aligned} \quad (5.5)$$

where n is the total number of radicals, V is the system volume, $2n-1$, 2 , is the degree of propagation of the smallest molecule not relative to the system and

$$\begin{aligned} & k_1, \text{ if the termination is first order} \\ + & k_3 + \frac{k_4}{V}, \text{ if it is a second-order disproportionation} \\ & \frac{1}{V} \sum_{j=1}^n \sum_{k=1}^n \frac{k_4'jk}{j+k}, \text{ if it is a second-order recombination} \end{aligned}$$

It can be shown that

$$k_1 \frac{\partial \bar{Q}}{\partial T} = \sum_{j=1}^n \frac{\partial}{\partial T} \bar{Q}_j = k_1 \bar{Q}_n \frac{\partial \bar{Q}}{\partial Q_n} \quad (3.10)$$

where k_1 is the density of the sample, Q_n is the molecular weight of the monomer

Equation 3.3 can be rearranged to give

$$\begin{aligned} \frac{\partial \bar{Q}}{\partial T} = & - (n+1)k_2 + k_2 \bar{Q} \bar{P}_n - k_2 \bar{P}_n + k_2 \frac{k_1}{Q_n} \bar{Q}_n \\ & + k_2 \bar{Q} \sum_{j=1}^n \frac{\partial}{\partial T} \bar{P}_j + k_2 \bar{Q}_n \end{aligned} \quad (3.11)$$

The rate of change of concentration of radicals, k_p , is obtained in the same manner and is given by

$$\begin{aligned} \frac{\partial \bar{Q}}{\partial T} = & k_2 \bar{Q} + k_2 \bar{Q} \sum_{j=1}^n \frac{\partial}{\partial T} \bar{P}_j + k_2 \bar{P}_{n+1} - \left(\frac{k_1 k_2}{Q_n} \right) \bar{Q}_n + k_2 + k_2 n \bar{Q}_n \\ & + k_2 \bar{Q}_{n+1} \end{aligned} \quad (3.12)$$

where

$$n = \begin{cases} 1, & \text{For first-order termination} \\ 2/T - 1, & \text{For second-order termination} \end{cases}$$

If a steady-state concentration of radicals is assumed, then

$$R = (k_{tr} + k_p \bar{X}_n) C_0 = k_{tr} \frac{C_0}{\bar{X}_n} + k_p \bar{X}_n \quad (2.11)$$

$$\text{or } \bar{X}_n = \left(\frac{k_{tr} C_0}{k_p \bar{X}_n} + \frac{k_{tr} C_0}{k_p \bar{X}_n^2} \right)^{1/2} \quad (2.12)$$

where \bar{X} is 1 for first-order termination and \bar{X} for second-order termination, \bar{X} is the number-average degree of polymerization. The step length, $\frac{1}{\bar{X}}$, can be expressed as

$$\begin{aligned} \frac{1}{\bar{X}} &= \frac{k_t \bar{X}}{k_p \bar{X} + k_t k_p \frac{C_0}{\bar{X}_n}} \\ &= \frac{\text{probability of termination}}{\text{probability of termination} + \text{probability of transfer}} \quad (2.13) \end{aligned}$$

The variation in the total number of polymer molecules is

$$\begin{aligned} \frac{d \sum_{n=1}^{\infty} P_n}{dt} &= - \frac{dR}{dt} = - (k_{tr} + k_p \bar{X}) \left(\sum_{n=1}^{\infty} P_n C_{P_n} + k_{tr} \sum_{n=1}^{\infty} P_n \right) \\ &\quad + k_p \bar{X} \sum_{n=2}^{\infty} n P_n + \left(\frac{k_{tr} C_0}{\bar{X}_n} + k_p \bar{X} \right) \sum_{n=1}^{\infty} P_n \\ &= - (k_{tr} + k_p \bar{X}) C_0 - k_{tr} C_0 + k_p \bar{X} C_0 \\ &\quad + \left(\frac{k_{tr} C_0}{\bar{X}_n} + k_p \bar{X} C_0 \right) = 0 \quad (2.14) \end{aligned}$$

where $\bar{M}_0 = \bar{M}_0^0$ and $\bar{M}_1 = \bar{M}_1^0 \bar{M}_0^0$. Adding equations 5.13 and 5.14 gives

$$\frac{d\bar{M}_0}{dt} = -k_p \bar{M}_0 = -k_p \bar{M}_0^0 \bar{M}_1 = -k_p \bar{M}_0^0 \left(\frac{k_p \bar{M}_0^0}{k_t} \right) = -k_p^2 \bar{M}_0^0 \quad (5.17)$$

The first two terms represent the gain in molecules by initiation or chain transfer, and the second, the loss of molecules by termination at \bar{M}_1 .

The rate of weight loss can be obtained in a similar way by multiplying equation 5.15 by n and summing, to give

$$\frac{d\bar{M}_0}{dt} = - \left[\frac{k_p^2}{k_t} \bar{M}_0^0 + k_p \bar{M}_0^0 (\bar{M}_1 + \bar{M}_2) \right] \quad (5.18)$$

The first term represents weight loss due to termination by \bar{M}_1 , and the second, loss by disproportionation.

The rate of weight loss as a function of slip length can be obtained if \bar{M}_1 and \bar{M}_2 in equation 5.18 are eliminated with the aid of equations 5.13 and 5.17:

$$\frac{d\bar{M}_0}{dt} = - \left(1 + \frac{1}{\bar{Q}} \right) \frac{d\bar{M}_0}{dt} = - \left(1 + \frac{1}{\bar{Q}} \right) k_p \bar{M}_0^0 = - \left(1 + \frac{1}{\bar{Q}} \right) k_p \bar{M}_0^0 \quad (5.19)$$

If initiation is random, the number of possible initiation sites is independent of molecular weight. If the slip length, \bar{Q} , is much larger than the degree of polymerization, $\bar{Q} \gg \bar{n}$ and the termination is third order, then

$$\frac{dM_1}{dL} = - \frac{1}{2} k_p M_1 \quad (5.20)$$

The overall rate of recombination is proportional to k_p . However, if the degree of polymerization is much larger than the slip length ($\alpha \gg \frac{1}{2}$), then

$$\frac{dM_1}{dL} = - \frac{1}{2} k_p \left(\frac{1}{\alpha} \right) M_1 \quad \text{for first order and disproportionation termination} \quad (5.21)$$

or

$$\frac{dM_1}{dL} = - \frac{1}{2} k_p \left(\frac{1}{\alpha^2} \right) M_1 \quad \text{for recombination termination} \quad (5.22)$$

The rate of weight loss is independent of the initial molecular weight.

For chain-end initiation reaction, if the slip length $\frac{1}{\alpha}$ is much larger than the degree of polymerization α , then

$$\frac{dM_1}{dL} = - k_p M_1 \quad (5.23)$$

If the degree of polymerization is much larger than the slip length ($\alpha \gg \frac{1}{\alpha}$),

$$\frac{dM_1}{dL} = - \frac{k_p}{\alpha} \left(\frac{1}{\alpha} \right) M_1 \quad \text{for first order and disproportionation termination} \quad (5.24)$$

or

$$\frac{dM_1}{dL} = - \frac{1}{2} k_p M_1 \quad \text{for recombination termination} \quad (5.25)$$

More studies [18]-[19] have confirmed these conclusions and further

show that the termination is bimolecular at low temperatures and changes to unimolecular at high temperatures.

From the previous discussion, it is suggested that end groups generated during the termination of the free radical polymerization of methyl methacrylate (MMA) have a profound effect on the thermal stability of the resulting polymer. Bartsch et al. [196] demonstrated by ¹³C NMR spectroscopy that the termination by disproportionation in the radical polymerization of MMA occurred mostly through route a of the following reaction and not through route b.



The peaks at 5.1 and 6.15 ppm were assigned to the methylene protons of the vinylidene group formed through route a). In the absence of transfer agents, the termination of MMA polymerization occurs by oxidation or disproportionation. Disproportionation results in a saturated structure, i.e., not an unsaturated end group, *B*, while oxidation of growing radical chains yields a head-to-head (H-H) linkage, *A*, within the chain.





A detailed evaluation of the thermal stability of PMA was conducted recently by Australian researchers [108] and synthesized model compounds containing structures 4, 5 and 6. The unsaturated copolymer, 4, was prepared by employing methyl tetrahydrofurfurylcarboxylate (MTHFC), which yields exclusively unsaturated end groups [109] with relatively narrow distributions.



These mixtures were subsequently hydrogenated using a 5% Pd/C catalyst to yield the fully saturated copolymer, 6. The copolymer 7 containing a B-E linkage was prepared by decomposing diethylidene-2'-methylsuccinate, 8, in micro-wave oven containing PMA at 50°C for 24 hrs.



They then used variable NMR (differential scanning calorimetry) and DSC to test the thermal stability of oligomers 4, 5, and 7. It was shown that the onset of decomposition for unsaturated oligomer 4 is around 220°C, whereas the breakdown of saturated oligomer 5 commenced at 200°C. In comparison to molecular weight was observed up to $M_n = 18,000$. Model compounds containing head-to-head linkages (oligomer 7) decomposed at 190°C, clearly showing that head-to-head linkages are the least stable groups arising from termination of polymerization. The evidence for the reduced stability of the H-H linkage-configuration was provided by the crystallographic data obtained by Poppelet al. [110]. Poppelet al. stated that H is in the plane of the head-to-head link that when it is preferred side of chain selection. Furthermore, the bond dissociation energy of the head-to-head linkage is estimated to be about 84 kJ/mol (20 kcal/mol) less than that of C-C backbone bond, $E_{\text{C-C}}$, due to the large steric hindrance and inductive effect of vicinal ester groups [110]. Therefore, weight loss initiated by chain selection at the head-to-head linkage should occur at the lowest temperatures compared with

those due to end initiation (roughly 50-60 times less than k_{app}) or random scission. Schultz and May [110] reported that, within a given sample of PNB obtained by free radical polymerization, longer chains are more thermally stable than their shorter counterparts. Most work of the higher molecular-weight molecules are expected to arise by combination of the growing chains and these would contain the most head-to-head linkages; degradation of these chains, therefore, should be observed during the early stages of pyrolysis. Thus, Corbell [109] concluded that the use of a hydrophilic chain transfer agent, which would eliminate head-to-head linkages as well as unsaturated end groups, would substantially increase the overall thermal stability of PNB. The influence of chain ends and end links to the thermal stability of PNB were also studied by several other researchers [111-113].

1.2. McNeill [108] studied the thermal degradation of PNB and its copolymers and found that the thermal stability is highly dependent both on the method of preparation and on the molecular weight of the polymer. In his study, thermal gravimetric analysis (TGA) was used to monitor the thermal stability of PNB samples with different molecular weights prepared by free radical and anionic mechanisms. As shown in Figure 5.12(a), for PNB samples prepared by the free radical mechanism, two peaks were observed in the thermograms corresponding to different mechanisms of initiation of the chain depolymerization process. (Peaks below 300°C, which were attributed to trapped radicals migrate as the polymer softens, are not discussed.) At the first peak, the rate of degradation between 300°C and 350°C is lower for samples of higher initial molecular weight

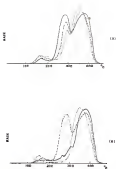


Figure 3: TGA results showing (a) the effect of initial molecular weight on the thermal stability of poly(methyl methacrylate) samples prepared by the free radical mechanism at 60°C: (solid line, polymer A, $\bar{M}_n = 40,000$; dashed line, polymer B, $\bar{M}_n = 100,000$; full line, polymer C, $\bar{M}_n = 50,000$), and (b) dependence of TGA thermograms for high and low molecular weight poly(methyl methacrylate) samples prepared by an anionic mechanism with the thermogram for a low molecular weight free radical sample: (solid line, polymer B, $\bar{M}_n = 1,000,000$; full line, polymer C, $\bar{M}_n = 50,000$; dashed line, free radical polymer A, $\bar{M}_n = 50,000$). Sampled from [180]2.

T_{max} is higher for samples of higher molecular weight. For the second peak, the onset of degradation between 300° and 350°C is higher for samples of higher initial molecular weight. T_{max2} is lower for samples of higher molecular weight. These observations are consistent with the assumed view that the first stage is not initiated and the second is initiated by random chain scissions. In Figure 5-1(C) thermograms for high and low molecular weight PPA samples prepared by an anionic mechanism are compared. The corresponding trace for the low molecular weight polymer C, prepared by the free radical mechanism, is also given. The initial stages of the first stage is evident for the high molecular weight sample D, which shows a similar T_{max1} value to the high molecular weight sample A prepared by the free radical mechanism (see Figure 5-1(B)). More striking, however, is the change of the first peak in the low molecular weight anionic sample, E. This indicates that the unstable vinylidene units present in the free radical sample are not produced in PPA-Pol prepared by the anionic process.

Kricheldorf and co-workers [19] used thermogravimetry to examine the effect of amount of vinylidene chain ends on the thermal stability of PPA. In their study, when the polymerizations were carried out in the presence of butyl-ethyl borophos (a chain transfer agent), the amount of vinylidene chain ends decreased greatly, i.e. from 0.3% to 0.025% and 0. The DTG results shown in Figure 5.2 indicate that, for all three samples, the most stable linkages generate the largest peak corresponding to degradation caused by random chain scissions within the polymer chains. Samples A (0.3%) and B (0.025%) do not show any detectable weight loss from least stable linkages (around

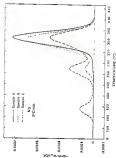


Figure 3.2 Effect of sample degradation on the 2DFT spectra of samples A, B, and C. (Sample A: 100 nm, 150 nm, 250 nm; Sample B: 100 nm, 150 nm, 250 nm; Sample C: 100 nm, 150 nm, 250 nm)

101°C), and hardly any weight loss as shown by the second peak due to oxidation from the vitrified state (260°C) appears for sample 4. Bartlberg and co-workers also studied the effects of molecular weight (Figure 3-34A) and polymerization method (Figure 3-35B) on the thermal degradation behavior of PBRs. Their results are in good agreement of work of Kricheldorf [100]. Similar observations were also reported by other researchers [101-103].

The influence of tacticity is another important factor affecting polymer degradation behavior [104-106]. Kelen [107] studied the thermal degradation behavior of PBRs of different tacticities by pyrolyzing samples in a flowing helium atmosphere at a heating rate of 10°C/min. The thermal degradation responses during pyrolysis of PBRs showed some differences for the different tactic forms (Figure 3-36A-C). Analysis of the pyrolysis products formed in the temperature range 300°-600°C shows, however, that all the tactic forms revert almost exclusively to methyl methacrylate monomer. The mass chromatograms are shown in Figure 3-36D. However, the issues of high molecular weight coefficients observed in the isotactic polymer were not characterized. Jellinek and Lee [108] studied the influence of tacticity on the rate of PBR degradation in a closed system over a range of temperatures 300°-400°C in the absence of air. The degradation rate shown by kinetic analysis is governed by random initiation, depropagation, and disproportionation in the termination reaction. Their results also show that syndiotactic PBR appears thermally more stable than isotactic PBR. However, the overall

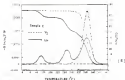
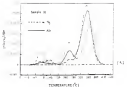


Figure 8.3. Thermal analysis results showing (a) effects of initial molecular weight on DTG curves for samples degraded in nitrogen, Sample 1 ($\bar{M}_n = 44,400$), 2 ($\bar{M}_n = 74,000$), and 3 ($\bar{M}_n = 100,000$), and (b) effects of substitution level on DTG curves for samples degrading in nitrogen, Series C (randomly polyacrylate) and B (alternately polyacrylate). Adapted from [108].



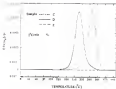
3-4

3-5

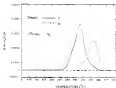
Figure 3-4 Raman scattering spectra showing (a) linear polyethylene with resonance during separation of crystals ($\lambda = 1.05 \mu\text{m}$, $\lambda_{\text{res}} = 1.15 \mu\text{m}$), amorphous (crystalline) (crystalline) ($\lambda = 1.05 \mu\text{m}$, $\lambda_{\text{res}} = 1.15 \mu\text{m}$), and (b) linear polyethylene ($\lambda = 1.05 \mu\text{m}$, $\lambda_{\text{res}} = 1.15 \mu\text{m}$) polyethylene amorphous (crystalline) and (c) same spectra of the various products of ethylene formed in the temperature range 2000–3000°C at static 10% crystallinity (a) and (b) and (c) polyethylene amorphous (crystalline). The values of the values (a) show the values for the products formed from the linear polyethylene in the temperature range 100–1000°C (copied from [10]).

energy of activation for aliphatic polymer is smaller, the reason for this similarity is not yet understood.

Detailed investigations of the role of oxygen in the thermal degradation of PMA were made recently by a group of researchers at MIT (United States of Massachusetts [71b,72b-73]). The DSC curves for randomly polymerized PMA sample B and radically polymerized sample C degraded in air are compared with those degraded in nitrogen as shown in Figures 5.5 (a) and (b) (iv), respectively. Only one peak shows up for sample B degraded in N_2 and air, according to Figure 5.5 (a). However, sample B degraded in air at much lower temperatures than in nitrogen. The effects of gas-phase oxygen on the degradation of radically polymerized PMA are much more complex than those in randomly polymerized PMA as shown in Figure 5-6 (B) for sample C. With sample C, the first peak caused by the breakdown of backbone linkage during nitrogen pyrolysis completely disappears when the sample degrades in air. The second peak caused by acid initiation in nitrogen is slightly shifted (i.e.) shifted toward high temperatures. The third peak caused by random scission is barely present in air. Instead, a new major peak appears at around 500°C in air between the second and third peaks observed in nitrogen. Therefore, Rothlaup et al. suggest that gas-phase oxygen plays a dual role in the degradation of radically polymerized PMA, by suppressing the degradation caused by the weak linkages at low temperatures and by enhancing the degradation at high temperatures. The reported activation energy for the random scission initiation is 231 kJ/mol for thermal degradation and 39 kJ/mol for oxidative degradation. Because



(a)



(b)

Figure 5.5 DSC curves for (a) anionically polymerized PNB (Sample B), and (b) free radically polymerized PNB (Sample C) degrading in nitrogen and air. (adapted from [153].)

[138,139] also reported that the presence of oxygen promotes more chain scission than when oxygen is not present, probably due to the formation of peroxides and hydroperoxides. The enhanced scission was supported by the molecular weight measured results which showed that the number average degree of polymerization of PMS degraded in air decreases more rapidly than that of PMS degraded in nitrogen. Kashiwagi et al. [140] also reported that the relative degradation in air is not as sensitive to differences in PMS structures as is in nitrogen, since scissions involving different initial molecular weights, mechanisms and polymerization methods show basically the same pattern [141] when they degraded in air.

In this study, the pyrolysis behavior of PMS resins was investigated using a variety of techniques as described in the next section. More importantly, degradation behavior of PMS in the presence of various plasticizers was also investigated. Finally, the effects of important processing variables (e.g., pyrolysis atmosphere, heating PMS, weight loss) as well as strategies for enhancing the degradation reactions were discussed.

Materials and Methods

Materials

Polymers. The polymers used in this study were poly(methyl methacrylate) resins,¹ PMS. According to the manufacturer, they were

¹ Elconite 300F, 300L and 3001, DuPont Co., WILMINGTON, DE.

made by a free radical polymerization process. The molecular weights, molecular weight distributions, and tactic distributions are given in Table 5-1. The molecular weights and molecular weight distributions were obtained using gel permeation chromatography (GPC)² with monodisperse polystyrene as a standard and tetrahydrofuran, THF, as the solvent. A sample concentration of 20 mg per milliliter was used. The polymer solutions were filtered through a 0.45 μ m filter to remove any undissolved material. A total volume of 50 μ l solution was then injected into the GPC, which has a set of four 4 mm \times 25 cm μ STABODIL columns³ (packed with crosslinked styrene-divinylbenzene polymer) operated at a flow rate of 1 ml/min. Both UV and RI (refractometer) detectors were used simultaneously. The elution chromatograms are shown in Appendix A.

The tactic distributions [T], [S] were calculated from the relative ^1H peak areas of the α -olefin comonomer using deuterated octadecane, $\text{C}_{18}\text{D}_{32}$, as solvent and tetramethyl silane, TMS, as internal standard. The polymer concentration was 100 mg/ml $\text{C}_{18}\text{D}_{32}$. A 0.25 ml RF probe and a ten minute sweep time were used during the run. The ^1H NMR spectra are shown in Appendix C.

Isotane standard specimens, 99.99-10 were used in most experiments.

¹ Model 8000, Waters Associates, Milford, MA.

² Millipore, Waters Chromatography Division, Milford, MA.

³ Varian 10-000, 40 mm ^1H and ^13C spectrometer.

TABLE 5.1 Molecular Weight, Molecular Weight Distribution, and Tensile Strength of PPSA resins

Polymers	Molecular Weight and Molecular Weight Distribution			Tensile Strength		
	\bar{M}_w	\bar{M}_n	\bar{M}_w/\bar{M}_n	(bar)	(psi)	(psi)
PPSA-8	27,399	10,400	2.63	0.15	0.46	0.67
PPSA-10	35,605	13,589	2.62	0.19	0.56	0.80
PPSA-40	152,432	120,047	1.27	0	0.86	0.98

Coagulation. Coagulate/polymer mixtures were prepared using the same Al_2O_3 powder as described in Chapter IV. The TGA curve of the as-received powder showed a gradual weight loss of ~0.28 from 30°C to 500°C due to loss of adsorbed water. The Al_2O_3 was then as received and after calcination at 1000°C for 24 hours.

High purity, amorphous, spherical SiO_2 , prepared by Baker's method [14], was also used in some experiments. The precipitated powder was calcined at 600°C for 24 hours. The number average diameter, as determined by scanning electron microscopy,¹ was 0.4 μm and specific surface area was $0.4 \text{ m}^2/\text{g}$.

Sample preparation. Both the polymer and ceramic powders were dried in vacuum for 24 hours at 50°C and 150°C, respectively, to remove adsorbed water before use. Coagulate/polymer mixtures were initially prepared as suspensions, using chloroform as the solvent for PMS. In some studies, acetone was used as the solvent as specified. The suspensions, consisting of 5 wt% polymer, 25 wt% ceramic, and 70 wt% solvent, were cast onto Nylar-covered glass slides and the solvent was allowed to evaporate at room temperature. The cast samples were then ground to a powder in a mortar and dried at 50°C for 24 hr under vacuum to remove any residual solvent. The final $\text{Al}_2\text{O}_3/\text{PMS}$ mixtures contained 0.3 wt% PMS.

¹ Model JSM-500F, Japan Electron Optics Co., Ltd., Tokyo, Japan. The number average diameter value was provided by C. S. Robinson, Department of Materials Science and Engineering, University of Florida, Gainesville, FL.

In some experiments, low concentrations of stabilizers were used to analyze the polymer degradation pathways. These additives were ground to a powder and were carefully weighed and added to the polymer solutions, where acetone was used as the solvent. (The viscosities of these solutions were much higher in acetone than in chloroform.) The solutions were cast into KBr-infrared glass plates and left dry for 48 hr at room temperature. The cast thin films were then cut into 2 in X 4 in plates and dried at 50°C under vacuum for 24 hr before use.

Analysis

Elemental Analysis (IR-FTIR): The sample size was approximately 10 mg for pure polymer, and 171 mg and 1000 mg for mixture-FTIR studies. The heating rate was 5°C/min, and the gas flow rate (air or nitrogen) was approximately 60 cc/min.

Elemental Analysis (FTIR) (FTIR Spectroscopy): The sample preparation and experimental procedures for FTIR analysis were similar to those described previously in Chapter IV, except that nitrous gasifier was used as diluent in most of the experiments.

Gas Chromatography (GC): The conditions of collecting the reaction and the GC operational variables are given in Tables 5.2 and 5.3, respectively.

The GC was also equipped with a flame ionization detector (FID) and a peak integrator to obtain the retention volume measurements

Table S.1 Conditions of Collecting FTIR Potentials

	Pt/Al	Al ₂ O ₃ /Pt/Al
Atmosphere	Air and H ₂	Air and H ₂
Heating rate (°C/min)	5	5
Initial temperature (°C)	30	30
Final temperature (°C)	600	1000
Heat time (min)	5	5

Table 8.3 GC Operational Variables for PMMA Volatile Degradation Products

	PMMA	CL ₂ D ₂ /PMMA
Carrier gas	Helium	Helium
Flow rate (mL/min)	8	8
Column length (m)	5	20
Injection port temperature (°C)	180	150
Initial oven temperature (°C)	50	50
Injection time (s)	0	0
Heating rate (°C/min)	10	0
Final oven temperature (°C)	250	200
Final time (s)	10	10
FTD temperature (°C)	230	200

Pyrolysis and Degradation

Pyrolysis Behavior of PEMA Beads

A study of various methods has suggested that PEMA degrades by the depolymerization mechanism. Figure 5-4 shows the TGA results for pyrolysis of PEMA (PMMA-4) in air and nitrogen. Under both atmospheres, the polymer can be heated and degraded at relatively low temperatures compared to that of PET. The derivative of the TGA curve (DTG), i.e., the derivative of a peak of weight loss vs. temperature, for pyrolysis of PEMA in air is shown as the top curve in Figure 5-5. It shows that all of the polymer weight loss occurs in a relatively narrow temperature range (180-200°C) as expected for a polymer that degrades by a single stage mechanism such as depolymerization. The lower curve (DTG) in Figure 5-5 shows that the reaction is endothermic which is also consistent with degradation by depolymerization. Similar results were obtained for nitrogen pyrolysis as shown in Figure 5-6, except that the degradation was shifted to higher temperatures by approximately 50°C. The absence of weight residue in the degradation reaction... (the bump appearing before the endothermic peak in Figure 5-6 was eliminated by adding the period of closed piston as shown in Figure 5-7 to maintain the furnace, which tends to decrease weight loss in the rapid volatilization of the monomers.)

Similar thermal analysis results, i.e., single stage end endothermic reaction, were also observed for lower molecular weight

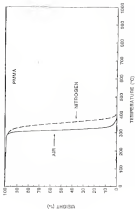


Figure 3-4 TGA results for PMMA in air and nitrogen.

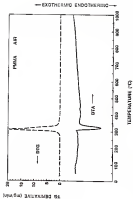


Figure 3.1 DSC and DTA results for PMAA in air.

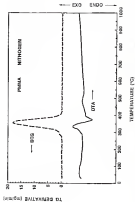


Figure 3. DSC and DTA results for PABA in nitrogen.

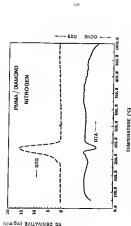


Figure 5. DSC and DTA results for diamond/nitrogen powder at 100°C.

PMD, i.e., PMD-6 ($\bar{M}_n = 17,110$, $\bar{M}_w = 19,881$), as shown in Figures 5.10 and 5.11. However, more complex results were observed when a much higher molecular weight sample, i.e., PMD-11 ($\bar{M}_n = 251,408$, $\bar{M}_w = 311,051$), was used as shown in Figures 5.12 and 5.13. Instead of the single-stage degradation process observed in PMD-6 and PMD-10, the results for PMD-11 show that degradation occurs in several stages. From Figure 5.12(a) as an example, three well defined stages occurred at 175°C, 200°C and 225°C even in nitrogen pyrolysis. Consistent with the observations by other researchers [10-15,205,118,119,200], these three stages represent three different initiation mechanisms due to the head-to-head head-to-head linkage (-THPC), unactivated chlorine chain ends (-CHCl₂), and the most stable carbon chain linkages (-CHCl₃). In the other hand, in air pyrolysis [Figure 5.12(b)], the second and third peaks observed in nitrogen pyrolysis overlap and the first peak caused by the head-to-head linkage completely disappears. This is again consistent with the results by Kricheldorf et al. [118], who stated that gas-phase oxygen plays a vital role in the degradation of radically polymerized PMD by suppressing the degradation caused by the weak linkage at low temperatures and by enhancing the degradation at high temperatures. Comparison of the weight loss curves for these three polymers are shown in Figures 5.15(a) and (b) for air and nitrogen pyrolysis, respectively. It can be seen that polymers with higher molecular weights show less thermal stability than the lower ones.

Figure 5.15 shows the TGA spectra for the polymer residues at different temperatures during pyrolysis of PMD. PMD-11 in air-

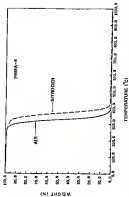


Figure 2-10 TGA results for cross-linked $\bar{M}_w = 37,000$, $\bar{M}_n = 20,000$ in air and nitrogen

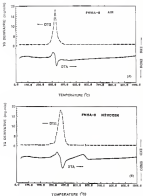


Figure S-11 DTG and DTA results for PMAA-6 in (a) air and (b) 10% nitrogen.

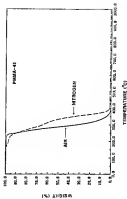


Figure 8. TG results for (PMMA-41) $\bar{M}_w = 100,000$, $\bar{M}_n = 100,000$ in air and nitrogen.

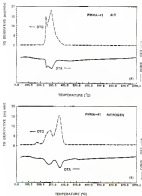


Figure S.13 DSC and DTA analysis for P466-91 in (a) air and (b) nitrogen

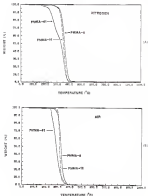


Figure 5-18 TGA results for PMMA resin with different molecular weight in (A) air pyrolysis and (B) nitrogen pyrolysis

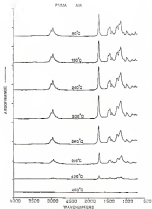


Figure 3-15. FTIR spectra of the polymer residue at the indicated temperatures during pyrolysis of PMMA in air.

A list of the FTIR peak assignments for the initial polymer is given in Table 3-4 [19,20]. All of the absorption peaks increase in intensity on the temperature increase. Figure 3-11 shows the plots of the relative peak intensities as a function of temperature for the carbonyl (C=O) stretching peak at $\sim 1730\text{ cm}^{-1}$, the C-O stretching peak at $\sim 1177\text{ cm}^{-1}$, and the O-H asymmetric stretching peak at $\sim 2815\text{ cm}^{-1}$. The increase in all peak intensities, as well as the observation that no new peaks develop during pyrolysis, is consistent with the depolymerization mechanism. Similar FTIR spectra were also obtained for nitrogen pyrolysis as shown in Figures 3-12 and 3-13, except that degradation was shifted to higher temperatures.

The application of infrared spectroscopy in studying the thermal reactions of PMs has been reported by other researchers. Szymanski and Bialins [12] studied the degradation of polypropylene and PMs films on silver plates by an infrared emission spectroscopy technique. Similar study was carried out by Miers and Pyrie [14] using external reflection infrared spectroscopy (ERIR) technique. However, due to the limitations of their instruments, pyrolysis atmosphere and heating schedule could not be properly controlled. Moreover, direct chemical effects on the PMs decomposition were observed when different substrate materials were used such as Au, Ag, Cu, Al, Ni, SiC. Thus, the hot-stage coupled diffuse reflectance infrared spectroscopy used in this study seems to be the most suitable method for in-situ characterization of high temperature degradation behavior of polymers.

Table 3-1 FTIR Peak Assignments for PHEMA Sample

Peak (cm^{-1})	Assignment
3064	overtones $\nu(\text{C-H})$
2981	$\nu_{\text{as}}(\text{CH}_2-\text{O}) + \nu_{\text{as}}(\text{CH}_2)$
2948	$\nu_{\text{as}}(\text{CH}_2-\text{O}) + \nu_{\text{as}}(\text{C}-\text{CH}_2) + \nu_{\text{s}}(\text{CH}_2) + \nu_{\text{s}}(\text{C}-\text{CH}_2)$
2892	combination band associated with other CH_2 group
1728	$\omega(\text{C=O})$
1481	$\nu_{\text{as}}(\text{C}-\text{CH}_2)$
1448	$\nu(\text{CH}_2)$ overlapped with $\nu_{\text{s}}(\text{CH}_2-\text{O})$
1428	$\nu_{\text{s}}(\text{CH}_2-\text{O})$
1383	$\nu_{\text{s}}(\text{C}-\text{CH}_2)$
1378	$\nu_{\text{s}}(\text{C}-\text{CH}_2)$ overtones
1299	$\nu_{\text{as}}(\text{O}-\text{C}-\text{O})$ coupled with $\omega(\text{C=O})$
1198	$\nu_{\text{as}}(\text{O}-\text{C}-\text{O})$ coupled with $\nu(\text{O-H})$
1159	isolated stretching, coupled with isolated $\nu(\text{CH}_2)$
1101	$\nu_{\text{s}}(\text{O}-\text{C}-\text{O})$
981	$\nu_{\text{s}}(\text{O}-\text{C}-\text{O})$ coupled with $\nu(\text{CH}_2-\text{O})$
961	$\nu(\text{C}=\text{CH}_2)$
753	$\nu(\text{CH}_2)$ coupled with isolated stretching

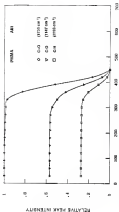


Figure 5(d) Relative peak Intensity (from 100 MPa) as a function of temperature for the polymerization of MMA at 50 MPa.

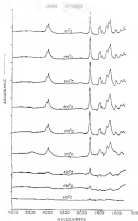


Figure 5-11 FTIR spectra of the polymer residue at the indicated temperatures during pyrolysis of PMA in nitrogen.

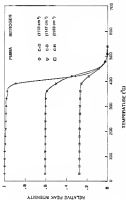


Figure 3-11 Relative peak intensities (from the PMA spectra) as a function of temperature during condensation of PMA in nitrogen.

Direct evidence for the depolymerization reaction is provided by GC-FTIR analysis of the volatiles. Figure 3-19 shows the gas chromatogram of PMMA volatiles collected in air. The major component (peak 44) had a concentration of 85.8 wt% and was identified as methyl methacrylate monomer as shown in Figure 3-20. Other minor degradation products are listed in Table 3-3. Traces of low molecular weight substances such as methanol and acetone were also detected, presumably due to side chain scission. Gas chromatogram of PMMA volatiles collected in nitrogen is shown in Figure 3-21. Again, the major degradation product is methyl methacrylate monomer (peak 45) and had a concentration of 79 wt%. Very low percentages of other volatile monomers were also identified as minor degradation components as listed in Table 3-4.

Thus, all of the results confirm that the PMMA resin used in this study degrades almost exclusively by depolymerization. PMMA resins with higher molecular weights showed less thermal stability than that of the lower ones due to initiation at the ends through. The presence of oxygen accelerates the depolymerization reaction; however, no direct evidence (i.e., formation of peroxide or hydroperoxide) for the participation of oxygen in the degradation process was observed. GC-FTIR spectra and structural formulae of degradation products are shown in Appendix C (Tables C.1-C.3).

Pyrolysis Behavior of Garamic/PMMA Blends

1. Degradation Behavior of Garamic/PMMA Blends

Figure 3-22 shows the results for the pyrolysis of a Al_2O_3 /PMMA mixture in air. The degradation behavior is similar to that of the

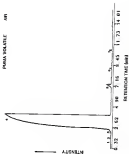


Figure 3.10 Gas chromatogram of 1000 volatiles collected in air from 30°C to 100°C.

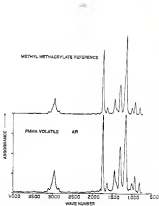


Figure 5.24 The IR spectrum of the primary acrylic product as compared to the reference spectrum for methyl methacrylate.

Table 1.3. Decomposition Products from the Synthesis of PBO in air.

	Concentration
Peak # 1: Nitrogen	~ (trace)
2: Acetone	~ (trace)
3: Nitro2 amide	0.11
4: Nitro2 acetoxyamide ^a	94.88
5: Nitro2 amide acid	0.05
6: Nitro2 amide acid	0.05
7: Nitro2 acid, Nitro2 ester	0.05

^a Major decomposition product.

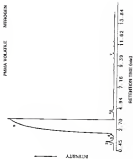


Figure 2.17. IR spectrum of para-iodoaniline obtained by difference from KIO₄ reagent.

Table S.1 Quantitative Products from the Pyrolysis of PBD in Nitrogen^a

		Quantification
Peak # 1	Hexane	0.15
2	Isobutane	0.39
3	Methyl acrylate	— (Trace)
4	Ethyl acrylate	0.15
5	Methyl methacrylate ^b	50.68
6	Ethyl methacrylate	0.25
7	Acrylonitrile, Methyl acry	0.15

^a Major decomposition products

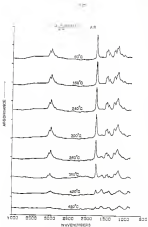


Figure 5-22 IR spectra of the polymer residue at the indicated temperatures during pyrolysis of Mg_2Si (run 24, 25).

polymer without the nitrate (Figure 5-11) is that the major absorption peaks (e.g., C-H, C=O, and C-N) of the PMA all increase in intensity with increasing temperature. However, the important difference is that a new peak at $\sim 1575\text{ cm}^{-1}$ develops in the $\text{Al}_2\text{O}_3/\text{PMA}$ system at temperatures $\geq 100^\circ\text{C}$ (Figure 5-12). This peak, assigned to the carboxylate ion [$\text{O}=\text{C}(\text{O}^-)$], indicates that there is an interaction between the PMA side groups and the Al_2O_3 surface. A proposed reaction reaction is shown as follows:



At the surface of alumina the normal octahedral coordination of Al^{3+} apply, and these sites can generally be considered as being due to exposed aluminum ions fixed in a tetrahedral configuration but attached to only three oxygen atoms.



This species is exactly analogous to the aluminum halides (Lewis acids) and would be expected to undergo reaction with Lewis bases,

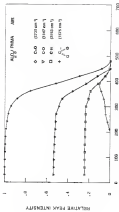


Figure 1-13 Relative peak intensities (from the PIR spectra) as a function of temperature for the degradation of Alkylphenyl siloxanes in air.

such as PMA (19), to give surface oxides. In this case the ion-polymer interaction is via the lone pair of electrons associated with the carbonyl oxygen to form carboxylate complexes as shown in equation 5.20.

This surface reaction complicates the PMA pyrolysis behavior so that degradation no longer occurs exclusively by the depolymerization reaction. As shown in Figure 5-29 and Table 5.7, in addition to initial volatile weight losses (peak III), several other components, including a variety of acids, were detected and the amount of initial volatizable residue (peak IV), several other components, including a variety of acids, were detected and the amount of initial volatizable residue decreased to 40% of the total residues. Most of the degradation process is still controlled by depolymerization. However, the surface reaction delays the final stages of pyrolysis, i.e., considerably higher temperatures are needed to achieve complete burnout. This is illustrated in Figure 5-35 which shows a comparison of the TGA behavior in air for the polymer alone and the polymer/ceramic mixture. The total weight loss in the polymer/ceramic mixture was corrected to 100% in order to directly compare the results with the TGA curve for the polymer alone. It can be seen that not only the final stage of pyrolysis was delayed but the degradation rate, which is the slope of TGA curve, also decreased for the ceramic/polymer mixture. Similar high-temperature TGA and Q-TGA analyses were conducted to attempt pyrolysis as shown in Figures 5.29-5.38 and Table 5.7, except that the degradation temperatures were 50°C higher (Figure 5.29). These observed results indicate that the interaction between PMA

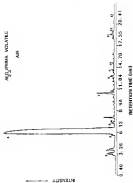


Figure 3.21 Gas chromatogram of hydrogen sulfide collected in air from 20 to 240 min.

Table S.7 Decomposition Products from the Pyrolysis of $\alpha,\beta,\gamma,\delta$ -tetra-*tert*-butyl-1,3,5,7-tetraoxacyclooctane in air

		Concentration
Peak # 1	Acetone	1.00
2	Acetone	1.40
3	Methyl acrylate	0.70
4	Methyl methacrylate ^a	70.00
5	Methyl methacrylate	0.00
6	2-Hydroxyethyl methacrylate acid	0.10
7	Hexanoic acid, dimethyl ester	0.00
8	Hex-3,5-dimethyl heptanoic acid	0.00
9	3,4-Dimethyl glutaric acid	0.00
10	2-Ethyl, 3-methyl pentanoic acid	0.00
11	3-Isopropylpentanoic acid	0.00
12	Adipic acid, dimethyl ester	-- (Trace)
13	Septanoic acid	-- (Trace)

^a Major decomposition product

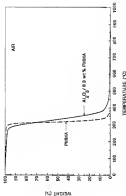


Figure 3-15 TGA results for PMMA and Al_2O_3 -PMMA at $10^{\circ}\text{C}/\text{min}$.

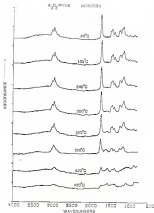


Figure 9-26 FTIR spectra of the polymer residue as the induced temperature during pyrolysis of $\text{Al}_2\text{O}_3/\text{PMA}$ mixture in nitrogen.

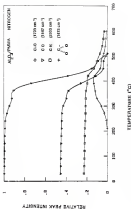


Figure 1.17 Relative peak intensities (from the PHS spectra) as a function of temperature during synthesis of Alkyltrimethylammonium bromides in solution

ALIPHATIC VOLATILE
RETENTION

RETENTION

— ALIPHATIC



RETENTION TIME (min)

Figure 3. 20 Gas chromatogram of aliphatic volatile collected in nitrogen from 20% to 100%.

Table 1.1 Decomposition Products from the Pyrolysis of $\text{Al}_2\text{O}_3/\text{TiO}_2$ Mixture in 851 Pages.

	Concentration
Peak # 1 Methanol	2.05
2 Acetone	0.05
3 Methyl acrylate	0.75
4 Methyl acrylate	0.75
5 Methyl methacrylate ^a	80.75
6 Acrylic acid	0.05
7 Methyl methacrylate	1.05
8 2-Methyl acrylate acid	1.05
9 Succinic acid, dimethyl ester	4.55
10 Maleic acid, dimethyl ester	4.55
11 3-Carboxy cyclohexanecarboxylic acid	0.05
12 Maleic acid, dimethyl ester	0.55
13 3-Bromobenzene	0.75
14 2-Bromobenzene	-- (trace)

^a Major decomposition product



Figure 5.29 TGA results for Al_2O_3 /PMMA mixtures in air and nitrogen

OH group and Al_2O_3 surface serve a "blocking effect" [16] on the depolymerization process, so that depolymerization cannot pass through the original OH bond as much (see reaction).

One of the features which affects the nature of the surface reaction between PPH and Al_2O_3 is the degree of hydroxylation of the catalyst surface. Figures 5.22 and 5.23 show that higher intensities of the carboxylic ion peak are observed during heat treatment when a oxidized Al_2O_3 (1000°C, 24 hours) is used. Furthermore, the surface hydroxylation is observed at much lower temperatures. This increased hydroxylation may reflect greater extent of the exposed porosity (which is about 10% of the total surface area) [17-19] so the OH group is the polymer/catalyst interface. It is also possible that the effect arises from an increase in the acid-base interaction between the catalyst and polymer. (The ester group in the PPH has a weak character while the Al_2O_3 may develop a more acidic character after calcination [20].) However, the latter interpretation is not supported by experiments carried out with another acidic catalyst, V_2O_5 . The low-temperature FTIR results of the oxidized V_2O_5 /PPH mixture in air are shown in Figures 5.24 and 5.25. Due to the difficulty of subtracting out the strong Al-O-Si absorption peak between 1000-900 cm^{-1} , only the C=O and C-O stretching band intensities are shown in Figure 5.25. Surface interaction between PPH and Al_2O_3 was not observed during pyrolysis, i.e., the carboxylic ion peak did not develop during heat treatment. The speculated increased acid-base interaction between the heat-treated Al_2O_3 and PPH was also demonstrated with the absorption results during

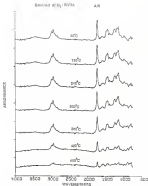


Figure 8.35 FTIR spectra of the polymer region at the isotactic temperature during synthesis of isotactic ΔT_g PPSA obtained in air.

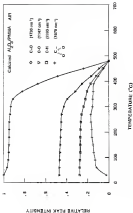


Figure 5.21 Relative gas ionization cross section (σ) as a function of temperature for the polymorphs of various Al_2O_3 polymorphs in air.

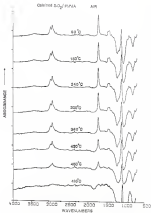


Figure 5.30 FTIR spectra of the polymer residue at the indicated temperatures during synthesis of oxidized poly(THFA) in air.

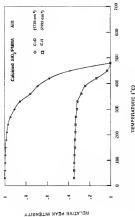


Figure 3-20 Relative peak intensities from the FTIR spectra as a function of temperature during oxidation of polypropylene in air.

1700-1600 cm^{-1} as shown) [14], which showed a decreased infrared band fraction, from $F = 0.20$ to $F = 0.17$, after covering SiO_2 of a monolayer of surface hydroxyls of heat-treated Al_2O_3 . These results suggest that an important factor in determining the extent of the catalyst/polymer interaction during pyrolysis is the character of the catalytic layer in the catalyst. Additional absorption results are shown in Appendix B. The carbon fraction occurred in the material (i.e., Al_2O_3) in which the catalytic layer was more inert (less reactive) compared with this observation were pyrolysis experiments with mixtures of PPA and glassy polymer (which complete carbon binding) which showed no surface interaction. In contrast, experiments with highly reactive materials, such as silica gel, showed an even greater degree of reaction with PPA than in the Al_2O_3 /polymer mixtures (as shown in Figures 5.18 and 5.21).

The reaction mechanism between PPA and transition metals (TM) was obtained by analyzing the relative decomposition products of the PPA/TM mixtures. The reactions were analyzed by heating the PPA/TM mixtures (cast from chloroform) in air from 100°C to 1000°C and held at 1000°C for 1 hour. The mixture analysis results are shown in Figure 5.20 and Table 5.3. Again, methyl methacrylate is the major degradation product. However, more important, methyl bromide (Figure 5.20) and the other brominated alkanes were also detected. The presence of methyl bromide (CH_3Br) along with the development of acrylonitrile then indicates the following important reaction mechanism:

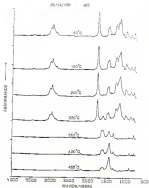


Figure 3.28 FTIR spectra of the polymer residues at the indicated temperatures during pyrolysis of PBD-ODR mixture in N_2 .

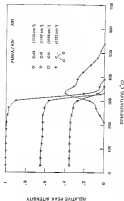


Figure 5.20 Relative peak intensity (from FTIR spectra) as a function of temperature during pyrolysis of polyurethane (PU).

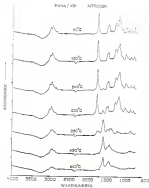


Figure 5-36 IR spectra of the polymer residue at the indicated temperatures during pyrolysis of PMMA in nitrogen as storage.

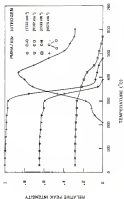


Figure 5.37 Relative peak intensities (from FTIR spectra) as a function of temperature during degradation of copolyester systems in air.

Table 4.5 Decomposition Products from the Pyrolysis of PMMA at 500°C

Peak #	1	Carbon dioxide
	2	Water
	3	Methanol
	4	Chloroform
	5	Acetic acid
	6	Isobutyl acrylate
	7	Isobutyl methacrylate ^a
	8	Isomeric vinyl dimethyl ether
	9	2,4-Dimethyl glutamic acid
	10	Isobutyl formate
	11	Malic acid, dimethyl ether
	12	2-Hydroxyethyl methacrylate acid
	13	2,2-Dihydroxyethyl methacrylate acid
	14	Hexa/2,4-dimethyl succinic acid
	15	Propionic acid, ethyl ether
	16	1,2-Ethanedithione
	17	1,2,3-Trithione ethane
	18	Formic acid, isopropyl ether

^a Major decomposition product

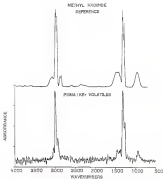


Figure 3.25 The IR spectrum of the volatile product (Peak #10) is compared to the reference spectrum for methyl bromide.



Further verification of this surface-polymer interaction was made using other surfaces. Other materials used to demonstrate this surface-polymer reaction include AgI , silicones glass, SnO_2 , and BaO as shown in Figures 3 to 5 VI. This silicon glass/PMS mixture is an example, as expected, since the glass contains both SiO_2 , Si_2O_5 , and PbO AgI . The carboxylic acid does not interact as strongly as in the case of Al_2O_3 or AgI /PMS mixtures. These observed results were surprisingly in good agreement with those obtained by Lepelowski and Gerschlager¹¹ (1961), who studied the interaction between PMS carboxylic acids and surfaces of various acid strengths (acid salts) over the temperature interval from 100° to 1050°. They indicated that the formation of chemical bonds between the acid groups of PMS and the labile regions of acid Al_2O_3 , AgI occurs involving the thermal degradation products of the polymer and is reflected in decreases in the activation energy of PMS thermal degradation on the surface of $\alpha\text{-Al}_2\text{O}_3$ and of AgI . Consistent with the results shown in Figures 3, 4, and 5, VI, a stronger chemical bond was observed between PMS and AgI than that of PMS and $\alpha\text{-Al}_2\text{O}_3$. More interestingly, similar to the case of tetrahydrofuran Al_2O_3 (Figure 3-3), enhanced surface interaction (i.e., stronger carboxylic acid polymer surface bond formation) was also observed by Lepelowski and Gerschlager¹¹ when a carboxylic

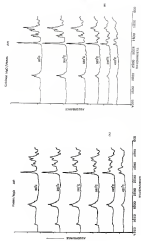


Figure 8.40 FTIR spectra of the polymer residues at the indicated temperatures during synthesis at (a) 100 °C and (b) 200 °C. The spectra show the characteristic peaks of the polymer residues.

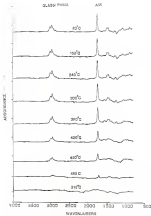


Figure 5.11 IR spectra of the polymer residue at the indicated temperatures during synthesis of glassy films at 450°C.

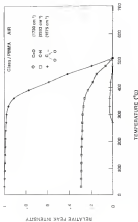


Figure 5.40 Relative peak intensities (from FTIR spectra) as a function of temperature for the products of Glass/PMMA. Sampled at 100°C.

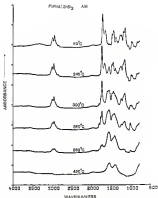


Figure 5.43 FTIR spectra of the polymer residue at the different temperatures during pyrolysis of (Formaldehyde)₂ measured in air.

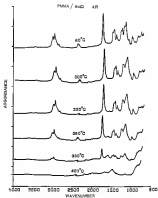
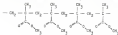


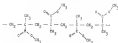
Figure 5.14 FTIR spectra of the polymer residue at the indicated temperatures during synthesis of PMMA/NaCl solution in air.

Ag₂SO₄ was used. [However, no significant enhancement was observed (Figure 3.40XII) in our study.] The observation of carboxylate ion formation was also reported by Higginbotham [1960], who investigated the thermal degradation behavior of titanium dioxide filled PPMs. He reported that formation of the carboxylate groups was due to coordination of the highly polarizable carbonyl groups with the transition metal ions. [The relatively weak interaction between PPM and NaCl is presumably due to the residual moisture on the NaCl, since NaCl was not dried as vigorously as in the case of Ag₂.]

Further examination of the reaction between PPM ester groups and metal ions was carried out for solutions of potassium benzoate (KBr) and stereoregular polymers, i.e., isotactic and syndiotactic PPMs.¹



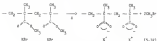
Isotactic PPM



Syndiotactic PPM

¹ P. C. Challa, Inc., Birmingham, Al. The number average molecular weights of isotactic and syndiotactic PPM are 152,000 and 100,000, respectively.

IR, ^{13}C , and ^1H results of the pure isotactic and syndiotactic PPhs are shown in Figures 3.15-3.17. It should be noted, however, that the molecular weights of these two polymers differ greatly. As shown in Figures 3.18 and 3.19, both stronger conjugation in poly and, more importantly, significant development of anionic structure as indicated by the appearance of 1550 cm^{-1} , 1705 cm^{-1} and 1026 cm^{-1} bands were observed in isotactic PPhs/Br mixtures at 300°C. These observations indicate that the isotactic PPh is more reactive toward Br than that of the syndiotactic one. A proposed reaction mechanism is shown as follows:



Since all the ester groups of the isotactic PPh are in the same side of the polymer chain, the possibility of these ester groups reacting with protonic ions and thus maintaining its pure anionic structure between the adjacent ester groups is much larger than that of the syndiotactic PPhs:

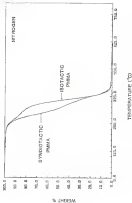


Figure 5-10 The results for isotactic and syndiotactic PPA in storage.

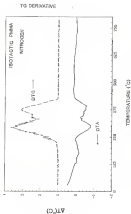


Figure 1. TG, DTA and DTG results for isotactic PMA in nitrogen.



Figure 5.47 DTG and DTG curves for syndiotactic PMMA in nitrogen.

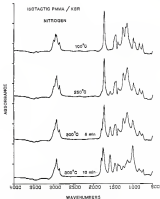


Figure 3-44 FTIR spectra of the polymer residues at the indicated temperatures during pyrolysis of isotactic PMMA in nitrogen at 1000°C.

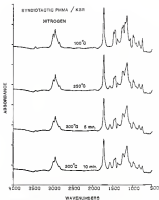


Figure 3.9: IR spectra of the polymer residue at the different temperatures during synthesis of syndiotactic monomer obtained in nitrogen.

$\text{Al}_2\text{O}_3/\text{PMS}$ mixtures were compared with those of $\text{Al}_2\text{O}_3/\text{PM}$ mixtures² in order to determine the effects of processing variables on the wetting loss behavior and the mechanism of degradation. The mechanism of the continuous residue formed under different firing conditions was assessed by a SEM/EDS analyzer.

Figure 5-20(a) shows the TGA results for $\text{Al}_2\text{O}_3/\text{PMS}$ mixtures that were processed in air and nitrogen. As discussed earlier, the degradation mechanism of PMS is not affected by the gas atmosphere. Thus, unlike $\text{Al}_2\text{O}_3/\text{PM}$ mixtures (Figure 5-20(b)), the TGA curve of $\text{Al}_2\text{O}_3/\text{PMS}$ mixture in nitrogen atmosphere is just simply shifted to higher temperatures. The effect of gas flow rate was also investigated. Figure 5-21(a) shows the TGA curves for pyrolysis of $\text{Al}_2\text{O}_3/\text{PMS}$ mixtures carried out in static air and flowing air (100 sccm). Under the static condition, the oxygen supply is limited, thus the degradation reaction is delayed. Also, since the volatile species cannot be removed efficiently from the sample interior, complete pyrolysis is not achieved and the fired sample appeared black. For $\text{Al}_2\text{O}_3/\text{PM}$ mixtures (Figure 5-21(b)), the TGA curve is very similar to the behavior observed in a nonoxidizing atmosphere (e.g. nitrogen in Figure 5-20(b)). This can be explained by the difficulty in getting oxygen in and in removing volatile

² The TGA results on $\text{Al}_2\text{O}_3/\text{PM}$ mixtures were provided by G.R. Jenaiphala, Department of Materials Science and Engineering, University of Florida, Gainesville, FL.

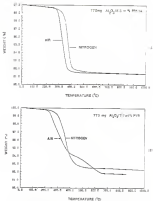


Figure 3.40 The results for (a) $\text{Al}_2\text{O}_3/\text{PMMA}$ matrices and (b) $\text{Al}_2\text{O}_3/\text{PMMA}$ matrices in O_2 and nitrogen. (Adapted from [164].)

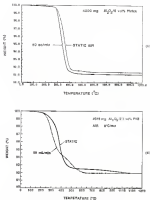


Figure 5.8 TGA results for (a) Al₂O₃/TMS mixtures and (b) Al₂O₃/TMS mixtures in static air and flowing air (collected from [154]).

degradation species from the sample interior layer, the degradation mechanism is less selective [754].

Pyrolysis is also delayed in samples with larger size as shown in Figures 3-55(a) and (b). This is again attributed to the diffusivity in entering radicals from the sample interior. The superoxidized carbon particles (TO-150%) and other volatile species need to be transported out of the sample through such longer diffusion path. Evidence for this delayed transport was obtained by monitoring the residual carbon concentrations of the samples taken out from the top and bottom of the crucibles. Table 3.16 shows that concentrations profiles did shift for samples with larger size. Carbon concentrations for samples fired under other conditions are also listed in Table 3.16. However, the difference between various sample size for $\text{Al}_2\text{O}_3/\text{Pyb}$ mixtures is minimal. (i.e., degradation mechanism did not change) compared to that of $\text{Al}_2\text{O}_3/\text{Pyb}$ mixtures. As shown in Figure 3-55(c), pyrolysis of Pyb in air is initiated in samples with larger size due to the lower oxygen partial pressure within the samples. Thus, not only does the weight loss kinetics change, the degradation mechanism also changes from oxidation to nonselective [754].

Decreasing the heating rate affects the weight loss behavior of $\text{Al}_2\text{O}_3/\text{Pyb}$ mixtures in a similar manner to increasing the sample size. Since it takes less time to reach a given temperature and there is less time for pyrolysis to occur when the heating rate increases [755], the TGA curves were just shifted to higher temperatures as

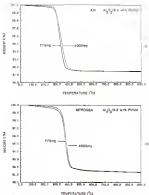


Figure 5.32 TGA results for $\text{Al}_2\text{O}_3/\text{PMMA}$ mixtures with different weight ratio in (a) air and (b) nitrogen atmosphere.

Table 1-10 Carbon Residue Concentrations of $\text{Al}_2\text{O}_3/\text{TiO}_2$ Pigment Fired Under Pollution Conditions

Atmosphere	Heating rate	Temperature	Sample size	Carbon concentration
Air	5° C/min	800°C	4000 mg (Total)	186
Air	5° C/min	800°C	4000 mg (Residue)	268
Air	5° C/min	1000°C	4000 mg (Total)	139
Air	5° C/min	1000°C	4000 mg (Residue)	166
Air	5° C/min	800°C	775 mg	24.7
Air	5° C/min	1000°C	775 mg	1.07
Nitrogen	5° C/min	800°C	775 mg	14.0
Nitrogen	5° C/min	1000°C	775 mg	1.0

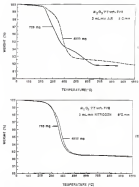


Figure 5.8: TGA results for $\text{Al}_2\text{O}_3/\text{TiO}_2$ coatings with different TiO_2 contents (10 and 30 wt%) in air and nitrogen atmospheres. (Adapted from [194].)

shown in Figure 5.10(a). The swelling ratio also affects the local oxygen partial pressure (i.e. in the matrix interior) during pyrolysis. For example, at higher swelling ratios, the local oxygen partial pressure tends to decrease due to the large concentration of oxidation generated during a short period of time. Thus, as shown in Figure 5.10(b), once again, the change in local partial pressure of oxygen changes the degradation mechanism of PVB (10), i.e. from an oxidative mechanism at a low swelling ratio to a less oxidative mechanism at a higher swelling ratio.

3. Swelling Degradation of PVB Beads

In order to lower the pyrolysis temperatures and reduce the polymer residues, low concentrations of oxidizers were used to catalyze the degradation reactions. As discussed earlier, the polymer-oxidizer samples were dried in films from acetone. Figure 5.11 shows the weight loss curves for the air-oxidized polymer (bead) and polymer films cast from acetone (bead) and nitroethane (bead). Results show that the weight loss curves of the polymer film cast from acetone resemble that of the air-oxidized polymer, however, polymer film cast from nitroethane shows much higher temperatures are needed to remove the residual solvent due to stronger acid-base interaction [187]. Similar acid-base interaction was also observed for PVB (solid) cast from acetone in H₂O₂-initiated solution as shown in Figure 5.12 [188].

TM results in Figure 5.13 show that addition of 0.1 wt% aqueous perchloric, $Hg(ClO_4)_2$, or ammonium perchlorate,

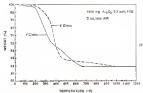
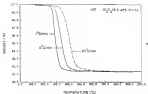


Figure 5-51 TGA results for (a) Al_2O_3 /PMMA mixtures and (b) Al_2O_3 /PMMA mixture in air at the indicated loading rate.

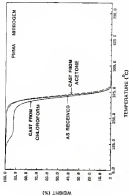


Figure 1.10 TGA results for poly(vinyl)ene and copoly films cast from chloroform and acetone in air.

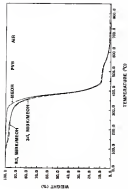


Figure 3.16 TGA results for PET film and two different mixtures. (adapted from [108])

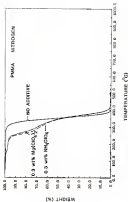


Figure 5-27 TGA results showing the effect of nitrogen permeation and generation products on PMMA weight loss in nitrogen

$\text{H}_2\text{O}/\text{H}_2$, significantly increases the early stage degradation of PBA by as much as 40%. PTO and PTA results in Figures 3 (B) and 3 (C) also show the degradation reactions are far more complicated than that of the pure polymer (Figure 3.4). (The initial weight loss between 100° and 200°C was possibly due to the evaporation of the trapped solvent, i.e., water.) Losses are more low-molecular compounds with initial loss in the low pair of electrons associated with the carbonyl oxygen (C=O). As a consequence, thermally higher temperatures may be required to remove the strongly held electron molecules. Similar behavior was also observed in HNO_3/H_2 mixtures and from analysis, as shown in Figure 3.4, the electron carbonyl structure was at $\sim 100 \text{ eV}^{-1}$ with shifted up strongly at 200°C, indicating the formation of coordination complexes with the transition metal ion Zn^{+2} . (Although water would be expected to act as a stronger ligand than the ester group of the polymer, the replacement of before by water in Figure 3 during film formation by continuous removal of water from the film surface by evaporation.) This observed enhancement in degradation with Dwyer's kinetic results [20], which show that the activation energy required for the decomposition of Dwyer (an aliphatic polyether polyurethane) increased by 18 (25.8 kJ/mol) vs. 7.4 kJ/mol, in H_2 with addition of electron permeation. In the same study, the decomposition rates were compared for vinyl alcohol polymers with different metal permeation additives. He stated that the more acid character the ester has, the more effective the substance is in decreasing the thermal stability of vinyl alcohol

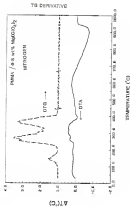


FIGURE 3-18 DSC and DTA results for poly(3-vinylpyridine) in nitrogen.

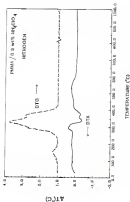


Figure 3-53. DTA and DSC results for poly(vinylidene fluoride) (PVDF) samples in nitrogen.

polymers. Further, it was found the prepared for poly(α -olefin) sulfoxylates.

Despite the early stage information about in Figure 3.33, the final degradation stages were delayed. This is not surprising about the last-stage FTIR results (Figure 3.34) about the development of carbonyls not observed even during high temperature pyrolysis, i.e. similar to the results with $\text{Al}_2\text{O}_3/\text{PMS}$ catalyst. Thus, although $\text{HfO}_2/\text{Al}_2\text{O}_3$ concentration only stage degradation, the decomposition is accompanied with increased carbonization at high temperatures. Chatterjee et al. [160] proposed that the carbonization is due to splitting off of the acid groups of PMS catalyzed by $\text{H}_2\text{SO}_4/\text{Al}_2\text{O}_3$. They also found that the carbon concentration of the carbonized samples increases with increasing perfluorinated concentration. Further, details of carbonization effect were also observed when PMS was supported on metal fluoride salts of platinum, palladium, iridium, zircon, niobium, and alloy of iron and nickel [161,162].

Summary and Conclusions

A variety of catalysts were used to investigate the pyrolysis behavior of PMS and various/PMS catalysts. Information concerning the degradation mechanism was obtained by analyzing both reaction and reaction.

As expected, TGA, DTA, FTIR, and GC results showed that PMS degraded by the degradation mechanism. PMS reacts with higher molecular weights showed less thermal stability than the lower ones

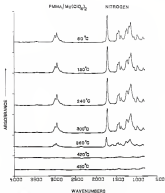


Figure 5-46. FTIR results of the polymer reaction at the indicated temperatures during the synthesis of PMMA/ $\text{Mg}(\text{ClO}_4)_2$ mixture in nitrogen.

due to presence of more weak linkages. Also depolymerization temperature was accelerated by the presence of oxides.

Degradation of PBA in $\text{Al}_2\text{O}_3/\text{PBA}$ mixtures also occurred primarily by depolymerization. However, a surface reaction between PBA and Al_2O_3 at higher temperatures was indicated by observation of an FTIR absorption peak for the carbonyls (as an additional) visible component in the IR spectra. This interaction between PBA carbonyl groups and alumina ions on the Al_2O_3 surface causes a "fixing effect" on the depolymerization process, so the depolymerization reaction was retarded and even higher temperatures are required to achieve complete burnout. This surface reaction was more extensive with reduced (dehydroxylated) Al_2O_3 (due to greater amount of the positively charged alumina ions) and with highly ionic oxides (i.e., alkali halides). Besides also showed that isotactic PBA residues were strongly bound potassium ionside than that of syndiotactic PBA. This was shown by the much stronger development of carbonyls as peak and, more importantly, the development of anhydride structure at higher temperatures in the isotactic PBA/COE mixtures. No reaction was observed when the oxides had a more neutral character (i.e., SiO_2 , alumina).

The effects of processing variables on the pyrolysis behavior of $\text{Al}_2\text{O}_3/\text{PBA}$ mixtures were also investigated. Pyrolysis was delayed for larger sample size, higher heating rate, and nonoxidizing atmosphere. However, unlike PBA, the degradation evolution is not affected by these variations.

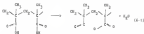
Addition of low concentrations of perchlorates (ClO_4^- , ReO_4^- , BrO_4^-) and MnO_4^- significantly enhanced the early stage degradation of PPA by as much as 40%. However, the final degradation stages were delayed due to increased carbonization.

CHAPTER XI THERMAL DEGRADATION OF POLY(ACRYLIC ACID) ESTERS

Literature Review

Thermal degradation of poly(acrylic acid), PAA, was first studied by French and Braggie [vi] in 1940. Examination of the infrared spectra of the polymer residues after heating at 1000° indicated that the major reaction is the formation of anhydride of the glutaric (intramolecular) type due to elimination of water between neighboring carboxyl groups. A similar reaction was observed in poly(methyl acrylate), PMA. McCough and Gohls [ix] reported the formation of both glutaric and isomeric (intermolecular) anhydride groups in PAA in the range of 100-1100° as a first order reaction.

Formation of cyclic anhydride structures in PAA, as shown in equation (1), was observed later on by a number of researchers [xii-xix].



Their results are in close agreement with those of Braggie. Figure 11 shows the IR spectra of PAA before and after heat treatment.

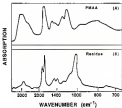


Figure 8-1 Infrared spectra of (A) poly(methylmethacrylate) and (B) PMMA residue after heating at 200°C. (Adapted from [102].)

After heating, the broad acid hydroxyl absorption band in the region $3400-3500\text{ cm}^{-1}$ and the strong acid C=O absorption band at 1700 cm^{-1} are replaced by intense C-H-C absorption at 1200 cm^{-1} and splitting of the carbonyl peak at 1715 cm^{-1} and 1730 cm^{-1} . These changes are characteristic of anhydride structure. Closer observation of the nature of the carbonyl splitting [39,45,146] seems to point to the fact that the water has been eliminated intramolecularly to form cyclic structures rather than intermolecularly to form anhydrides.

Reisman et al. [146] investigated the effect of acidity on the rate of water elimination. Examination of the infrared spectra of isotactic and syndiotactic PMMA heated for 18 min at 150°C shows that the isotactic sample dehydrates at much higher rate than the syndiotactic sample.

Thermogravimetric analysis of the rate of water loss between 100°C and 250°C in vacuum was performed by Graham et al. [148,150] for atactic and isotactic PMMA. Three distinct stages are observed in the weight loss curves as shown in Figure 5-11. During the initial temperature rise 100°C , a rapid weight drop corresponding to about 25 weight loss occurs. The rate of weight loss in this region is independent of the polymer tacticity and the degradation temperature, and is due to water absorbed in the polymer. The second stage is characterized by a slower weight loss and is temperature dependent. The rate of weight loss is faster for the isotactic than for the atactic polymer. Finally, in the third stage, there is a further weight loss which varies between 15 and 35 depending on the sample. These results are first order kinetics and indicate that the

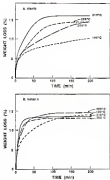


Figure 5.2: Weight-time curves of (a) styrene and (b) isoprene in PMA between 100°C and 200°C. [isoprene from (150)-2]

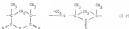
rate of water loss is about four times higher for the linear PBA than for the starlike polymer. However, the activation energies are almost identical (40 kJ/mol). They concluded that it is probable that the enhanced reactivity of the linear polymer is the result of a higher frequency factor in the rate constant of the reaction. The arrangement of neighboring reacting groups is more favorable to the formation of a cyclic intermediate in the case of the linear polymer than for the starlike polymer.

Blomquist et al. also reported that water was the only volatile product produced in this temperature range. No carbon dioxide or methane was detected. These results agree with those of Okamoto [14] but not with those of Blomberg et al. [17] who detected methane during the degradation of PBA.

The dehydrohalogenation reaction was also proven by other experimental techniques. Jackson and Bellill [17] reported that extensive volatilization of water was observed in the thermal volatilization analysis in the range of 300°-350°C.

Byn and McGowan [19] used high-resolution solid-state NMR spectroscopy to analyze the structural changes occurring in high temperature degradation of PBA. In their work, a combination of cross-polarization CP and magic-angle spinning (MAS) with high-power proton decoupling was used to give high-resolution ^{13}C NMR spectra of solid samples. Figure 5.8 shows the spectra for various heat-treated PBA samples. As shown in the figure, the resonance at δ 161, assigned to the acid functionality of the polymer, becomes broader after heating at 300°C for 1 h (Figure 5-8(c)). The new

acetyl resonances peak at δ 19 is due to formation of cyclic anhydrides. This cyclization also gives rise to a shift in the methyl resonances which are observed at δ 16. Heating the sample at 250°C for 2 h (Figure 8.28 and 8.29) results in the complete loss of the methyl peak due to the acid functionality and there are no isolated unreacted acid groups existing. Pyls and Williams indicated that at this stage a cyclic polymer appears to have formed since heating this sample at temperatures up to 300°C results in no further change in the IR spectrum. At a higher temperature of 350°C, the sample undergoes extensive degradation. After 30 min (Figure 8.30 and 8.31), the spectrum shows peaks due to the cyclized polymer (1600) as well as resonances due to aromatic degradation (1700). There is also a peak at δ 200, indicating the presence of ketone functionality. They propose that ketones could be formed by the decarboxylation of the anhydride...



After 1 hour (Figure 8.32 and 8.33), the sample is mainly aromatic in nature. There is a shoulder at δ 121, which possibly indicates the formation of some phenol rings. The work of Pyls and Williams provides us with a new approach to yield information about the structure of the solid degradation products that is spectroscopically cannot fulfill due to peak overlapping.

Kurita and Seikei [110] studied the variation of molecular weight in the thermal decomposition of PMMA as a function of temperature. Two polymer samples ($\bar{M}_n = 150,000$ and $300,000$) prepared by a solution polymerization reaction were tested by thermogravimetric analysis at 10°C/min in air. Results show that both polymers have the same activation energy of 10 kcal/mole in the range of 345-400°C (33.7% weight loss). Only a slight variation of the percentage weight losses was observed in the depolymerization step. No major differences are reported between these two polymers.

In 1958, Defendi and Battaglin [111] studied the degradation behavior of polymers of isobutene, styrene, propylene, and various ratios of acrylonitrile and styrene. Their results show that these polymers degrade in a totally different manner from PMMA. They reported that these small-molar-mass polymers are stable to about 300°C in vacuum; at higher temperatures, oxidation in the main chain and side groups takes place yielding monomer, carbonates, oxides, carbon dioxide, and a variety of ketenes and aldehydes as the principal degradation products. The main degradation reaction can be summarized in the following scheme:



In addition, structures were found in the partly degraded polymers. This indicates that intramolecular migration of metal cations or carbonate involving adjacent carboxylate groups does not occur. They also observed a gradual enhancement of carbon dioxide production as the total cation increases ($\text{Ca}^{2+} + \text{Mg}^{2+}$).

In 1979, Pinnell and Laflamme (1980) reported a study on properties of polymers of aliphatic earth metal salts of methacrylic acids. Their results show that chain extension and depolymerization, which was found to be an important process in the aliphatic metal polymethacrylate series, did not occur to the same extent in the aliphatic earth metal series where, except in the case of magnesium salt, the monomers are recoverable and cannot distill out of the reaction zone. Thus, the alternative process, involving formation of carbon and metal distribution or metal, predominates.

In this study, pyrolysis behavior of PMAA resins were investigated using a variety of techniques, including TGA, DTA, FTIR (Fourier-transform infrared spectroscopy), and GC. More importantly, degradation behavior of PMAA in the presence of various products were also investigated. Finally, strategies for reducing PMAA pyrolysis were discussed.

Materials and Methods

Materials

Colony. The polymer used was a commercial poly(methacrylic acid) (PMAA)¹ resin. The resin was made up a free radical

¹ Scientific Polymer Products, Inc., Geneva, NY.

polymerization process. The molecular weight obtained from the intrinsic viscosity measurement was 145,200 g/mol. The intrinsic viscosity measurement was made using a capillary viscometer. The Rouse-Zimm-Brenner equation [18] was used for the viscosity-average molecular weight, M_v , calculations:

$$[\eta] = K + B^2 \quad (15.4)$$

where the intrinsic viscosity, $[\eta]$, is defined as

$$[\eta] = \lim_{c \rightarrow 0} \frac{\eta - \eta_0}{c\eta_0^2} = \lim_{c \rightarrow 0} \frac{1 - \eta/\eta_0}{c\eta_0^2} \quad (15.5)$$

in terms of the solvent viscosity, η_0 , the solution viscosity η , solute concentration c , solvent flow time t_0 , and solution flow time t_s . The Rouse-Zimm constants B and K in (15.4) are 0.202 and 0.81, respectively, for PMMA-solvent solution at 40°C [19]. Since PMMA is very hydrophobic, the polymer was dried at 80°C under vacuum for 24 hours and stored in desiccator before use. No further purification was made.

Characterization. The materials used in this study were mainly high purity (99.999%) Al_2O_3 powder as described in Chapter 12. The Al_2O_3 was used as received and after calcination at 1050°C for 24 hours.

High purity, monodisperse, and spherical PS- SiO_2 described in Chapter 7 was also used in some experiments. The precipitated powder was calcined at 850°C for 24 hours.

Sample Preparation

Similar sample preparation procedures as reported in Chapter 7 were used to prepare the various/PSMA mixtures, except wet-pressed and

used as the solvent for PMA. The fused Al_2O_3 /PMA element contained 1.8 wt-% PMA.

Analysis

Thermal analysis (TGA/DTG). The scan rate was approximately 50 °C per run (polymer, and/or 175 °C and 1000 °C for Al_2O_3 /PMA blends). The heating rate was 10 °C/min and the gas flow rate (air or nitrogen) was approximately 50 mL/min.

Fourier transform infrared (FTIR) spectroscopy. Similar sample preparation and experimental conditions were used for FTIR analysis as described in Chapter 10.

Gas chromatography (GC). The conditions of collecting the volatiles and the GC operational variables are listed in Tables 5.1 and 5.2, respectively.

Resin and Glass/Resin

Resin: Structure of PMA and PMA

Although the structure of PMA differs from PMA only in the replacement of a methyl group by a hydrogen atom (i. e., a methylene end group instead of the ester group),



PMA



PMA

Table 6.1 Conditions of Densifying PMA Polystyrene

Heating Schedule	Atmosphere			
	N_2		Air	
Step 1	200°C (program) 5 min	200°C (hold) 0.5 hr	200°C (program) 5 min	200°C (hold) 0.5 hr
Step 2	200°C (program) 5 min	250°C (hold) 0.5 hr	250°C (program) 5 min	250°C (hold) 0.5 hr
Step 3	250°C (program) 5 min	300°C (hold) 0.5 hr	300°C (program) 5 min	300°C (hold) 0.5 hr
Step 4			300°C (program) 5 min	300°C (hold) 0.5 hr

Table 6.1 GC Operational Parameters for MMA and $\text{Al}_2\text{Cl}_3/\text{MMA}$ Fractional Separation Products

	PMMA	$\text{Al}_2\text{Cl}_3/\text{PMMA}$
Carrier gas	Helium	Helium
Flow rate (mL/min)	1	1
Column length (m)	30	30
Injection port temperature ($^{\circ}\text{C}$)	150	150
Initial oven temperature ($^{\circ}\text{C}$)	50	50
Initial time (min)	10	0
Ramping rate ($^{\circ}\text{C}/\text{min}$)	5	0
Final oven temperature ($^{\circ}\text{C}$)	200	200
Final time (min)	10	20
PS temperature ($^{\circ}\text{C}$)	200	200

The pyrolysis behavior is dramatically different for these two polymers. Instead of the stage-stage process observed in PMA (Figure 5.4), the TGA curves for pyrolysis of PMA (Figure 5.4) show that degradation occurs in three stages.

Consistent with the results of Grant et al.¹² [74], [75], [76] the first weight loss stage results in approximately 10% weight loss in the range of -100°C – 250°C and is dominated by the condensation reaction between the neighboring carbonyl groups as shown in equation 5.1. Evidence for this reaction is provided by the results obtained by FTIR. A list of FTIR peak assignments for PMA is shown in Table 5.2. As shown in Figure 5.6, the strong acid carbonyl peak at 1770 cm^{-1} and the broad carboxyl peak in the range 3000 – 2500 cm^{-1} that originally exist at 10°C are diminished after heating to approximately 300°C (i.e., the end of the first stage in the TGA curve). The FTIR spectra in Figure 5.6 also show the development of several strong peaks which are consistent with the polymer structure on the right-hand side of equation 5.1. For example, Figure 5.6 shows plots of the relative peak intensities as a function of temperature for the C–O–C stretching peak at $\sim 1200\text{ cm}^{-1}$ and two peaks associated with the suboxide carbonyl structure, i.e., the asymmetric C=O stretching peak at $\sim 1800\text{ cm}^{-1}$, and the symmetric C=O stretching peak at $\sim 1750\text{ cm}^{-1}$. The observation that the 1750 cm^{-1} carbonyl peak is stronger than the 1800 cm^{-1} carbonyl peak indicates that the unsaturated suboxide rings were formed predominantly. This is consistent with the results obtained by Grassie and Smith [77]. Similar reactions



Figure 5.4. TGA thermogravimetric curves for poly(4-vinylpyridine).

Table 8-3 FTIR Peak Assignments for PMA Acids

Peak (cm^{-1})	Assignment
3300-2500	$\nu(\text{O-H})$
2911	$\nu_{\text{as}}(\text{CH}_2) = \nu_{\text{as}}(\text{CH}_2)$
2854	$\nu_{\text{s}}(\text{CH}_2) = \nu_{\text{as}}(\text{CH}_2) = \nu_{\text{s}}(\text{CH}_2)$
1670	overtones and combinations of $\nu(\text{C-H})$ and $\delta(\text{C-H})$
1568	$\nu(\text{C=O})$
1480	$\delta_{\text{as}}(\text{CH}_2)$
1454	$\delta(\text{CH}_2) = \delta_{\text{s}}(\text{C-H})$
1380	$\delta_{\text{s}}(\text{CH}_2)$
1261	$\nu(\text{C-H})$ coupled with $\nu(\text{C-C-H})$
1123	isolated deformation coupled with $\delta(\text{CH}_2)$
993	$\nu(\text{C-CH}_3)$
733	$\nu(\text{CH}_2)$ coupled with isolated in-plane bending

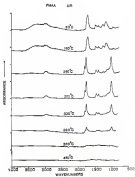


Figure 4.8 FTIR spectra of the polymer reaction at the indicated temperatures during polymerization of PMMA in AIBN.

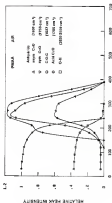


Figure 8.8

Evolution of chemical species during the synthesis of polyacetylene. The x-axis represents Temperature in degrees Celsius. The y-axis represents Arbitrary Units.

were also observed in nitrogen pyrolysis as shown in Figures 6.7 and 6.8.

Additional evidence for this condensation reaction is provided by GC-FTIR results. Figure 6.9 shows the GC chromatogram of volatiles collected from 50% to 250°C in air. The major volatile product (peak P2) was identified as water by comparing the mass spectra with the reference spectra shown in Figure 6.10. This is again consistent with the dehydration reaction. It should be noted that if all the methyl groups were converted into water (with the release of water), the theoretical weight loss should be 10.5%. However, the TGA results show approximately 18 weight loss at the end of the first stage (Figure 6.4) suggesting that the water weight loss might be the result of a limited depolymerization reaction along with organic acid (HAc) release as detailed as shown in Figure 6.11. The detection of HAc species was also reported by Sato et al. [176] in their ion-mobility study of PFPO. Other minor degradation compounds are listed in Table 6.4. (The EPR detector does not respond to H_2O , thus, volatile condensation was not reported.) Similar results were also observed in nitrogen pyrolysis as shown in Figures 6.11, 6.12 and Table 6.4b.

This dehydration reaction was observed to be substantial as shown by the TGA curves in Figures 6.13 and 6.14 for air and nitrogen pyrolysis, respectively.

In both air and nitrogen pyrolysis of PMMA, most of the weight loss (~55%) occurs during the second weight loss stage (Figure 6.5). This stage is indicated by the breakdown of the poly(methylol) structure formed in the first stage. The two-stage TGA results as seen in Figures 6.3 and 6.4 show that the post-degradation of PMMA

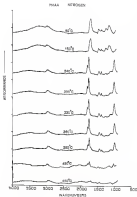


Figure 4-7 IR spectra of the polymer residues at the indicated temperatures during synthesis of PMMA in *n*-hexane.

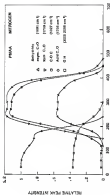


Figure 8.8 Relative peak intensities from the FTIR spectra as a function of temperature during the degradation of PMMA in nitrogen.

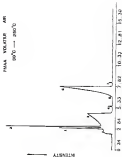


Figure 5.1. Infrared spectrum of red poly(vinylidene fluoride) in air from 3000 to 200 cm^{-1} .

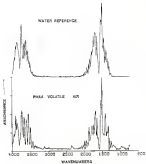


Figure 4 to The IR spectra of the primary volatile product is compared to the reference spectrum for water.

Table 4.8 Decomposition Products from the Pyrolysis of PMMA in Air, 30-350°C.

From 1	ethyl alcohol
2	acetone
3	water ^a
4	acetic acid
5	ethyl acetate
6	2-ethyl vinylidene acid
7	acetic acid

^a Major decomposition product.

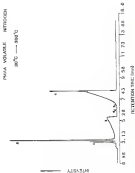


Figure 8.11 Gas chromatogram of PMMA solution collected in nitrogen from 20% to 200%.

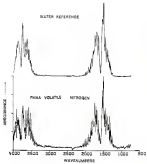


Figure 6 To The IR spectrum of the primary whistle product is compared to the reference spectrum for water

Table 4.5 Decomposition Products from the Pyrolysis of PMA in Nitrogen, 30-300°C.

Peak #	Ident. chemical
1	methane
2	water ^a
3	acetic acid
5	methyl isocyanide
6	n-butyl acrylate ester

^a Major decomposition product



Figure 4.13 DSC and TGA results for PMA in air

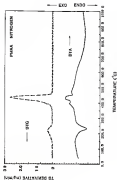


Figure 5.14. DSC and TGA results for PMAA-NITROGEN.

sharply intense (287° and 294°) for the carbonyl C=O stretching peak, the symmetric and asymmetric S-H stretching peaks, and C-H stretching and bending peaks. Similar behavior was observed in nitrogen pyrolysis (Figure 4.4). However, the polyphosphazene structures seem more thermally stable in nitrogen since the corresponding peaks extend to much higher temperatures.

Another important development in the second stage is the formation of crosslinked and cyclic structures. Evidence that crosslinking occurs at this stage was obtained by monitoring changes in solubility of the polymer residues in 0,0-dichloro(p) benzene (DCP) after heat treatment. Initially, the polyphosphazene is completely soluble in DCP. As crosslinking occurs during heat treatment, the percentage of the polymer that becomes insoluble in DCP increases. Figures 4.15 and 4.17 show that almost 100% of the residues formed after 5 hours at 250°C in air and 400°C in nitrogen is insoluble, while less than 1% of the residue is insoluble after 18 hours at 200°C in both air and nitrogen. Further examination of the solubility curves at 250°C for both air and nitrogen pyrolysis as shown in Figure 4.16 indicates that, contrary to the case of PM (Figure 4.15), carbon does not have significant effects on the crosslinking reaction of the polyphosphazene.

The development of cyclic structures is indicated by GC-FTIR results. The gas chromatograms of PMB residues in air and nitrogen are shown in Figures 4.18 and 4.19. Tables 4.5 and 4.6 show that volatile products collected at high temperatures (200-400°C) include cyclic compounds. The development of degradation-resistant polyphos-

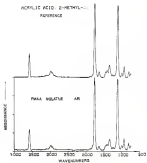


Figure 4.15 The IR spectrum of peak 16 in the gas chromatogram is compared to the reference spectrum for acrylic acid monomer.

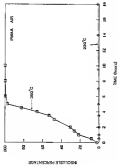


Figure 8. (a) PMAA; (b) PMAA-APM. Percentage of the insoluble precipitate vs. time (hours) at 100°C and 120°C.

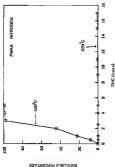


Figure 8.10 Rate of the insoluble percentage of the PMAA reaction in acid treatment time at 100°C and 100% H₂O.

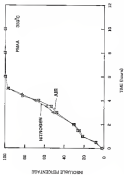


Figure 5. 10. Points of the distribution (percentage of the total residue in the acid residue) as a function of total residue in the acid residue.

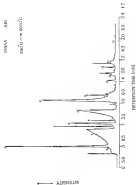


Figure 3-19 Gas chromatogram of PMMA volatiles collected in air from 200°C to 1000°C.

Table 8.8
Decomposition Products from the
Pyrolysis of PMMA in Air,
300–1000°C.

Peak #	1	Retention
	2	Carbon
	3	Water
	4	Formic acid
	5	Acetic acid
	6	2-Methyl acrylic acid
	7	Methyl formic acid
	8	Lactic acid
	9	1-Methyl-2-oxocyclohexanone
	10	3-Methyl glutaric acid
	11	5-Hydroxy-2-methyl hexanoic acid
	12	Cyclopentanone-3-one
	13	Carbaldehyde acid
	14	1,2-Dithiodipropyl carboxylic acid

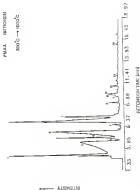


Figure 4.10 Gas chromatogram of PMA solution subjected to nitrogen flow 80°C to 100°C

Table 4.1 Identification Products from the Pyrolysis of PBA in Nitrogen, 350–1000°C

Peak #	1	Structure
2	Water	
3	Acetic acid	
4	Propionic acid	
5	4-Methyl, acetic acid	
6	1,3,5-Trimethyl benzene	
7	3-Methyl, 2-hydroxybenzoic-3-methyl	
8	Methyl, acetic acid	
9	1,3,5,7-Tetramethyl benzene	
10	Residue	
11	1-Methyl, acetic acid	
12	1,3,5-Tetramethylbenzene	
13	4-Methyl, acetic acid	
14	3-Methyl, acetic acid	

structure is also indicated by the higher temperatures required to degrade the last 10-15 wt.% of the polymer, i.e., a third stage is observed in the TGA curves (Figure 4.4). In nitrogen pyrolysis, there is still a large amount of residue at very high temperatures (approximately 8.5 wt.% at 1000°C), suggesting that a charred stage exists. In air, the cyclic and crosslinked structures can be degraded completely by an oxidative mechanism. It is noted, however, that the final degradation temperature is still considerably higher for this than in pure pyrolysis. The oxidative mechanism in air pyrolysis is indicated by the PR curve in Figure 4.11 which shows a strong exotherm during the third weight loss stage. It should be noted that this exotherm is much larger than the second-stage exotherm, despite the much smaller weight loss. This is associated with the development of the cyclic and crosslinked structures during the earlier stages in air pyrolysis, since a large amount of heat energy will be released when these structures are broken down oxidatively.

Pyrolytic Behavior of α -MethylTHA Polymers

1. Degradation Mechanism of α -MethylTHA Polymers

Pyrolysis studies were also carried out with Al_2Cl_3 /THA mixtures. As in the case of "pure" THA, degradation of Al_2Cl_3 /THA mixtures also occurs in three stages as shown by the TGA results in Figure 4.15. The DT record shown in Figure 4.16 and Table 4.8 again indicates that the first stage is dominated by the coordination reaction between the neighboring carbonyl groups, since unlike in the

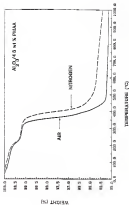


Figure 3 (b) TGA curves for Al_2O_3 -coated alumina in air and nitrogen.

H_2O_2 -PMAA VOLATILE AIR

$20^\circ C \rightarrow 100^\circ C$

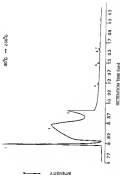


Figure 4.22 Gas chromatogram of H_2O_2 -PMAA volatile collected in air from 2000 to 20000

Table 4.1 Decomposition Products from the Pyrolysis of $\text{Al}_2\text{O}_3/\text{PMMA}$ Mixtures in Air, 50–600°C

Peak #	Assignment
1	H_2O^a
2	3-Methyl acrylate acid
3	Hex-5,6-dimethyl, undecanoic acid
4	3-Methyl isocyanuric
5	1-Cyanoacetic-3-one
6	2,6-Di-tert-butyl-1,4-dioxane

^a Major decomposition product

major volatile product collected in this stage. Similar IR results in also obtained for nitrogen precipitate as shown in Figure 3.12) and Table 3.3. Volatile products collected at high temperatures (>100°C) are listed in Tables 3.10 and 3.11 for air and nitrogen precipitates, respectively. As shown in Tables 3.10 and 3.11, very high percentages of cyclic compounds, i.e., oxirane and acetylene, were detected in both atmospheres. However, according to the data obtained from the FTIR analyzer, much higher percentages of 1-vinylcyclohexane and 1,2-epicyclohexanecarboxylic anhydride were detected for nitrogen precipitate than air precipitate. This is consistent with the results for "pure" polymer in that acetylenic anhydride can be more effectively broken down to smaller molecules in air but not in nitrogen.

Although PMMA and PMA have very different degradation mechanisms, similar surface reactions are observed in monomer/polymer mixtures. The late-stage FTIR spectra of Al_2O_3 /PMMA mixtures in Figures 4.16 and 4.17 show the development of the carbonyl peak at $\sim 1775\text{ cm}^{-1}$ in air and nitrogen. In contrast with PMMA, the reaction was more extensive with the oxidized (carboxylated) Al_2O_3 (Figures 4.18 and 19) and with more Lewis acidic oxides (germanium trioxide) (Figures 4.20 and 4.21). No reaction was observed with more reduced materials, i.e., SnO_2 (Figures 4.22 and 4.23) and silicon (Figures 4.24-4.25).

The observation of surface carboxylate species was also reported by Rochester [19], who studied the conversion of carboxylic acids on metal oxides such as alumina and titania. He also reported that,

Table 5.3 Decomposition Products from
the Pyrolysis of $\text{Al}(\text{C}_2\text{H}_5)_3/\text{TMAC}$
Mixture in N_2 30–500°C

Peak # 1 Unknown

2 Acetone

3 Water^a

4 *n*-Butyl acrylate acid

5 *n*-Butyl butene

6 Mono-*n*,*i*-Butylal acrylate acid

7 Butyl-*n*,*i*-butyl acrylate acid

8 1-Cyclopentyl-1-prope

^a Major decomposition product

Table 3.16 Decomposition Products from the Pyrolysis of Al_2O_3 -PAA Mixtures in N_2 (200–1000°C)

Peak #	1	Carbon dioxide
	2	Methanol
	3	Propanol
	4	Acetone
	5	Water
	6	Acetic acid
	7	Acetone (acetylaldehyde)
	8	2-Butanone
	9	Methyl methacrylate
	10	Propionic acid
	11	2,4-dimethyl 2,3-heptadien-4-one
	12	8-Carvone
	13	Methyl ^a
	14	2-methyl butyric acid
	15	1,1,3-Trimethyl benzene
	16	1,2-Cyclopropanedimethylacetic acid
	17	5-Hydroxy-3-methyl acid
	18	2-Methyl-4,5-dihydro-2,3-furandione
	19	1-Cyclopropyl acetic anhydride ^a
	20	5-Hydroxy-3-methyl-malic acid
	21	2-Methyl acrylic acid
	22	2-Methyl-3-butanone
	23	2,3-Dimethyl-1-butanone
	24	2,4-Dimethyl-3-pentanone
	25	2-Methyl-3-butanone
	26	1,2-Cyclohexanedimethylacetic anhydride ^a
	27	4-Butanone
	28	2-Methyl-3-butanone
	29	2-Methyl-2-butyl acetoacetic acid

^a Major decomposition products

ALIPHATICS VOLATILE

AIR 200°C → 1000°C

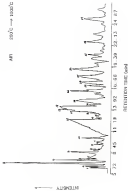


Figure 8.44 Gas chromatogram of aliphatic volatiles collected in air from 200°C to 1000°C

ALDOPHOSPHATE MONOCRYSTAL

WATERGAS 3000°C → 1000°C

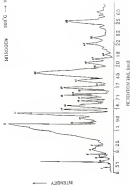


FIGURE 1. X-ray diffraction pattern of Aldophosphate Monocrystal. The x-axis is reciprocal lattice space (Å⁻¹).

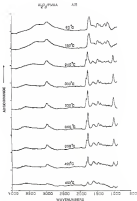


Figure 8.28 FTIR spectra of the polymer matrix at the indicated temperatures during synthesis of $\text{Mg}_2\text{P}_2\text{O}_7$ mixture in air.

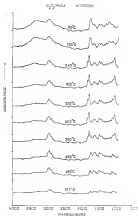


Figure 3-45 FTIR spectra of the polymer reaction at the indicated temperatures during synthesis of $\text{Al}_2\text{O}_3/\text{PMMA}$ clusters in air (1 atmosphere).

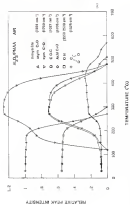


Figure 6. Relative peak intensities (from the FTIR spectra) as a function of temperature for the spectra of poly(2-vinylpyridine) in air. The symbols (a) through (z) are used to identify the peaks in the spectra. The symbols (aa) through (ae) are used to identify the peaks in the spectra of poly(2-vinylpyridine) in air. The symbols (a) through (z) are used to identify the peaks in the spectra of poly(2-vinylpyridine) in air. The symbols (aa) through (ae) are used to identify the peaks in the spectra of poly(2-vinylpyridine) in air.

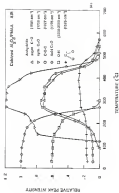


Figure 4. DSC curves.

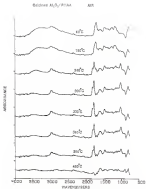


Figure 6-25 FTIR spectra of the polymer residues at the indicated temperatures during pyrolysis of solvent $\text{Al}_2\text{O}_3/\text{PMMA}$ obtained in air.

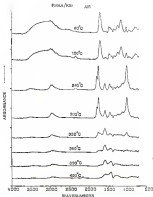


Figure 5.30 FTIR results showing 17 spectra of the polymer residues at the indicated temperatures, for (21) relative post-irradiation as a function of temperature during pyrolysis of PMMA/MDI mixture in air.

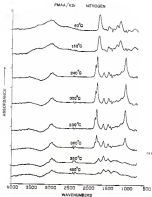


Figure 4.31 FTIR results showing (I) spectra of the polymer residues at the indicated temperatures and (II) relative peak intensities as a function of temperature during pyrolysis of PMAA/AN mixtures in nitrogen.

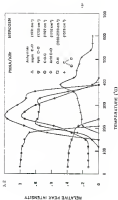


Figure 14. TGA and DSC curves of poly(amide-imide) 14.

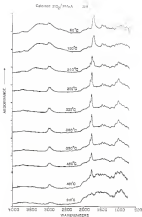


Figure 4-20 FTIR spectra of the polymer at the indicated temperatures during synthesis of isolated $\text{Si}_2\text{P}_{10}\text{O}_{28}$ clusters in air

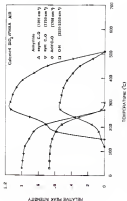


Figure 4-33 Infrared peak intensities (from the FTIR spectra) as a function of temperature during pyrolysis of oxidized poly(vinylidene fluoride) in air.

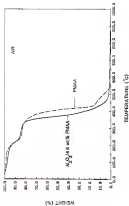
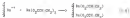


Figure 4.10 TGA results for PMAA and $\text{Al}_2\text{O}_3/\text{PMAA}$ nanocomposites in air.

Although the isophthalic acids can be readily separated from nitroisobutyric acids adsorbed on silica surface via hydrogen bonding, the chlorinated isophthalates are kinetically retained on the surfaces of silica oxides.

Although the surface interaction between AlH_3 and PMA could contribute from the hindered hydrogen bonding, i.e. much higher temperatures are needed to achieve complete burning as shown in Figure 8.18, this surface interaction may be utilized to improve the reinforcement of plastics and elastomers. For example, isophthalic (substituted) crystallites are formed with the siliceous layer as the external surface of the structure. This layer was coated with isophthalic acids to form chlorinated isophthalates. Thus, treatment of isophthalic diisocyanates with isophthalic acid has been used for the preparation of elastomer-silica fillers [10].

The reaction of polymeric acids, for example, polyisophthalic acid, with metal oxides such as organosilica or silica oxides, or with metal-organosilica or metal-organosilicates, has been used in the formation of composites and films grafted [10]. The hardening effect occurs as a result of the organosilica acid on the mineral, followed by diffusion of the released silicic acid into the acid phase. This results in the formation of a hard isophthalic composite containing the silicic particles in an acidic cross-linked polymeric matrix. The improved bonding was also reported for SiO_2 or Fe_2O_3 -nanofiller treated with a solution isophthalic acid of the same acid, followed by drying at elevated temperatures [10]. The improved bonding arises from the formation of isophthalic ligands with the nanocomposite surface.



3. Enhancing Degradation of PBAA Resin

Polymer pyrolysis can be enhanced by using selectively low concentrations of additives which catalyze the degradation reactions. For example, Figure 4-10 shows that 0.1 wt% addition of potassium permanganate, KMnO_4 , or silver acetate, $\text{AgC}_2\text{H}_3\text{O}_2$, significantly decreases the degradation temperatures during the final stage of PBA pyrolysis in air. DTA results in Figures 4-11 and 4-12 also show very strong and sharp exotherm development at this stage as opposed to the pure polymer. Similar effects were also observed with nickel acetate, $\text{Ni}(\text{C}_2\text{H}_3\text{O}_2)_2$, as shown in Figure 4-10, although the enhancement is not as strong as the addition of potassium permanganate and silver acetate. Consistent with this are the DTA results in Figures 4-11 and 4-12, which show less strong and sharp exotherms as in Figures 4-10 and 4-11.

These catalytic additives were also tested for their catalytic effects in $\text{Al}(\text{C}_2\text{H}_3\text{O}_2)_3/\text{PBA}$ mixtures. Table 4-13 shows the exotherm reaction temperatures of various $\text{Al}(\text{C}_2\text{H}_3\text{O}_2)_3/\text{PBA}$ mixtures fired in air. After being fired at 100%, $\text{Al}(\text{C}_2\text{H}_3\text{O}_2)_3/\text{PBA}$ mixtures with 0.1 wt% addition of potassium permanganate show about the same exotherm temperatures as $\text{Al}(\text{C}_2\text{H}_3\text{O}_2)_3/\text{PBA}$ mixtures without additive fired at 100%. The enhancement of PBA pyrolysis can be explained by the strong oxidizing nature of potassium permanganate.

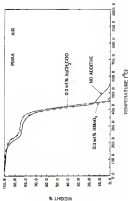


Figure 1.10 TGA curves showing the effects of silver acetate and potassium persulfate on PBD weight loss in air.

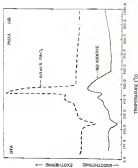


Figure 4.16 DSC results showing the effects of titanium persulfate on PMA pyrolysis solution 9.



Figure 4-20

Effect of silver nitrate on PMMA crystallization behavior. The effect of silver nitrate on PMMA crystallization behavior is shown in Figure 4-20.

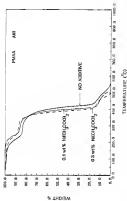


Figure 4. (a) TGA results showing the effects of acetal content on PMA weight loss in air.

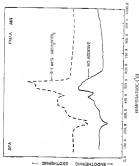


Figure 5.40 DSC results showing the effects of 2,4-dinitrophenol on thermal degradation of PMMA and ABS.

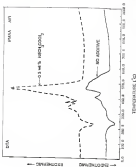


Figure 5.30 DSC results showing the effects of 0.8 minutes of cure on PMA and PMMA (curves are for the).

Table 4.12 Carbon Residue Concentrations of $\text{Al}_2\text{O}_3/\text{TiO}_2$ Residues Fired in the Presence of Low Concentration Additives.

Sample	Temperature	Atmosphere	Carbon Concentration
$\text{Al}_2\text{O}_3/\text{TiO}_2$			
(no additive)	1500°C	Air	166 ppm
$\text{Al}_2\text{O}_3/\text{TiO}_2$			
(as sintered)	800°C	Air	325 ppm
$\text{Al}_2\text{O}_3/\text{TiO}_2$ with			
0.5 wt% KNO_3	800°C	Air	17% ppm
0.5 wt% $\text{Al}(\text{CH}_3\text{COO})_3$	800°C	Air	120 ppm
0.1 wt% $\text{Al}(\text{CH}_3\text{COO})_3$	800°C	Air	980 ppm
0.5 wt% $\text{Al}(\text{CH}_3\text{COO})_3$	800°C	Air	817 ppm

Summary and Conclusions

Although the structure of PMA differs from PMB only in the replacement of a methyl group by a hydrogen atom in carboxylic acid group (instead of the ester group), the pyrolytic behavior is essentially different for these two polymers. Instead of the single-stage process observed in PMB, the TGA results for pyrolysis of PMA showed that degradation occurs in three stages. FTIR and GC results indicated that the first stage was dominated by intramolecular degradation reaction between the neighboring carboxyl groups with the formation of six-membered polycyclic structures. The second stage, accounting for most of the weight loss, was dominated by the breakdown of the polycyclic structures formed in the first stage. Crosslinking and cyclization also occurred during the process. These degradation reactions yielding rigid crosslinked structures can be broken down relatively at higher temperatures in air pyrolysis. In contrast, there is a large amount of residue at high temperatures in nitrogen pyrolysis.

Despite the difference in degradation mechanism for PMA and PMB, similar surface reactions were observed in catalytic polymer reactions. In comparison of carboxylation between highly polarized acid groups (carboxyl and carbonyl) and Al_2O_3 surface. As observed with PMB, the reaction was more intensive with the retained (oligomerized) Al_2O_3 and with more basic supports (high silanol

breaked. No reaction was observed with the oxidized materials, Li_2O , Al_2O_3 and diamond.

Pyrolysis of PMMA was enhanced by using relatively low concentrations of oxidizer. Results showed that 0.3 wt% addition of KMnO_4 or KNO_3/O_2 significantly decreases the final stage degradation temperatures of PMMA by as much as $\sim 10^\circ\text{C}$. Results further showed that Al_2O_3 /PMMA mixtures with the addition of KMnO_4 showed about the same carbon residue distributions at a 100°C lower firing temperature than those without the addition of KMnO_4 .

CHAPTER VII SUMMARY AND CONCLUSIONS

A variety of techniques, including thermal gravimetric analysis (TGA), differential thermal analysis (DTA), Fourier transform infrared (FTIR) spectroscopy, and gas chromatography (GC), were used to investigate the pyrolysis behavior of poly(vinyl butyral), PVB; poly(vinyl acetate), PVAc; poly(methacrylic acid), PMAA; and poly(methacrylic alcohols). Information on the degradation mechanism was obtained by analyzing both residues and volatiles.

Pyrolysis Behavior of PVB and Poly(vinyl Alcohols)

The initial pyrolysis of PVB is controlled by the elimination of butyrol and hydroxyl ester groups. Available evidence indicates that main chain scission, crosslinking, and cyclization also occur during the early stages of pyrolysis. Higher temperatures are required to break down the degradation-resistant cyclic and crosslinked structures.

Degradation behavior of PVB is highly dependent on the pyrolysis atmosphere. Pyrolysis is initially accelerated in air as compared to nitrogen due to oxidative scission. Oxidative degradation is followed by the extensive development of carbonyl groups during air pyrolysis. At intermediate temperatures, a larger weight loss was observed in nitrogen as compared to air. This apparently reflects the

slow development of carbonyl groups and the less rapid development of crosslinked structures during nitrogen pyrolysis. During the late stages of pyrolysis, degradation to the extent of steps is extremely difficult due to carbonization.

FTIR observed with Al_2O_3 surfaces via hydrogen bonding between hydroxyl side groups in the polymer and hydroxyl groups on the particle surfaces. During pyrolysis, the FTIR degradation mechanism was found very similar to that of the polymer alone. In direct chemical reactions took place between PTH and Al_2O_3 at higher temperatures.

Pyrolytic Reaction of PTH and Carboxy-PTH Polymers

As expected, TGA, DTG, FTIR, and GC results showed that PTH degraded by the depolymerization mechanism. PTH resins with higher molecular weights showed less thermal stability than the lower ones due to presence of more weak linkages. The reaction was accelerated by the presence of oxygen.

Degradation of PTH in Al_2O_3 /PTH mixtures also occurred primarily by depolymerization. However, a surface reaction between PTH and Al_2O_3 at higher temperatures was indicated by observation of an FTIR absorbing peak for the carbonyls (as not exhibited volatile components in the GC results). This interaction between PTH carbonyl groups and alumina ions on the Al_2O_3 surface results a "blocking effect" on the depolymerization process, so the existing reaction was retarded and much higher temperatures are required to achieve complete burnout. This surface reaction was more extensive

with reduced (overoxidized) Al_2O_3 (due to greater amount of the positively charged aluminum ions) and with higher chain entanglement (i.e., higher inherent). Results also showed that oxidized PPA reacted more strongly toward potassium bromate than that of acetylated PPA. This was shown by the much stronger development of carboxylic end group, and more importantly, the development of amorphous structure at higher temperatures in the oxidized PPA/PPA mixtures. In reaction, we observed that the process had a more complex character (i.e., Al_2O_3 , diamorph).

The effects of processing variables (i.e., synthesis atmosphere and flow rate, heating rate, and sample size) on the synthesis behavior of Al_2O_3 /PPA mixtures were also investigated. Synthesis was delayed for larger sample size, higher heating rate, and oxidizing atmosphere. However, unlike PPA, the degradation mechanism is not affected by these variations. It was also shown that addition of low concentration of peroxide, i.e., $\text{H}_2\text{O}_2/\text{Al}_2\text{O}_3$ and $\text{H}_2\text{O}_2/\text{Al}_2\text{O}_3$, significantly enhanced the early stage degradation of PPA.

Synthesis Behavior of PPA and Oxidized PPA Mixtures

Although the structure of PPA differs from PPA only in the replacement of a methyl group by a hydrogen atom (i.e., a carboxylic acid group instead of the ester group), the synthesis behavior is drastically different for these two polymers. Instead of the single-stage process observed in PPA, degradation of PPA showed three stages in PPA. FTIR and GC results indicated that the first stage was

initiated by a deprotection reaction between the neighboring carboxyl groups with the formation of a six-membered polycyclic structure. This structure breaks down during the second stage, but crosslinking and cyclization apparently occur during the process... These degradation-resistant cyclic and crosslinked structures can be broken down selectively at higher temperatures in air pyrolysis. In contrast, there is a large amount of residue at high temperatures in nitrogen pyrolysis.

Despite the differences in the degradation conditions for PBA and PBA, similar surface reactions were observed in various polymer systems. As observed with PBA, the reaction was more vigorous with the reduced (dehydrogenated) Al_2O_3 and with more active components (e.g., potassium bromide). No reaction was observed with more inert materials, i.e., SiO_2 and diamond.

Pyrolysis of PBA was enhanced by using small amounts (~0.3 wt.-%) of SnO_2 or AgClO_4 . Addition of SnO_2 was shown significantly lower the carbon residue concentrations of $\text{Al}_2\text{O}_3/\text{PBA}$ mixtures fired at 800°C in air.

APPENDIX I
LISTED SPECIMENS OF THE BIRD

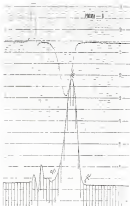


Figure A-1 Liquid chromatogram of PMA-2

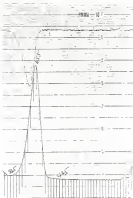
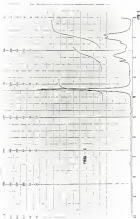


Figure A.2: Liquid chromatogram of P99A-10



Figure 8.2 Liquid chromatogram of 900a-11.

APPENDIX B
B.1 THE EFFECTS OF TPOA REDUCTION


 Figure 1-5. R_p vs. t for polymerization of styrene.

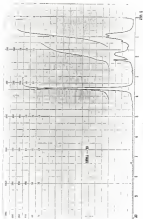


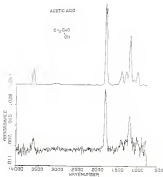
Figure 8.2 IR and Raman spectra of PMMA-13.

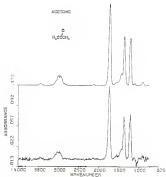


Figure 4-3. % of control of area (A).

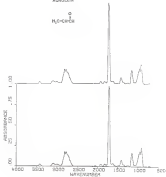
APPENDIX C
FTIR SPECTRA AND STRUCTURAL FORMULA
OF THE VOLATILE PRODUCTS

Note: FTIR spectrum (top) of the volatile product is compared to the reference spectrum (top) for the indicated compound.

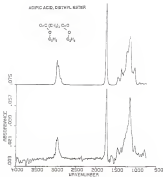




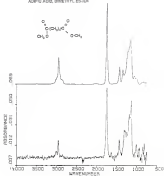
ADONOLIN



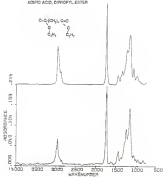
ACIDIC ACID, INTERNAL, BRON



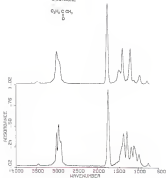
ADIPIC ACID, DIMETHYL ESTER



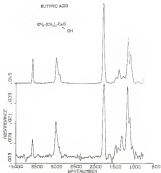
ACETIC ACID, DIETHYLESTER

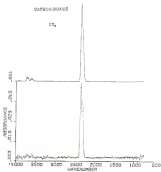


8-ETHYL-2-ONE

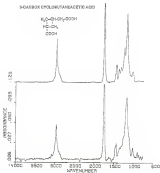


BUTYRIC ACID





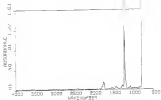
4-CARBOXY-6-POLYMERACETIC ACID



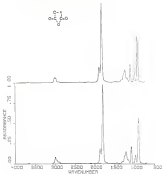
280

CHLOROPHORM

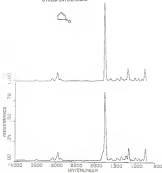
CHCl_3

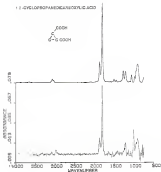


1,3-DICHLOROBUTANEDIOIC ACID HYDRIDE

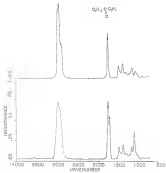


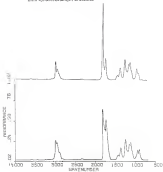
OXYCLOPENTANE-2-ONE

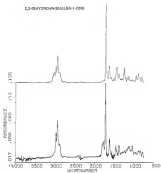




8-DECANONE



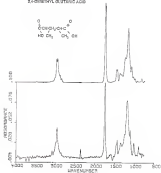
2.0H⁺ 4,8-DICHLORO-2,6-DIMETHYLPHENOL



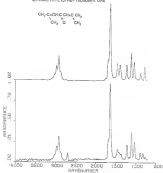
1. **IDENTIFY THE PROBLEM**



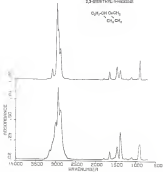
2,4-DIMETHYL GLUTARIC ACID



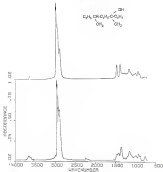
3,4-DIMETHYL-2,5-HEPTADIENE-4-ONE



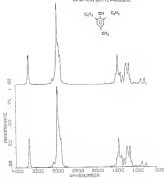
2,3-DIBENZO-1,4-DIOXANE



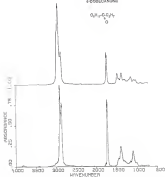
3,6-DIBUTYL-3-OCTANOL



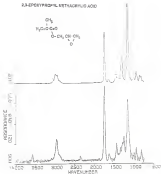
2,4-DI-TERT-BUTYL P-CRESOL



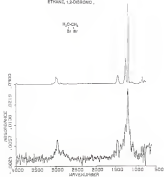
4-COSBUOXANONE



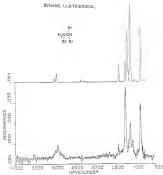
2,3-EPIHYDROXYL METHACRYLIC ACID



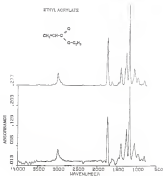
ETHANE, 1,2-DIBROMO-

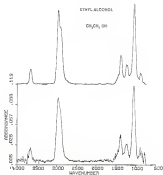


ETHYLENE, 1,1,2,2-TETRABROMO-

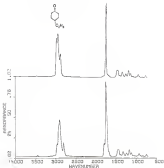


ETHYL ACRYLATE

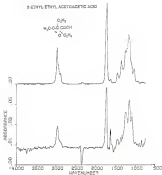




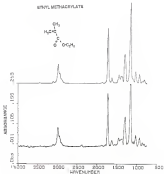
4 ETHYL CYCLOHEXANONE

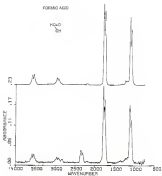


B-ETHYL-ETHYL ACETOACETIC ACID

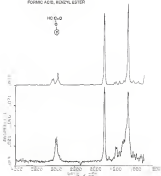


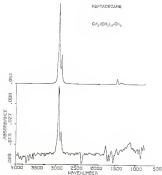
VINYL METHACRYLATE



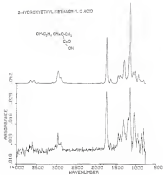


FORMIC ACID, BENZYL ESTER

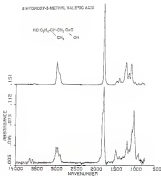




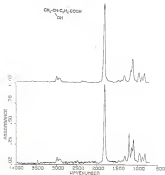
2-HYDROXYETHYL CITRADELPH-2-ACID

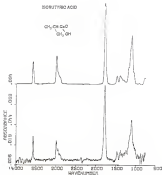


2-HYDROXY-3-METHYL-3-ALLOXIC ACID

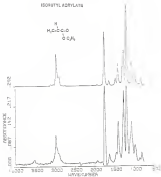


4-HYDROXY-8-HELENIC ACID

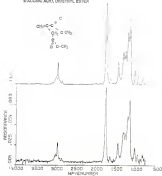




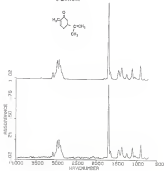
ISOBUTYL ACRYLATE

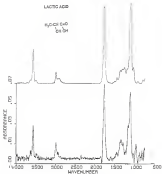


ITACIC ACID, DIMETHYL ESTER

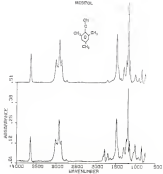


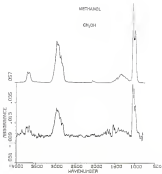
L-CARVONE

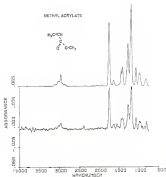


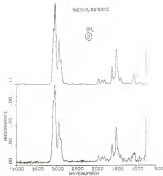


MADDFOL

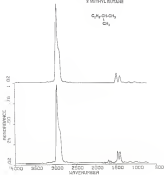




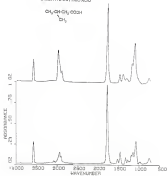


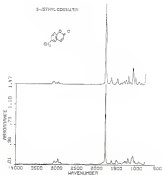


2-METHYL BUTANE

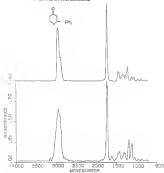


3-METHYL BUTYRIC ACID

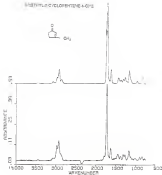




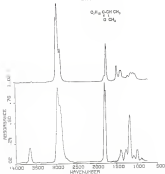
3 METHYL-CYCLOHEXANONE



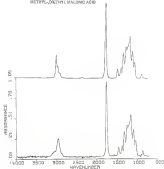
3-METHYLCYCLOHEPT-4-EN-2-ONE



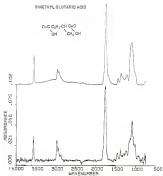
3-METHYL-2-DECANONE



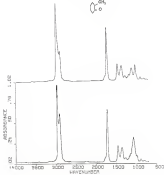
METHYL-DIPHENYL MALONIC ACID



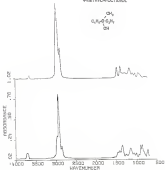
BIMETHYLSUCARIN-403



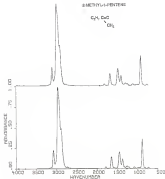
3-METHYL-3-PENTANONE

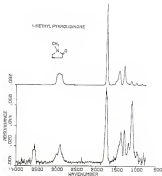


4-ETHYL-4-OCTANOL

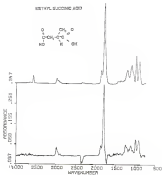


2-METHYL-1-PENTENE

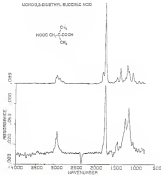


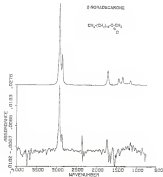


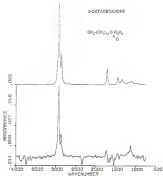
DIETHYL SUCCINATE, 850

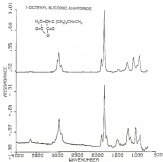


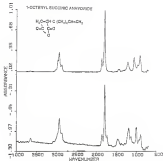
MONO(3,3-DIETHYL SUCCINIC ACID

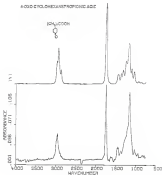


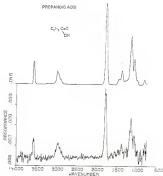




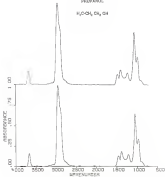




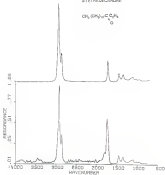




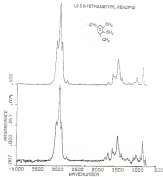
PROPANOL



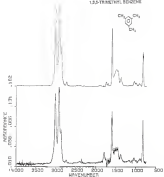
3-TETRADECANONE



1,2,3,4-TETRAMETHYL BENZENE



1,3,5-TRIMETHYL BENZENE



APPENDIX B
ABSORPTION SPECTRUM OF PPSA BEADS INTO
 Al_2O_3 SURFACE THROUGH POLYMER SOLUTIONS

SYNOPSIS

To obtain the absorption spectrum for Al_2O_3 /PPSA suspensions prepared with various solvents,

Materials

<u>Polymer</u>	PPSA-10 (as described in Chap. 8.1)
<u>Solvents</u>	Al_2O_3 (as described in Chap. 17.1)
<u>Solvents</u>	Acetone
	Benzene
	Chloroform
	4:1 benzene/tetrahydrofuran

Procedure

1. Prepare eight to ten polymer solutions with concentrations from 0 to 4.5 g/dl. for each solvent.
2. After the polymer dissolves completely, add the preweighed Al_2O_3 powder (200 mesh) into the polymer solutions at last time. The total volume of the suspension is 100 ml.
3. Mix by ultrasonication (15 min) to break down polymer agglomerates.
4. Age the suspensions for 24 hours at room temperature.

- 6) Centrifuge the suspensions at 11,000 rpm for 20 min.
8. Take out the centrifuge tubes, and carefully pour the supernatants into clean bottles.
7. Carefully withdraw without upset or vigorous agitation from the bottom in the provided vialine and wet dry at 60°C for 48-68 hours.
8. Weigh the sample pans after the drying procedure is complete.
9. Calculate the weight difference before and after absorption equilibrium has been achieved.
10. Construct the absorption isotherms. (See Figure 5-1.)

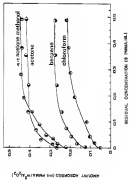


Figure 2. Dependence of the rate of polymerization on the initial concentration of monomer for different solvents.

REFERENCES

1. S.Y. Kato, Trans. Indian Cer. Soc., 31, 81 (1950).
2. H.C. Williams, Am. Ceram. Soc. Bull., 50, 577, 586 (1971).
3. H.C. Sheng, Japanese Patent 2,443, June 13, 1950.
4. E. Maier, U.S. Patent 2,953,347, Apr. 23, 1958.
5. E. Maier, T. Tanaka, and T. Wicks, U.S. Patent 3,046,365, Sep. 29, 1969.
6. E.A. Bell, T.D. Wilson, and J.E.H. Guder, U.S. Patent 3,025,756, May 5, 1963.
7. E. Maier and J.E. Guder, U.S. Patent 3,017,748, Aug. 5, 1964.
8. J. Shultz, Ceram. Bull., 49 [11], 1096 (1969).
9. F.A. Castiglione, R.D. Frost, and C.R. Williams, U.S. Patent 3,779,384, Sep. 11, 1974.
10. J.E. Guder, Trans. Am. Cer. Soc., 52, 141 (1969).
11. E.E. Goss, Jr., "The Kinetics of Organic Matter Reactions", p. 225 in Organic Reactions (P. D. Bartlett, Ed.), Vol. 1, Wiley & Sons, New York, 1955.
12. E.E. Goss and E.J. Gilman, Am. Ceram. Soc. Bull., 51, 579 (1972).
13. E. Maier and E.E. Guder, Am. Ceram. Soc. Bull., 52, 1294 (1973).
14. F.A. Williams, E.A. Bell, and T.D. Wilson, Am. Ceram. Soc. Bull., 52, 744 (1973).
15. T.D. Wilson and E.F. Johnson, Am. Ceram. Soc. Bull., 52, 218 (1973).
16. H. Siefert, Zeitschrift für Naturwissenschaften, 22, 81 (1977).
17. H.A. Rabinow, U.S. Patent 3,928,719, June 7, 1976.

14. J.R. Braveman and T.L. Frazee, *U.S. Patent 3,774,211*, (1969), 2.
15. K. Suzuki and R. Ogihara, *Topol-Synthes-Rei.*, 22 (11), 25 (1994).
16. K. Suzuki and R. Ogihara, *Topol-Synthes-Rei.*, 22 (4), 210 (1994).
17. R.H. Weisler, *Bull. Am. Chem. Soc.*, 22 (11), 280 (1941).
18. G.H. Smith, Jr., *J. Am. Chem. Soc.*, 21 (3-4), 426 (1944).
19. D.F. Bailey, *U.S. Patent 3,084,871*, Mar. 19, 1964.
20. J.R. Harvey and R.H. Weisler, *Am. Chem. Soc. Bull.*, 22 (8), 497 (1941).
21. R.H. Weisler, C.H. Warkoff, and J.R. Lewis, *Advances in Catalysis*, 5, 284 (1954).
22. I. Pollman and H. Pollman, *Isotopenum.*, 5, 54 (1961).
23. R.E. Ryan, *Nuclear Reaction Section Symposium*, Vol. 24, *IAEA-CN-24/24*, New York, 1961.
24. F.L. Wiley and R.H. Goodwin, *J. of Catalysis*, 1, 319 (1945).
25. L. Karlsson, *Chemical Engineering Science*, 26, 495 (1971).
26. W. McILWAIN and L. Wiley, *Am. Chem. Soc. Bull.*, 21 (8), 545 (1940).
27. J.R. Topp, *J. Nuclear Materials*, 1, 307 (1963).
28. R.D. Fisher, *Proc. Nuclear Energy*, 12 (3), 146 (1966).
29. R.H. Weir, "New Oxide Catalysts", p. 147-161 in Advanced Catalysis in Organic Chemistry, R.D. Fisher, Ed., New York, 1967.
30. R. Fieser and R.H. Weir, *J. Am. Chem. Soc.*, 83, 4971 (1961).
31. R.F. Fieser, *J. of Catalysis*, 5, 371 (1963).
32. R.H. Weir and R. Fieser, *J. Am. Chem. Soc.*, 83, 2988 (1961).
33. R.E. Greenhill, "Nuclear Reaction and Associated Problems: Reaction and Commercial Processes", p. 275 in Organic Syntheses and Catalysis by Homocatalysis, Edited by J.F. Greenhill, R. Adams and R. Garwood, J. Wiley Publishing Co., Boston, MA, 1962.

25. J. Baker, "Geometry in Catalysis by Transition Metal Salts", p. 1 in Surface Properties and Catalysis by Solids, Edited by J.F. Kuntz, R. Imura, and C. Sereno. N. Reidel Publishing Co., Dordrecht, 1984.
26. E.A. Milder, "The Heat Induction of Spontaneous", p. 29 in Catalysis, Vol. 3, Edited by E. Eichel and A. Imura. The Chemical Society, Burlington House, London, England, 1980.
27. E. Finke, The Kinetics of Catalytic Reactions, Dover, p. 1. Academic Press Inc., New York, 1987.
28. G.L. Thomas, Catalytic Processes and Product Analysis, p. 203. Academic Press Inc., New York, 1970.
29. E.A. Milder, Aspects of Degradation and Stability of Polymers, Edited by E.A. Milder, Elsevier, Amsterdam, 1978.
30. E. Gracia and E. Smith, "Thermal Degradation", p. 23-24 in Polymer Degradation and Stabilization, Cambridge University Press, Cambridge, 1980.
31. T. Kelen, "General Aspects of Polymer Degradation", p. 3 in Polymer Degradation, Van Nostrand Reinhold Co., New York, 1970.
32. E.T. Conley, Thermal Stability of Polymers, p. 12-15. Marcel Dekker, New York, 1950.
33. G.A. Johnson, J. Kharasch - Sci.-Chem., 177 (2), 127 (1942).
34. E. Schmidt, "Thermal Degradation", p. 25 in Polymer Degradation, Mechanisms and Practical Applications, Marcel Dekker, New York, 1977.
35. E. Gracia, History of High Polymer Degradation Processes, Interscience, New York, 1980.
36. E. Kelen, "Degradation", p. 33-34 in Polymer Degradation, Van Nostrand Reinhold Co., New York, 1970.
37. E. Schmidt, Polymer Degradation, Mechanisms and Practical Applications, Marcel Dekker, New York, 1977.
38. J.F. Pignatelli and E.A. Finke, "Degradation and Synthesis Mechanisms", p. 175 in Synthesis and Use of Polymer Materials, Edited by E.A. Finke and E.A. Levy. Marcel Dekker, Inc., New York, 1985.
39. E. Gracia and E. Smith, "Thermal Degradation", p. 12-13 in Polymer Degradation and Stabilization, Cambridge University Press, Cambridge, 1980.

33. E. Grassie, "Fundamental Chemistry of Polymer Degradation", pp. 3-11 in Weathering and Degradation of Plastics, Edited by E. A. Fisher, Reinhold Publishing Co., New York, 1964.
34. E. Grassie and E. Scott, "Thermal Degradation", p. 14 in Polymer Degradation and Stabilization, Cambridge University Press, Cambridge, 1973.
35. F. Sauer, "General Aspects of Polymer Degradation", p. 4 in Polymer Degradation, Van Nostrand Reinhold Co., New York, 1960.
36. F. S. Dainton, *J. Appl. Polym. Sci., Appl. Polym. Symp.*, **1968** (1969).
37. J. A. Ryan and E. B. Flint, "Degradation and Pyrolysis Mechanisms", p. 169 in Pyrolysis and G. in Polymer Analysis, Edited by E. A. Mahan and E. J. Levy, Marcel Dekker, Inc., New York, 1964.
38. E. Doubly and E. Sael, *Angew. Chem.*, **71**, 387 (1959).
39. E. Doubly and E. Sael, *J. Polym. Sci. A*, **11**, 171, 199 (1963).
40. G. A. Farnham, *Int. Rev. Standards Spec. Pub.*, **37**, pp. 29-46, 1972.
41. J. F. Jackson and A. Ledwith, Spontaneous, Radiation and Chemical in Polymer Chemistry, John Wiley & Sons, New York, 1964.
42. J. F. Nixon, "Thermal Degradation of Polymers", p. 425-446 in Quartz Analysis, Vol. 14, Edited by G. B. Beards and C. R. B. Cooper, Elsevier Publishing Co., Amsterdam, 1975.
43. E. Azziz, T. Hill, and F. S. Mayo, *J. Org. Chem.*, **31**, 1976 (1966).
44. E. V. Degale, *Pure Appl. Chem.*, **11**, 91 (1967).
45. B. Bimberg and J. Talle, *Mon. Chem. Phys.-Org. Chem.*, **3**, 127 (1967).
46. L. Reich and E. B. Flint, Introduction of Macromolecules and Polymers, Marcel Dekker, New York, 1964.
47. E. J. Carlsson and G. B. Wilson, *Macromol.*, **3**, 377 (1964).
48. F. S. Mayo and E. B. Dineen, *Polym. Eng. Sci.*, **3**, 262 (1963).
49. E. J. Carlsson, F. Sato, and G. B. Wilson, *Macromol.*, **3**, 466 (1964).
50. J. A. Manson, E. B. Halpern, and F. S. Gay, *J. Polym. Sci., Part A*, **3**, 3871 (1965).

71. J.F. Longue, *J. Appl. Polym. Sci.*, **22**, 303 (1978).
72. J.F. Longue, *J. Polym. Sci., Part A*, **1**, 791 (1963).
73. L. Reich and E.R. Simcoe, *J. Polym. Sci., Part A-1*, **3**, 929 (1965).
74. R. Gratch and E. Sata, "Fundation of Polymer", p. 68 in Polymer Synthesis and Characterization, Cambridge University Press, Cambridge, 1968.
75. R.G. Wessell, P. Walla, and J. Katta, *J. Polym. Sci.*, **2**, 511, 521 (1962).
76. R. Gratch, N.S.J. Ryan, and P. Angermundtner, *J. Appl. Polym. Sci.*, **22**, 799 (1978).
77. R. Levi, M. Gerson, T. Schatz, and A. Yehoshua, *Rev. Polym. J.*, **15**, 377 (1983).
78. G.W. Michallia, E. E. Derogian, M. S. Melniker, and R.F. Ross, *Rev. Polym. J.*, **12**, 126 (1980).
79. E.F. Shostakov and G.M. Papisov, *Dokl. Akad. Nauk SSSR*, **22**, 1075 (1961).
80. E.F. Shostakov, *Polym. Sci. USSR*, **3**, 191 (1961).
81. M.F. Smith, *Parities A, Sci. and Res.*, **20**, 38 (1983).
82. C.H. Ho, unpublished work.
83. F.A. Og and E. Linton, *J. Appl. Polym. Sci.*, **22**, 1027 (1981).
84. W.R. Allen, R.H. Stone, G.R. Schaffner, E.W. Lee, and J.W. Williams, "Pyrolysis of Poly(Vinyl Acetate) Studied: 2. Reproduction Mechanism", p. 549-558 in Carbolic Polymer Science II, A. Gratch Symposium, Vol. 1, Edited by A.G. MacCall, T.H. Pinner, and A. Knappe, American Carbolic Society, Waterville, ME, 1981.
85. W.R. Collins, L.W. Daly, and R.E. Wheeler, Introduction to Polymer and Super Spectroscopy, Academic Press, New York, 1979.
86. C. Mariani, *Mater. Lett.*, **2**, 143, 389 (1981).
87. R.M. Silverstein, G.M. Bassler, and T.C. Morrill, Spectroscopic Identification of Organic Compounds, John Wiley, New York, 1981.

88. E. Gratch and E.M. McVillie, Macromol. Chemistry Rev., **1**, 375 (1967).
89. E. Gratch and E.M. McVillie, Proc. Roy. Soc. London, Ser. A, **221**, 1 (1954).
90. E.M. McVillie, J. Phys. Chem., **65**, 447 (1961).
91. E. Spenser, J. Phys. Chem., **65**, 875 (1961).
92. E. Gratch and E.M. McVillie, Proc. Roy. Soc. London, Ser. A, **221**, 18 (1954).
93. E. Gratch and E.M. McVillie, Proc. Roy. Soc. London, Ser. A, **221**, 28 (1954).
94. E. Schroeder and E. Jansson, Macromol. Chem., **18/19**, 282 (1960).
95. E. Gratch and E. Vanzo, Trans. Faraday Soc., **49**, 164 (1953).
96. E. Gordon, J. Phys. Chem., **65**, 71 (1961).
97. J.R. MacCallum, Macromol. Chem., **57**, 137 (1962).
98. E.B. Gerson and R.F. Kay, Macromol. Chem., **113**, 266 (1968).
99. E.B. Gloor, Analtical Chemistry of Polymers, Vol. 2 International, New York, 1968.
100. E.B. Jellinek, in Development of Polymer Polymers, Vol. 4, p. 760. Interscience, New York, 1969.
101. E.B. Jellinek, "The Relationship between the Kinetics and Mechanism of Thermal Depolymerization", p. 47-67 in Thermal Stability of Polymers. Edited by E.B. Corley. Marcel Dekker, New York, 1968.
102. L. Hsieh and E. Eyring, Elements of Polymer Polymerization. McGraw-Hill, New York, 1957.
103. L. Hsieh, E.B. Jellinek, J.R. Koch, and E. Kauterbach, Polymer, **9**, 503 (1968).
104. G.B. Smolensk, G.F. Ponomarev, and T.B. Nagel, Soviet Chem., **3**, 839 (1961).
105. E.B.E. Jellinek and E.B. Loh, Macromol. Chem., **123**, 70 (1968).
106. E.B.E. Jellinek and E.B. Loh, J. Phys. Chem., **72**, 3470 (1968).

107. G. Nagai, S.-I. Igarashi, and T.-O. Sato, *Polymers*, **12**, 3047 (1961).
108. E. Nakata and T. Kikugawa, *K. Kagaku J. (Tokyo)*, **18**, 110 (1961).
109. R. Gossell, G. Ward, E. Manning, J. E. Searles, and E. R. Zeman, *Polym. Bull.*, **1**, 325 (1960).
110. R. B. Sillescu, R. B. Nielsen, E. F. Fenneman, and J. R. Brighenti, *J. Polym. Sci.: Polym. Chem. Ed.*, **2**, 875 (1964).
111. R. Pappelen, *Polym. Bull.*, **1**, 341 (1961).
112. R. Tang, *private communication*.
113. R. G. Roberts, L. Hsu, and L. J. Fetters, *J. Macromol. Sci.-Chem.*, **2**(2), 875 (1967).
114. R. G. Jenkins, *J. Polym. Sci.*, **3**, 343 (1948).
115. R. G. Jenkins, *J. Polym. Sci.*, **3**, 1 (1948).
116. R. G. Jenkins, *J. Polym. Sci.*, **3**, 13 (1948).
117. E. Reineke, *Kolloid Beigeb. Kolloidchem. Ges.*, **3** (1), 21 (1973).
118. E. Eisenberg and E. Manoogian, *J. Polym. Sci.*, **6**, 23, 397 (1951).
119. T. Endrey, J. Jozsa, J. G. Brown, E. Nakata, T. Kikugawa, and E. Nakata, *Macromol.*, **15**, 2142 (1982).
120. J. E. Nakata, *Int. Polym. J.*, **3**, 21 (1966).
121. R. Gordon and L. J. Fetters, *J. Polym. Sci.*, **2**, 187 (1948).
122. L. J. Fetters and R. J. Behnken, *Int. Polym. J.*, **2**, 375 (1965).
123. A. Jenkins and L. E. Matlack, *J. Polym. Sci.: Polym. Chem. Ed.*, **1**, 1019 (1963).
124. E. Doran, R. Behnke, and G. Nagai, *Macromol.*, **2**(2), 113 (1973).
125. G. Ward, *Polym. Prepr.*, **22**(2), 156 (1975).
126. J. B. Longman, *Industrial Polymerization*, Academic Press Inc., New York, 1961.
127. E. Doran, Ph.D. Thesis, Department of Chemical Engineering, Princeton University, Princeton, NJ, 1974.

108. R.E.O. Anderson and R.E. Salt, *J. Phys. Chem.*, **75**, 2472 (1971).
109. T. Kawai, T. Kawaijiri and J.B. Grice, *Polym. Prepr.*, **25** (1), 176 (1984).
110. T. Kawaijiri, T. Kawai and J.B. Grice, *Macromol.*, **15**, 121 (1981).
111. T. Kawaijiri, T. Kawai and J.B. Grice, *Macromol.*, **15**, 140 (1981).
112. K. Iwama, *Polym. Prepr.*, **25** (2), 56 (1984).
113. K. Iwama, J.M. Martin and D. Kawanishi, *Polymer*, **25**, 958 (1984).
114. F.A. Bovey and G.E.B. Farn, *J. Polym. Sci.*, **25**, 73 (1957).
115. S.H. Byun, H. Kawai, O. Johnson, and K. Ito, *Macromol. Chem.*, **11**, 15 (1968).
116. H. Kawai, A. Fink, and K. Ito, *J. Colloid Interface Sci.*, **35**, 82 (1971).
117. K. Nagai, *J. Appl. Polym. Sci.*, **8**, 1697 (1964).
118. R.H. Jackson, *Anal. Spectrosc.*, **20** (4), 336 (1965).
119. K. Nakagawa and K. Okazaki, *Spectrochim. Acta*, **20**, 265 (1965).
120. D.R. Allen and C.A. Fryle, *Organic Chem. Plant Prod.*, **11**, 498 (1975).
121. K. Nakajima and K.H. Schmidt, *Infra-red Spectroscopy*, Springer-Verlag, New York, 1974.
122. A.W. Coyle, *Spectrochim. Acta*, **22A**, 1317 (1967).
123. A. Kawaijiri, H. Iwama and J.B. Grice, *J. Polym. Sci., Polym. Chem. Ed.*, **21**, 1963 (1983).
124. F.M. Pothan and R.E. Mustafa, *Int. Rev. Bio. Sci.*, **17** (1), 1 (1973).
125. K. Kawai and K. Nagai, *J. Colloid Interface Sci.*, **55**, 152 (1975).
126. S. Ota, H. Taniyama and K. Nakajima, *J. Phys. Chem. A*, **105**, 81 (1981).

147. E. E. John, G. Barnall, E. E. Palmer and E. J. Peerman, *J. Chem. Soc.*, 193, 4958 (1973).
148. E. E. John, E. Palmer, *ibid.*, Part C, 31, 389 (1973).
149. F. E. Lippman and E. E. Kornikowski, *Pyroanal. Technol.*, Ser. A, 22, 193 (1981).
150. F. E. Lippman, *Tr. Khim. Khim. Tekhnol.*, 3, 115 (1975).
151. L. E. McNeill and R. J. McQuinn, *Polym. Deg. and Stab.*, 3, 147 (1984).
152. L. E. McNeill and R. J. McQuinn, *Polym. Deg. and Stab.*, 3, 209 (1984).
153. L. E. McNeill, W. Gelfinger and C. Wile, *Polym. Deg. and Stab.*, 3, 229 (1984).
154. L. E. McQuinn, E. E. Lippman, L. E. Thomas and T. D. Donohue, *Adv. Polym. J.*, 13, 875 (1973).
155. E. E. Kornikowski, *Pyroanal. Technol.*, Ser. A, 2 (3), 343 (1974).
156. C. E. Schmittels and W. D. Burns, "Thermogravimetry of Poly(vinyl Alcohol) Standards. II. Effects of Resolving Techniques," p. 593-603 in *Gas-Liquid Chromatography*, L. J. CRAGG, Monograph No. 121, C. E. Hoyle, Ed., by C. E. Hoyle, W. D. Burns, and C. Schmittels, American Chemical Society, Washington, DC, 1978.
157. W. D. Burns and A. L. Schmitt, *J. Res. N. Plasmaville*, 13, 363 (1982).
158. C. E. Schmittels, unpublished work.
159. S. Sano, *Bull. Chem. Soc. Japan*, 33, 185 (1960).
160. E. Gossens, J. Puydy and E. Baey, *COLL. COORDINATION CHEM. COMM.*, 21, 203 (1973).
161. E. Anderson and L. Brinson, *J. Anal. Appl. Pyroly.*, 3, 95 (1981).
162. L. Brinson, *J. Anal. Appl. Pyroly.*, 3, 73 (1981).
163. R. E. Grant and R. Gossens, *Polymer*, 3, 185 (1962).
164. W. E. McLaugh and R. Batten, *Polym. Lett.*, 3, 417 (1965).

166. D. Guzman, D. Bellinger, and C. David, *Sur. Polym. J.*, **1**, 581 (1971).
167. E. Mecerdes, E. Guzman, A. Jodanis, and E. Selzer, *J. Polym. Sci.*, **26**, 1965 (1958).
168. A.S. Papirerian, Jr., *Kain. Kain. Tashm.*, **1**, 45 (1971).
169. A.S. Papirerian, *Polym. Science*, p. 1091. North Holland Publishing Co., Inc., New York, 1970.
170. Y.S. Papirerian, *Physicochem. Kinet.*, **4**, **13** (1971), 445 (1971).
171. F.E. Hunt and R.A. Gulderson, *Sur. Polym. J.*, **1**, 408 (1971).
172. A. Janssens and E.C. McNeill, *Sur. Polym. J.*, **12**, 277 (1971).
173. E.J. O'Hara, M. Sanger, and E.C. Janssens, *J. Polym. Sci., Polym. Chem. Ed.*, **11**, 159 (1973).
174. J.R. Lei, *Macromol.*, **17**, 1049 (1984).
175. B. Guzman and C. David, "Thermal Degradation", pp. 51-69 in *Polym. Degradation and Stability*. Interscience Publishers Press, New York, 1974.
176. C. David, "Thermal Degradation of Polymers", p. 10-51 in *Chemical Kinetics*, Vol. 19. Edited by E.R. Sanford and C.F.E. Tripp. Elsevier Scientific Publishing Co., Amsterdam, 1975.
177. E.A. Fyfe and R.S. Williams, *Macromol.*, **11**, 1001 (1978).
178. A. Eisenberg and F. Sauerbrey, *J. Polym. Sci.*, **21-2**, 1967 (1956).
179. B. Sauerbrey and E. Reineke, *Koll. Zent.*, **254**, 208, 210, 212, **2**, **21**, 25 (1975).
180. E.C. McNeill and M. Sanger, *J. Polym. Sci., Polym. Chem. Ed.*, **11**, 2001 (1973).
181. E.C. McNeill and M. Sanger, *Polym. Deg. and Stability*, **1**, 69 (1973).
182. B. Sauerbrey, "Elementary Molecular Weight Determinations", p. 1,3-17 in *Polym. Science*. Edited by J. Smets and E.R. Santer. Wiley, New York, 1975.
183. E.R. Sauerbrey, *Adv. Polymer Science*, Vol. **11**, 61 (1972).

- [19] P. G. DILLI, *SIAM Review* 3, 114, 117, Jan. 7, 1961.
- [20] E. GRIFF, D. HORTON, R. B. WILSON, J. R. KILPAT, and P. B. KERNING, *J. Polym. Sci.*, 33, 397 (1959).
- [21] R. B. HUNTER and R. M. THOMAS, *J. Am. Chem. Soc.*, 84, 348, Mar. 19, 1962.

BIOGRAPHICAL SKETCH

Ts Hsi Shu was born on January 22, 1921, in Taipei, Taiwan, Republic of China. In June, 1981, she received her Bachelor of Science degree in chemical engineering from the National Tsing Hua University, Taipei, Taiwan.

In May, 1984, she joined the Department of Materials Science and Engineering, University of Florida, Gainesville, Florida. Two years later, she received her Master of Science degree as a polymer major.

She is a member of the American Ceramic Society and Materials Research Society.

I certify that I have read this study and that, in my opinion it conforms to acceptable standards of scholarly presentation and is fully adequate, in scope and quality, as a dissertation for the degree of Doctor of Philosophy.


Richard D. Sack, Chairman
Associate Professor of Materials Science
and Engineering

I certify that I have read this study and that, in my opinion it conforms to acceptable standards of scholarly presentation and is fully adequate, in scope and quality, as a dissertation for the degree of Doctor of Philosophy.


Joseph L. Williams, Co-Chairman
Assistant Professor of Materials Science
and Engineering

I certify that I have read this study and that, in my opinion it conforms to acceptable standards of scholarly presentation and is fully adequate, in scope and quality, as a dissertation for the degree of Doctor of Philosophy.


E. Don Williams
Professor of Materials Science and
Engineering

I certify that I have read this study and that, in my opinion it conforms to acceptable standards of scholarly presentation and is fully adequate, in scope and quality, as a dissertation for the degree of Doctor of Philosophy.


Charles D. Bahl
Professor of Materials Science and
Engineering

I certify that I have read this study and that, in my opinion it conforms to acceptable standards of scholarly presentation and is fully adequate, in scope and quality, as a dissertation for the degree of Master of Philosophy.

Kenneth B. Weyman
Associate Professor of Philosophy

This dissertation was submitted to the Graduate Faculty of the College of Engineering and to the Graduate School and was accepted as partial fulfillment of the requirements for the degree of Master of Philosophy.

December, 1968

By: [Signature]
Dean, College of Engineering

Dean, Graduate School